Ph.D. Thesis

Non-perturbative analysis of phase structure in SU(3) gauge theory

Akio TOMIYA

akio@het.phys.sci.osaka-u.ac.jp

Osaka University Particle Physics Theory Group

February 27, 2015

Abstract

The phase structure of gauge theory is one of the most fascinating subject in particle physics. Because of its strong coupling feature, perturbation is not effective in general. Thus, non-perturbative approach is needed. In this thesis, we discuss the phase structure of SU(3) gauge theory through two different non-perturbative approaches.

In part 1, we discuss the fate of $\mathrm{U}(1)_\mathrm{A}$ anomaly in massless $N_f = 2$ QCD at finite temperature system by using lattice simulation. $\mathrm{U}(1)_\mathrm{A}$ symmetry is a symmetry of massless QCD Lagrangian, however it is not reflected in the particle spectra, because of quantum anomaly. Although anomaly is an explicit breaking, there is a possibility, $\mathrm{U}(1)_\mathrm{A}$ may be restored above the critical temperature. Most of lattice studies reported negative results, except for the simulation with the overlap fermion, which has exact chiral symmetry. In this thesis, we show significant difference between the spectrum of domain-wall type Dirac operator and the overlap-Dirac operator, which have been believed that almost same Dirac operators. We also show a volume insensitive gap in the overlap-Dirac spectrum. This may suggest $\mathrm{U}(1)_\mathrm{A}$ is restored above the critical temperature at quark mass vanishing and thermodynamic limit.

In part 2, we discuss supersymmetric $SU(3)$ gauge theory on $S^2 \times S^1$ in the context of the Hosotani mechanism by using the supersymmetric localization technique. The Hosotani mechanism is a mechanism, which breaks gauge symmetry by the Wilson line phase along compactified extra-dimension. The Wilson line phase is determined by the effective potential, which is calculated from the vacuum bubble of fermion and boson. The Hosotani mechanism does not occur in supersymmetric gauge theory in flat spacetime because of cancelation between fermion and boson loop contribution. We calculate the effective potential by using the supersymmetric localization technique. Thanks to the curvature of S^2, which couples to only scaler field, we obtain a nontrivial effective potential. We take large $\mathcal{R}$-charge limit in order to consider symmetry breaking. As a result, we reproduce the effective potential as obtained by the perturbation and lattice simulation. This approach has some difficulties, we comment on these issues.

Contents

1 Introduction to this thesis

Yang-Mills gauge theory is a fundamental language to describe the nature in the particle physics. Not only the standard model, but also candidates of beyond the standard model, the technicolor models, the gauge Higgs unification models, and the grand-unified theory are described by gauge theory. One of characteristics of Yang-Mills gauge theory is *asymptotic freedom*. The coupling of Yang-Mills gauge theory depends on the energy scale through the renormalization, and it becomes smaller and smaller at high energy regime. This phenomena called asymptotic freedom. Good concrete example for Yang-Mills gauge theory is Quantum Chromo-Dynamics (QCD), which is a fundamental theory of nucleus which is composed of quarks and gluons. QCD at high energy regime, since quark and gluon fields are weakly coupled each other, perturbation works well. In other words, system is described by gluons and quarks directly. Moreover, because of its striking properties, it has been investigated over 60 years from its discovery [1].

On the other hand, the phase structure is a important subject in the theoretical particle physics. The phase structure is inseparably related to the symmetries of the system. Again, QCD is a good example for importance of the phase structure. QCD at low energy regime, since quark and gluons are confined, they cannot be regard as dynamical degrees of freedom. However, the system is described by QCD Lagrangian as same as high energy regime, the dynamics of the system reflects its symmetry. One of global symmetry called *chiral symmetry*, play a key role to determine low energy dynamics. Chiral symmetry is a global symmetry of QCD Lagrangian at quark mass vanishing limit, which is broken by the quantum effect. Vestiges of chiral symmetry appear as the lightness of the pions, and light pions are dynamical degrees of freedom at low energy regime. In summary, in order to understand whole system in analytic way, we first classify the phase of the theory, and find lightest (massless) degrees of freedom at each phase.

Generally, the analysis of phase structure of gauge theory is difficult because of its large gauge coupling and non-perturbative effects. A variety of non-perturbative methods have been developed to analyze Yang-Mills gauge theory: Schwinger-Dyson equation, exact renormalization group equation, supersymmetric dualities, AdS/CFT, and so on. We employ lattice gauge theory (Part1) and supersymmetric localization technique (Part2) to analyze the phase structure of $SU(3)$ gauge theory.

In part 1, we study the axial $\mathrm{U}(1)_\mathrm{A}$ symmetry in massless two-flavor QCD at finite temperature using the lattice gauge theory. $\mathrm{U}(1)_\mathrm{A}$ is a global symmetry of massless quarks in the Lagrangian, which is broken in QCD physical state by the quantum effect. Originally, $\mathrm{U}(1)_\mathrm{A}$ symmetry is one of the chiral symmetry, however it is distinguished by quantization procedure. As we mentioned above, global symmetry connects to effective theory around phase transition, $\mathrm{U}(1)_\mathrm{A}$ restoration is relevant for the phase structure. Actually, if $\mathrm{U}(1)_\mathrm{A}$ symmetry is effectively restored, quark-hadron phase transition becomes first order.

The lattice gauge theory is an exact formulation of QCD and enable us a quantitative investigation of QCD phase structure. The lattice gauge theory is a gauge theory defined on a discrete space-time, which has exact gauge symmetry [14]. Because of the discretization, the path integral is regularized, and we can perform Monte Carlo integration without any approximation [15]. Over 30 years, QCD property has been investigated by using Monte Carlo simulation.

As we mention in following sections, most of studies by using the lattice gauge theory

reported negative result for $\mathrm{U(1)_A}$ restoration, and a few groups reported opposite results. Previous studies are not perfect simulation. Chiral fermion on the lattice is not uniquely defined. The overlap fermion realize exact chiral symmetry on a lattice, but numerical cost is too expensive to perform full-scale simulation. Moreover, the overlap fermion has difficulty on hybrid Monte Carlo algorithm. In the previous study, in order to overcome the difficulty, topology fixing term is introduced [17]. On the other hand, the domain-wall fermion is one of approximation of the overlap fermion. Goodness of the domain-wall are precise chiral symmetry and numerical performance. The domain-wall fermion is good at hybrid Monte Carlo calculation opposite to the overlap fermion. Unfortunately, the domain-wall fermion does not have exact chiral symmetry because of its approximation.

Two similar set-up , using the overlap fermion or the domain-wall fermion, should give a same result. However, as we mention in following section, numerical simulation with the overlap fermion and with the domain-wall fermion give different results. In this thesis, we employ both of fermion in order to judge which fermion gives the results with the chiral fermion. And we perform a calculation in two different volume, 2 fm and 4 fm in order to check finite size effect how affect to the results.

In part 2, we discuss the gauge symmetry breaking in the context of the Hosotani mechanism by using exact results on supersymmetric gauge theories based on the localization technique. In the Hosotani mechanism, gauge bosons acquire its mass from non-zero expectation value of the gauge field extended to extra-dimension, the Wilson line phase (Aharonov-Bohm effect in Yang-Mills theory). The expectation value is determined from an effective potential for the component *i.e.* the Wilson line phase. We consider a supersymmetric $SU(3)$ gauge theory on $S^2 \times S^1$ Euclidean space-time, and investigate how the effective potential for the Wilson line phase varies by running an imaginary chemical potential. We find that the large $\mathcal{R}$-charge is necessary in order to break the gauge symmetry. In addition, we confirm a finite size effect on our curved space for several small $\mathcal{R}$-charge. This method has some difficulties, which are discussed following section.

This thesis is based on following papers:

1. A. Tomiya, G. Cossu, H. Fukaya, S. Hashimoto and J. Noaki, arXiv:1412.7306 [hep-lat].
2. A. Tanaka, A. Tomiya and T. Shimotani, JHEP **1410**, 136 (2014) [arXiv:1404.7639 [hep-th]].

Detailed calculations are in the Appendix in order to clarify discussions.

Part I
Axial U(1) symmetry above the critical temperature

2 Introduction

The massless two-flavor QCD (*Quantum Chromo-dynamics*) Lagrangian has global $\mathrm{SU(2)_L} \times \mathrm{SU(2)_R} \times \mathrm{U(1)}_V \times \mathrm{U(1)}_A$ symmetries. Among them, the $\mathrm{U(1)_A}$ symmetry is considered to be special, because of existence of chiral anomaly. The anomaly is symmetry violation caused by a quantum correction. At zero temperature, anomaly appears through the heaviness of η' meson ($\sim$ 960 MeV) , which is heavier than π mesons ($\sim$ 140 MeV) in the real world. However the anomaly is not completely understood. Thus, the anomaly at finite temperature system is under active research in the last couple of years.

There is a possibility that $\mathrm{U(1)_A}$ is restored at finite temperature, although $\mathrm{U(1)_A}$ symmetry breaking is an explicit breaking. $\mathrm{U(1)_A}$ anomaly can be understood as the effect of instantons, which is suppressed by temperature. Since the effect of instantons is weakened by temperature, $\mathrm{U(1)_A}$ may be effectively restored at some finite temperature. Actually, Cohen argued, when $\mathrm{SU(2)_L} \times \mathrm{SU(2)_R}$ is fully restored, $\mathrm{U(1)_A}$ may be restored simultaneously.

$\mathrm{U(1)_A}$ symmetry and SU(2) chiral symmetry are related through the spectral density $\rho(\lambda)$ of the Dirac operator eigenvalue λ. SU(2) chiral symmetry is characterized by the chiral condensate $\langle\bar{\psi}\psi\rangle$. The chiral condensate is related to the spectral density $\rho(\lambda)$, which is main observable of this work [3],

$$\langle\bar{\psi}\psi\rangle = \lim_{m\to 0}\int d\lambda\ \rho(\lambda)\frac{2m}{\lambda^2+m^2}, \tag{2.1}$$

where m is the up and down quark mass in the isospin symmetric limit. When $\mathrm{SU(2)_L} \times \mathrm{SU(2)_R}$ symmetries completely restored, $\langle\bar{\psi}\psi\rangle = 0$ at quark mass vanishing limit. It is widely recognized that, above QCD critical temperature, this situation is realized. The spectral density is also related to the $\mathrm{U(1)_A}$ symmetry through the relation [3],

$$\chi_\pi - \chi_\delta = \lim_{m\to 0}\int d\lambda\ \rho(\lambda)\frac{4m^2}{(\lambda^2+m^2)^2}, \tag{2.2}$$

where χ_π and π_δ are the integrated correlator (*i.e.* susceptibilities) for iso-triplet pseudo-scalar and iso-triplet scalar channel, respectively. Since these channel are related by $\mathrm{U(1)_A}$ symmetry, if the $\chi_\pi - \chi_\delta = 0$, $\mathrm{U(1)_A}$ breaking is invisible in the correlators of these channels. It was argued that if there is a gap in the spectral density, *i.e.* $\rho(\lambda < \lambda_{\mathrm{gap}}) = 0$ with a finite $\lambda_{\mathrm{gap}} > 0$, $\chi_\pi - \chi_\delta$ vanishes [6]. It was further shown that if the $\mathrm{SU(2)_L} \times \mathrm{SU(2)_R}$ symmetry is fully restored above the critical temperature, the Dirac spectrum starts with at least cubic powers of λ and $\chi_\pi - \chi_\delta$ vanishes under this slightly relaxed assumption [13].

The argument above has been checked by using lattice QCD simulation, however results are controversial. Last couple of years, several group reported $\mathrm{U(1)_A}$ violation above the critical temperature except for JLQCD and TWQCD. [17, 18, 19, 20, 21, 22]. There are three possible causes of the difference. The first is the finite volume effect. There is always a gap in $\rho(\lambda)$ in the finite volume even below QCD critical temperature T_c. It is therefore

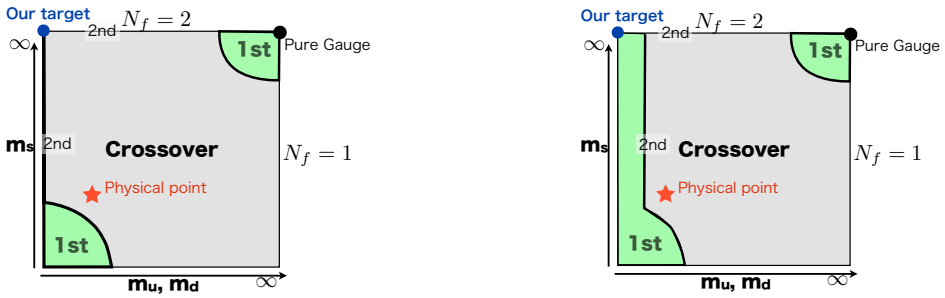

Figure 1: The Columbia plots. The left panel is conventional one. The right panel is possible one when $\mathrm{U(1)_A}$ is restored above the critical temperate. Vertical and horizontal axis corresponds to mass of strange and light two degenerated quarks, respectively. If quark mass is in gray (green) region, QCD phase transition is crossover (1st order). Boundary of these area is second order.

need to carefully check the volume scaling of the gap if it exists. The second is the accuracy of the chiral symmetry. As [13] suggested, the full $\mathrm{SU(2)_L \times SU(2)_R}$ symmetries play a key role to suppress the $\mathrm{U(1)_A}$ breaking effect in the correlators. The third is the effect of fixing topology.

Discretization of fermion is not unique, which is related to the treatment of chiral symmetry. Fermions on the lattice which have accurate chiral symmetry are the overlap fermion and the domain-wall fermion. The overlap fermion is a fermion on a lattice, which has an exact chiral symmetry. However its numerical cost is expensive, numerical calculation is difficult practically. On the other hand, the domain-wall fermion is an approximation of the overlap fermion, which can be extend the simulation to large volume rather easily. However it does not have exact chiral symmetry, the treatment of quark mass vanishing limit is not clear.

In this work, we compare domain-wall type fermions to the overlap fermion in order to understand how chiral symmetry is important for the issue. We perform Monte Carlo calculation of the lattice QCD at around $T = 200$ MeV ($> T_c$) employing the Möbius domain-wall fermion action, which allows us to simulate QCD on larger volumes than that of the overlap fermion. We use the code platform IroIro++ [23]. By the Möbius implementation of the domain-wall Dirac operator, we expect that the $\mathrm{SU(2)_L \times SU(2)_R}$ symmetry is kept to a good precision. We also study the effect of small violation of their symmetry by reweighting the Möbius domain-wall Dirac determinant to that of the overlap Dirac operator. This reweighting, if realizes, corresponds to the dynamical overlap fermion simulation without fixing topology.

As we will see below, we found a significant difference between the Möbius domain-wall and the (reweighted) overlap-Dirac operator spectra. By checking the chirality of each eigenmode, it turned out that the low-modes of the Möbius domain-wall Dirac operator violate the Ginsparg-Wilson relation, quite significantly even when their contribution to the residual mass is small. Such violation of the Ginsparg-Wilson relation in the low mode region may have a significant impact in the study of $\mathrm{SU(2)_L \times SU(2)_R}$ and $\mathrm{U(1)_A}$ symmetry restoration/breaking.

3 Symmetries in QCD

In this section, we briefly review the chiral symmetry and the anomaly in the context of QCD at zero temperature[1].

We start from the Dirac action in the continuum space-time, and introduce gauge interaction. If we take into account gauge interaction and quantize the system, a part of symmetry of the Dirac action is violated. This phenomenon is called the *anomaly*. As we review in this section, the anomaly can be understood as the Jacobian in the path integral [5]. On the other hand, there is another symmetry violation called *spontaneous symmetry breaking* [8]. Two of violations reflect to the particle spectrum as mentioned in this section.

Next, we review the vacuum of the gauge theory. Actually, there are infinite number of vacua which are not transformed each other continuously. The vacuum of the gauge theory should be gauge invariant. Thus, the superposed vacuum called θ vacuum is the physical vacuum. The anomaly can be understood as the tunneling between different vacua.

At the end of this section, we introduce meson correlators for later use. This is a preparation for the argument of the $\mathrm{U}(1)_\mathrm{A}$ restoration.

We discuss field theory in the Euclidean space-time throughout in this thesis.

3.1 The $\mathrm{U}(1)_\mathrm{A}$ anomaly in two-flavor QCD

The quarks in $N_f = 2$ QCD are described by the Dirac action,

$$S_F = \int d^4x \bar{\psi}(i\not{D} - m)\psi, \tag{3.1}$$

where,

$$\psi(x) = \begin{pmatrix} u(x) \\ d(x) \end{pmatrix}, \quad \bar{\psi}(x) = \begin{pmatrix} \bar{u}(x) & \bar{d}(x) \end{pmatrix}. \tag{3.2}$$

$\not{D}$ is the covariant derivative[2],

$$\begin{aligned} \not{D} = \gamma^\mu D_\mu &= \gamma^\mu(\partial_\mu - \sum_a igA_\mu^a T^a), \\ &\equiv \gamma^\mu(\partial_\mu - igA_\mu), \end{aligned} \tag{3.3}$$

where A_μ is a gauge field and T^a is a generator of the gauge group[3]. In the case of QCD, T^a is the Gell-Mann matrix. In other words, the covariant derivative act on quarks fields as a fundamental representation. This $\not{D}$ is diagonal for flavors. We consider $N_f = 2$ QCD, *i.e.* $m = \mathrm{diag}(m_u, m_d)$, $m_u = m_d = m$. At the end of the calculation, we take the quark mass vanishing limit, $m \to 0$.

The field strength of the gauge field can be obtained from a commutator of the covariant derivatives,

$$\begin{aligned} [D_\mu, D_\nu] &= -ig(\partial_\mu A_\mu^a - \partial_\nu A_\mu^a + g f^{abc} A_\mu^b A_\nu^c), \\ &= -igF_{\mu\nu}^a, \end{aligned} \tag{3.4}$$

[1] This section is a review of [5].

[2] Dirac operator $\not{D}$ is Hermitian in this section. Following sections, we use another convention.

[3] Generators satisfy, $[T^a, T^b] = if^{abc}T^c$ and $\mathrm{tr}\,(T^aT^b) = \frac{1}{2}\delta_{ab}$

where f^{abc} is the structure constant of the gauge group. The Yang-Mills action $S_{\rm YM}$ is defined using the field strength,

$$\begin{aligned} S_{\rm YM} &\equiv \frac{1}{4}\sum_{\mu\nu}\int d^4x F^a_{\mu\nu}F^a_{\mu\nu}, \\ &= \frac{1}{4}\int d^4x(\partial_\mu A^a_\mu - \partial_\nu A^a_\mu + g f^{abc}A^b_\mu A^c_\nu)^2, \\ &\equiv \frac{1}{2}{\rm tr}\int d^4x F_{\mu\nu}F_{\mu\nu}, \end{aligned} \tag{3.5}$$

where the tr is a trace over the gauge group. The gauge transformation is given by,

$$\psi(x) \to \psi'(x) = g(x)\psi(x), \quad \bar\psi \to \bar\psi'(x) = \bar\psi(x)g^\dagger(x), \tag{3.6}$$

$$A_\mu(x) \to A'_\mu(x) = g(x)A_\mu(x)g^\dagger(x) + \frac{1}{ig}(\partial_\mu g(x))g^\dagger(x). \tag{3.7}$$

where $g(x)$ is a function whose values are the gauge group. The fermion with the covariant derivative and the field strength of the gauge field are covariant under the gauge transformation. Then whole the QCD Lagrangian is invariant under the gauge transformation.

Taking the quark mass vanishing limit ($m \to 0$), another global symmetry arises which is called *chiral symmetry* : the Lagrangian is invariant under

$$\psi(x) \to \psi'(x) = e^{i\theta\gamma_5\tau^A}\psi(x), \quad \bar\psi \to \bar\psi'(x) = \bar\psi(x)e^{i\theta\gamma_5\tau^B}, \tag{3.8}$$

where θ is a real parameter. τ^A is a generator of U(2) group, $\tau^A = (\tau^0, \tau^a)$. τ^0 and τ^a represents the unit matrix and Pauli matrix, respectively. τ^0 corresponds to a U(1) subgroup of the U(2) chiral symmetry. This symmetry is supported from a fact,

$$\gamma_5 \not{D} + \not{D}\gamma_5 = 0. \tag{3.9}$$

In total, QCD Lagrangian has following global symmetry,

$$\mathrm{U(2)_L \times U(2)_R} \ \simeq \ \mathrm{SU(2)_L \times SU(2)_R \times U(1)}_V \times \mathrm{U(1)}_A \ , \tag{3.10}$$

where $\mathrm{SU(2)_L \times SU(2)_R}$ symmetry corresponds to

$$\psi \to e^{i\theta\gamma_5\tau^a}\psi, \tag{3.11}$$

$$\bar\psi \to \bar\psi e^{+i\theta\tau^a\gamma_5}, \tag{3.12}$$

(the SU(2) chiral symmetry) and

$$\psi \to e^{i\theta\tau^a}\psi, \tag{3.13}$$

$$\bar\psi \to \bar\psi e^{-i\theta\tau^a}. \tag{3.14}$$

On the other hand, the $\mathrm{U(1)_A}$ symmetry, equivalently the U(1) chiral symmetry, corresponds to

$$\psi \to e^{i\theta\gamma_5}\psi, \tag{3.15}$$

$$\bar\psi \to \bar\psi e^{+i\theta\gamma_5}. \tag{3.16}$$

Quantum field theory can be obtained from the path integral, thus all of information of QCD is calculated from the partition function[4],

$$Z = \int \mathcal{D}\bar{\psi}\mathcal{D}\psi[\mathcal{D}A_\mu] \exp\left[S_F - S_{\rm YM}\right], \tag{3.17}$$

where the path integral measure $[\mathcal{D}A_\mu]$ contains appropriate gauge fixing and ghost term. From now on, we derive the Ward-Takahashi identity, which corresponds to the Nöther theorem in quantum field theory, to clarify symmetries at the quantum level. Actually, the $\mathrm{U(1)_A}$ symmetry is violated at the quantum level. In order to see the violation, we employ the Fujikawa method. Take infinitesimal *local* $U(1)$ chiral transformation in order to derive the Ward-Takahashi identity,

$$\psi(x) \to \psi'(x) = e^{i\gamma_5\alpha(x)}\psi(x) = \psi(x) + i\alpha(x)\gamma_5\psi(x), \tag{3.18}$$
$$\bar{\psi}(x) \to \bar{\psi}'(x) = \bar{\psi}(x)e^{i\gamma_5\alpha(x)} = \bar{\psi}(x) + i\bar{\psi}(x)\alpha(x)\gamma_5. \tag{3.19}$$

The path integral is invariant under changing fermions fields,

$$\begin{aligned}&\int \mathcal{D}\bar{\psi}'\mathcal{D}\psi'[\mathcal{D}A_\mu] \exp\left[\int d^4x\bar{\psi}'(i\not{D} - m)\psi' - S_{\rm YM}\right] \\ &= \int \mathcal{D}\bar{\psi}\mathcal{D}\psi[\mathcal{D}A_\mu] \exp\left[\int d^4x\bar{\psi}(i\not{D} - m)\psi - S_{\rm YM}\right]\end{aligned} \tag{3.20}$$

With this transformation, the Dirac action is changed as,

$$\int d^4x\bar{\psi}'(i\not{D} - m)\psi' = \int d^4x\alpha(x)[\partial_\mu(\bar{\psi}\gamma^\mu\gamma_5\psi) - 2im\bar{\psi}\gamma_5\psi] + \int d^4x\bar{\psi}(i\not{D} - m)\psi. \tag{3.21}$$

If we neglect the Jacobian for the path integral, we obtain a conservation low of the axial current as same as the SU(2) chiral symmetry. The symmetry violating term arises from the Jacobian of the path integral. After a lengthy calculation, we obtain following expressions[5],

$$\mathcal{D}\bar{\psi}'\mathcal{D}\psi' = J\mathcal{D}\bar{\psi}\mathcal{D}\psi, \tag{3.22}$$

$$J \sim \exp\left[-2i\mathrm{Tr}\left(\alpha(x)\gamma_5\right)\right], \tag{3.23}$$
$$\to \exp\left[-2i\int d^4x\alpha(x)\frac{N_f g^2}{32\pi^2}\mathrm{tr}\,\epsilon^{\mu\nu\alpha\beta}F_{\mu\nu}F_{\alpha\beta}\right]. \tag{3.24}$$

If we combine (3.20) and (3.24), and we expand the linear order of $\alpha(x)$, we obtain,

$$\partial_\mu\langle\bar{\psi}\gamma^\mu\gamma_5\psi\rangle = \langle 2im\bar{\psi}\gamma_5\psi + 2i\frac{N_f g^2}{32\pi^2}\mathrm{tr}\,\epsilon^{\mu\nu\alpha\beta}F_{\mu\nu}F_{\alpha\beta}\rangle, \tag{3.25}$$

where $N_f = 2$ in this case. (3.25) shows that, even at the quark mass vanishing limit, the axial current is not conserved.

[4]Precisely speaking, all of information of QCD is obtained from the generating functional.
[5]Detail calculation is in Appendix B.

3.2 The instanton

In this subsection, we introduce another viewpoint of the anomaly: a classical solution of the Yang-Mills theory called the instanton [9, 10]. Here, we take a pure SU(2) gauge theory for simplicity. Since SU($N_c > 2$) gauge group has SU(2) subgroup, this result can be extended to general $N_c > 2$. The instanton is a solution of equation of motion of the Yang-Mills action on the Euclidean space-time, and describes transition between different vacua, which are characterized by the winding number, in the Minkowski space-time.

Intuitively, the vacuum of the gauge theory is characterized by,

$$A_\mu(x) = 0, \tag{3.26}$$

however this configuration is not gauge invariant. Actually, there are gauge equivalent energy-zero configurations described by,

$$A_\mu(x) = \frac{1}{ig}(\partial_\mu g(x))g^\dagger(x). \tag{3.27}$$

Here we choose temporal gauge, $A_0 = 0$, in which, residual gauge transformations are time-independent. In order to see the vacuum state, the residual gauge transformation letting them approach to a constant, unity at the spacial infinity,

$$g(\vec{x}) \to 1, \quad (|\vec{x}| \to \infty). \tag{3.28}$$

This condition (3.28) suggests, the spacial infinity cannot distinguish the gauge field *i.e.* the spacial infinity should be identified, thus our space is effectively compactified,

$$R^3 \simeq S^3. \tag{3.29}$$

This is the same as the stereographic map in the context of the Riemann sphere. Now, our gauge transformation function g define the map between spacial S^3 and $SU(2)$. Furthermore, $SU(2)$ group can be regard as S^3, therefore, the map (3.29) is topologically equivalent to the map (Fig. 2),

$$S^3 \to S^3. \tag{3.30}$$

There are topologically distinguished maps, which cannot be transformed each other continuously[6]. Each map is characterized by the so-called winding number n, where $n \in \boldsymbol{Z}$. This means that the vacuum characterized by (3.27) split into disjointed sets of vacua, and each of them is characterized by the winding number n. Note that, these vacua are transformed each other by the large gauge transformation.

The instanton describe the transition between the vacuum with the winding number n, $|n\rangle$ to the vacuum with the winding number m, $|m\rangle$ *i.e.* the instanton describes the transition between vacua which have different winding number. The instantons are characterized by the instanton number or the topological charge $\nu = m - n$. The explicit form of the instanton solution for ν is given in the Euclidean space-time by,

$$A_\mu(x) = \frac{r^2}{r^2 + \rho^2} ig(x)\partial_\mu g^\dagger(x), \tag{3.31}$$

[6]Mathematically because $\pi_3(S^3) = \boldsymbol{Z}$.

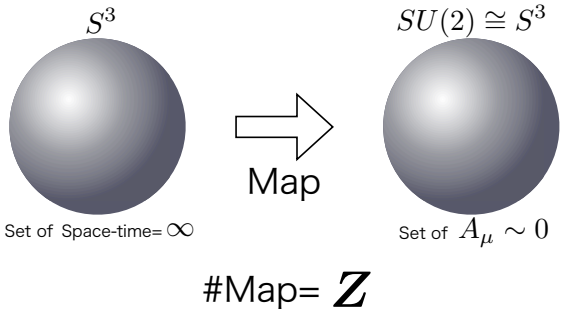

Figure 2: Topologically distinguished maps. Maps between S^3, can be regarded as wrapping. The number of wrapping corresponds to the winding number.

where ρ is an arbitrary real parameter and $r = x_\mu x^\mu$, and

$$g(x) = \left[\frac{x^4 + i\vec{x}\cdot\vec{\tau}}{r^2}\right]^\nu, \tag{3.32}$$

where $\vec{\tau} = (\tau^a)$ is the Pauli matrix. Actually, ν can be represented by the instanton solution,

$$\nu = \frac{1}{32\pi^2}\mathrm{tr}\int d^4x \epsilon^{\mu\nu\alpha\beta}F_{\mu\nu}F_{\alpha\beta}. \tag{3.33}$$

Physical vacuum must be invariant under not only infinitesimal gauge transformation but also large gauge transformation, and is given by a superposition of vacua,

$$|\theta\rangle = \sum_n e^{in\theta}|n\rangle. \tag{3.34}$$

This $|\theta\rangle$ is called theta vacuum[7].

Now, the gauge invariant partition function can be defined by

$$Z = \langle\theta|\theta\rangle, \tag{3.35}$$
$$= \sum_{n,m} e^{i\theta(n-m)}\langle m|n\rangle, \tag{3.36}$$
$$\propto \sum_\nu e^{i\theta\nu}Z^\nu, \tag{3.37}$$

where $\nu = m - n$ and $Z^\nu = \langle m|n\rangle$, which is a partition function describing transitions with the topological charge ν.

Let us get back to QCD. Recall (3.23) and (3.24), and we re-evaluate these equation from the viewpoint of the instanton. Substitute the instanton solution and choosing α to a constant, we obtain,

$$\mathrm{tr}_{\,\mathrm{reg}}[\gamma_5] = \frac{1}{32\pi^2}\mathrm{tr}\int d^4x \epsilon^{\mu\nu\alpha\beta}F_{\mu\nu}F_{\alpha\beta}, \tag{3.38}$$

[7] θ vacua satisfy cluster decomposition [4].

where $\mathrm{tr}_{\mathrm{reg}}$ is the trace over whole Hilbert space with appropriate regularization factor[8]. After expanding L.H.S in terms of the eigenmodes of the Dirac operator, we obtain,

$$n_+ - n_- = \nu. \tag{3.39}$$

where $n_\pm$ is the number of zero-modes with chirality $\pm$. Here we have used the fact that only paired eigenmodes appear except for the zero-modes. This is called the Atiyah-Singer index theorem [12]. This theorem is another appearance of the $\mathrm{U}(1)_{\mathrm{A}}$ anomaly.

3.3 SU(2) chiral symmetry

Because of the traceless property of th Puli matrix, the Jacobian $J = 1$ for the SU(2) chiral symmetry. Thus, the anomaly does not affect the SU(2) chiral symmetry. In other words, normal Ward-Takahashi identity is valid for the SU(2) chiral symmetry,

$$\partial_\mu \langle \bar{\psi}\gamma^\mu \tau^a \gamma_5 \psi \rangle = \langle 2im\bar{\psi}\gamma_5 \tau^a \psi \rangle. \tag{3.40}$$

This current conserve even at the quantum level after taking the quark mass vanishing limit.

However the SU(2) chiral symmetry is broken spontaneously. Then we get three massless bosons($\pi^{0,\pm}$) composed by $\bar{\psi}\tau^{3,\pm}\gamma_5\psi$, which are predicted from the Nambu-Goldstone theorem[9]. Note that, anomalous broken $\mathrm{U}(1)_{\mathrm{A}}$ part does not generate Nambu-Goldstone boson. In this case, corresponding would-be Nambu-Goldstone boson $\eta \sim \bar{\psi}\tau^0\gamma_5\psi$ does not have to be massless.

(3.25) is an operator identity, it looks that the equation holds always. However, at infinitely high temperature limit, finite temperature theory becomes field theory in three-dimensional space. In this case, the epsilon tensor $\epsilon^{\mu\nu\alpha\beta}$ does not exist. Then, the anomaly disappear at infinite temperature. Moreover, as we have seen in this section, the anomaly is a consequence of the instantons. The instanton effect is suppressed by the temperature. Thus, there is a possibility that the anomaly effectively disappear at finite temperate. We examine a possibility that the expectation value of $\mathrm{tr}\,\epsilon^{\mu\nu\alpha\beta}F_{\mu\nu}F_{\alpha\beta}$ vanishes just above the critical temperature, in following sections.

3.4 Correlators and Chiral symmetries

In this subsection, we review the relationship between meson correlators and the chiral symmetries. Let us define the *meson operators*,

$$\pi(x) = i\bar{\psi}(x)\gamma_5\tau\psi(x), \quad \sigma(x) = \bar{\psi}(x)\psi(x), \tag{3.41}$$
$$\delta(x) = \bar{\psi}(x)\tau\psi(x), \quad \eta(x) = i\bar{\psi}(x)\gamma_5\psi(x), \tag{3.42}$$

where $\psi = {}^T(u \;\; d)$. τ is the Pauli matrix, here we suppress index a for simplicity. Correlators of these composite fields are given by,

$$\Pi_J(x) \equiv \langle J(x)J(0)\rangle - \langle J(x)\rangle\langle J(0)\rangle, \tag{3.43}$$

[8]For example, heat kernel $\exp[-\not{D}/M^2]$, where M is a large real number (cut-off). After the calculation, M is taken to be infinity.

[9]See Appendix B.

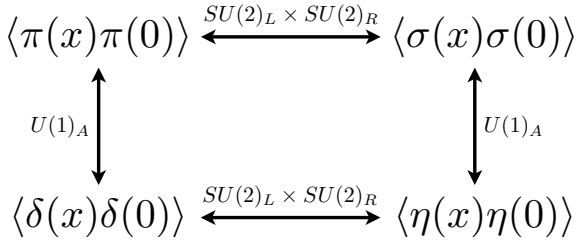

Figure 3: The relationship between meson correlators. Top and bottom correlators are paired via SU(2) chiral symmetry. Left and right are paired via U(1) chiral symmetry. Below the critical temperature, these are not degenerated.

where $J(x) = \bar{\psi}(x)\Gamma\psi(x)$. Γ corresponds to gamma matrices and flavor matrices which include unit matrix, $\Gamma = \gamma_5\tau^A, \mathbf{1}\tau^A$. We examine the symmetries of this correlators of there fields (Fig. 3). At zero temperature, all the correlators are not degenerate because of the existence of anomaly and spontaneous symmetry breaking. On the other hand, above the critical temperature, π channel and σ channel, δ channel and η channel are degenerate because of restoration of SU(2) chiral symmetry.

Let us summarize the symmetry of massless two-flavor QCD. The Lagrangian of Massless QCD has symmetry, $\mathrm{SU(2)_L \times SU(2)_R \times U(1)}_V \times \mathrm{U(1)}_A$. However whole symmetry cannot be realized in the particle spectra at zero temperature. SU(2) chiral symmetry is broken and accompanied with massless pions. This breaking is observed by splitting of π and σ channels. On the other hand, $\mathrm{U(1)_A}$ is breaking by anomaly. This breaking is observed by splitting of π and η. In this case, the mass of η meson is not constrained by the Nambu-Goldstone theorem.

3.5 Finite temperature system analysis

In this subsection we briefly review the Matsubara formalism. The Matsubara formalism is a formalism which enable us investigate finite temperature systems. This formalism is Euclidean formalism field theory with appropriate boundary condition for compact imaginary time direction. The path integral representation is obtained from the partition function (sum over state),

$$Z(\beta) = \sum_n e^{-\beta E_n}, \tag{3.44}$$

$$= \sum_n \langle n|e^{-\beta H}|n\rangle, \tag{3.45}$$

$$= \mathrm{Tr}\,[e^{-\beta H}], \tag{3.46}$$

where β is inverse temperature $1/T$. Eq. (3.45) can be understood as the imaginary time evolution, then the thermal partition function can be written in terms of the path integral,

$$Z(\beta) = \int \mathcal{D}\phi \exp\big[-\int_0^\beta d\tau \int d^3x \mathcal{L}[\phi]\big], \tag{3.47}$$

where ϕ represent all of fields in the system. In terms of the path integral, all of field must satisfy appropriate boundary condition for imaginary time direction. : periodic boundary

condition for bosonic fields and anti-periodic boundary condition for fermonic fields. In this representation, one can see that the infinite temperature limit corresponds to a field theory on three dimensional space as mentioned before.

4 Chiral symmetries and Correlators

In previos section, we have reviewed QCD and its symmetries. In this section, we discuss the chiral symmetry restoration based on Cohen's argument [6, 7]. As we have seen before, the SU(2) chiral symmetry is broken spontaneously at zero-temperature. It is widely recognized that, $\mathrm{SU(2)_L} \times \mathrm{SU(2)_R}$ symmetry is fully restored above the QCD critical temperature. On the other hand, $\mathrm{U(1)_A}$ symmetry is also violated at zero-temperature. Although the anomaly is an explicit breaking, by the instanton suppression, its effect is weakened with temperature increasing. Cohen pointed out, when SU(2) chiral symmetry is restored, $\mathrm{U(1)_A}$ may be restored simultaneously. Following subsection, we review his argument [6, 7] and introduce our observable, *i.e.* $\chi_{U(1)}$ and $\rho(\lambda)$.

Following sections, we employ anti-hermitian Dirac operator instead of hermitian Dirac operator[10].

4.1 Chiral symmetries and Dirac spectrum

The Dirac eigenvalue in the continuum theory is given by,

$$\not{D}\psi_j(x) = i\lambda_j\psi_j(x), \tag{4.1}$$

where $\not{D}$ is the anti-hermitian Dirac operator on a given background gauge field, and λ_j is a real eigenvalue. $\psi_j(x)$ is a eigen-mode (function) and after here we suppress the argument x. The eigenmodes satisfy the orthogonality $\int d^4x\psi_j^\dagger\psi_k = \delta_{jk}$. Since the Dirac operator, *i.e.* covariant derivative, $\not{D}$ includes the given back ground gauge field, λ_j reflects the gauge field configuration. In the continuum theory, the Dirac operator $\not{D}$ has the chiral symmetry (3.9). Therefore, all eigenvalues λ_j are paired with $-\lambda_j$ except for the zero-modes $\lambda_j = 0$.

Let us introduce the Dirac spectrum or the spectral density,

$$\rho_A(\lambda) = \frac{1}{V}\sum_n \delta(\lambda_n - \lambda), \tag{4.2}$$

$$\rho(\lambda) = \langle\rho_A(\lambda)\rangle, \tag{4.3}$$

$\langle\cdots\rangle$ is a weighted average with $e^{-S_{\mathrm{YM}}}\mathrm{Det}\,[\not{D} - m]$, if it needs to emphasize existence of the dynamical quark mass, we denote subscript m for the average as $\langle\cdots\rangle_m$. Note that, if $\not{D}$ has the chiral symmetry, $\rho(\lambda)$ is an even function for λ. In addition, $\rho_A(\lambda)$ is positive definite because it is a number density. If we neglect zero-modes, one can prove that $\rho(\lambda)$ is also positive definite. This $\rho(\lambda)$ is called the Dirac spectrum. This gives information of the symmetry of quarks in the quantum gauge field. For example, the chiral condensate $\langle\bar{\psi}\psi\rangle$, which is an order parameter of the chiral phase transition has a relation,

$$|\langle\bar{\psi}\psi\rangle_{m=0}| = \pi\rho(0), \tag{4.4}$$

[10]See Appendix A.

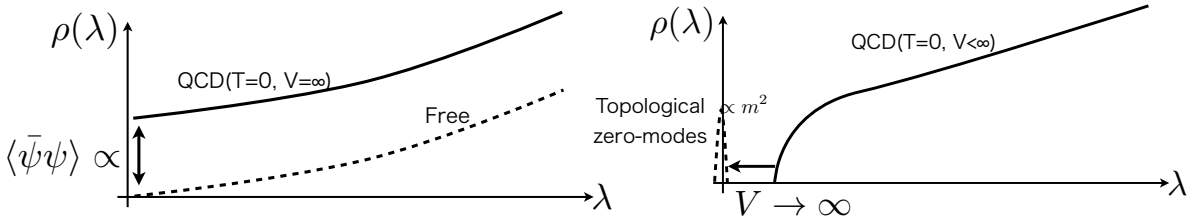

Figure 4: Symbolical figure of the Dirac spectrum at zero temperature. (Left panel) At thermodynamic limit, according to the Banks-Casher relation, the Dirac spectrum at the origin is proportional to the chiral condensate, $\rho(0) \propto \langle\bar{\psi}\psi\rangle$, at the quark mass vanishing limit. (Right panel) If the system volume is finite, chiral symmetry does not break. The gap is open in the spectrum and a peak from exact-zero modes appear at the origin (dotted curve). The hight of a peak at origin is proportional to the quark mass square. The gap size is proportional to inverse exponential of the volume, $\lambda_{\rm gap} \propto \exp[-V]$. As approaching thermodynamic limit, gap is closing.

this is called the Banks-Casher relation [11]. When the SU(2) chiral symmetry is broken spontaneously, $|\langle\bar{\psi}\psi\rangle_{m=0}| \neq 0$. The Banks-Casher relation(4.4) tells us $\rho(0) \neq 0$ (Fig. 4, Left panel). Precisely speaking, the symmetry breaking can be occurred at $V \to \infty$. At finite volume, symmetries are not broken spontaneously. In this case, both side of (4.4) 0. Approaching to $V \to \infty$, near-zero modes λ approaching to $\lambda \to 0$ (Fig. 4, Right panel). Finally the near-zero modes λ reach zero at the thermodynamic limit, then we obtain $|\langle\bar{\psi}\psi\rangle_{m=0}| \neq 0$ and $\rho(0) \neq 0$. Note that, near-zero modes must be distinguished from exact zero-modes, *i.e.* $\rho(0) \neq (n_+ + n_-)/V$.

If exact zero-modes are there, typically quarks on the instanton back ground, these contribution seems to be $\rho_A(\lambda) \propto \delta(\lambda)$. However, the number of zero-modes consists measure-zero-set in the path integral at the thermodynamic limit, in other words, topological zero-modes cannot contribute to the physical results after taking the continuum and thermodynamic limit. We will see this issue more rigid way.

4.2 Disappearance of $\mathrm{U}(1)$ anomaly above the critical temperature

In this subsection, we review Cohen's arguments. He argued that an existence of a gap in the spectral density is not inconsistent with an analysis of the connected part of correctors. In addition, he argued that if the Dirac spectrum has the gap, the disconnected part of correctors is identical above the critical temperature, precisely speaking, $\Pi_\pi(x) = \Pi_\eta(x)$ and $\Pi_\sigma(x) = \Pi_\delta(x)$ at $m \to 0$ above the critical temperature. Finally he concluded that $\mathrm{U}(1)_\mathrm{A}$ should be restored above the critical temperature. Here, "gap" in the Dirac spectrum means $\rho(\lambda) = 0$ for $\lambda <^\exists \lambda_{\rm critical}$ (Fig. 5).

Let us introduce $\mathrm{U}(1)_\mathrm{A}$ susceptibility,

$$\chi_{U(1)_A} = \frac{1}{V}\int d^4x(\langle\pi(x)\pi(0)\rangle - \langle\delta(x)\delta(0)\rangle). \tag{4.5}$$

If the $\mathrm{U}(1)_\mathrm{A}$ symmetry is restored above the the critical temperature, right hand side will vanish, *i.e.* this is an order parameter of $\mathrm{U}(1)_\mathrm{A}$ symmetry. This $\mathrm{U}(1)_\mathrm{A}$ susceptibility can be

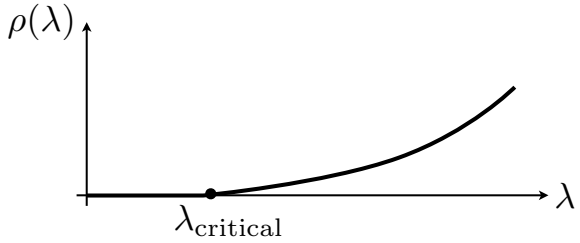

Figure 5: The Dirac spectrum with the gap. This situation may realize at finite temperature at the thermodynamic and the quark mass vanishing limit.

written in terms of the Dirac spectrum[11],

$$\chi_{U(1)_A} = \int d\lambda \frac{4m^2\rho(\lambda)}{(\lambda^2+m^2)^2}. \tag{4.6}$$

From the denominator in the right hand side of (4.6), one can understand that $\mathrm{U(1)_A}$ symmetry violation in the meson correlators come from the origin, $\lambda \sim 0$. On the other hand, from Banks and Casher's arguments,

$$|\langle\bar{\psi}\psi\rangle| = \int d\lambda \frac{2m\rho(\lambda)}{\lambda^2+m^2}. \tag{4.7}$$

One can see from above equation, spontaneous chiral symmetry breaking also comes from $\lambda \sim 0$. Both of order parameters depend on the behavior of spectral function $\rho(\lambda)$ at the quark mass vanishing limit, $m \to 0$.

Intuitively, if SU(2) chiral symmetry is restored above the critical temperature, $\mathrm{U(1)_A}$ symmetry seems to be also resorted in this representation. Actually, Cohen argued this statement in more precise way[12]. In following subsections, we discuss on the effect on $\mathrm{U(1)_A}$ anomaly on disconnected part of the meson correlator. *If* the spectral density took a form $\rho(\lambda) \sim m^2\delta(\lambda)$, we would $|\langle\bar{\psi}\psi\rangle| = 0$ and $\chi_{U(1)_A} \neq 0$ even at the quark mass vanishing limit. However as we mentioned before, the path integral measure of zero-modes contribution is zero at thermodynamic limit, this situation does not realized at least by the topological zero-modes.

4.2.1 U(1) anomaly on connected diagram

In this subsection, we review a constraint of $\rho(\lambda)$ from connected diagram based on [7]. He started from n-th derivative of logarithm of the partition function with respect to the quark mass,

$$\left.\frac{\partial^n \log(Z)}{\partial m^n}\right|_{m=0} = \frac{1}{V}\langle(\int d^4x\bar{\psi}\psi)^n\rangle. \tag{4.8}$$

In the right hand side, change the signature under the chiral rotation for odd n. Therefore $\log(Z)$ is a analytic even function of the quark mass. In the first order,

$$\langle\bar{\psi}\psi\rangle_m = \frac{1}{V}\frac{\partial \log Z}{\partial m}. \tag{4.9}$$

[11] See Appendix E.

[12] However a part of his treatment of UV is not rigorous. The rigorous treatment, see [13]

And also we have a relation between chiral condensate and the Dirac spectrum,

$$\langle\bar{\psi}\psi\rangle_m = \int d\lambda\rho(\lambda)\frac{m}{\lambda^2+m^2}. \tag{4.10}$$

We combine (4.8)-(4.10), then we obtain following formula.

$$\lim_{m\to 0}\frac{1}{V}\frac{\partial^n \log(Z)}{\partial m^n} = \lim_{m\to 0}\frac{\partial^{n-1}}{\partial m^{n-1}}\int d\lambda\rho(\lambda)\frac{m}{\lambda^2+m^2}. \tag{4.11}$$

In the derivation of (4.11), we used a fact that $\langle\bar{\psi}\psi\rangle$ is an even function. Here we assume $\rho(\lambda)$ *does not depend on quark mass.* Of course, $\mathrm{Det}\,[\not{D}-m]$ is included in $\langle\cdots\rangle$, $\rho(\lambda)$ implicitly depend on m. This assumption corresponds to neglect all of contribution except for connected diagram[13]. In order to emphasize, put "qlc", we obtain,

$$\begin{aligned}\lim_{m\to 0}\frac{1}{V}\frac{\partial^n \log(Z)}{\partial m^n}\bigg|^{\mathrm{qlc}} &= \lim_{m\to 0}\int d\lambda\rho(\lambda)\frac{\partial^{n-1}}{\partial m^{n-1}}\frac{m}{\lambda^2+m^2}\\ &= -(n-1)!\int d\lambda\rho(\lambda)\left(\frac{i}{\lambda}\right)^n\end{aligned} \tag{4.12}$$

Here we assume $\rho(\lambda)\sim|\lambda|^\alpha$ at $\lambda\sim 0$. Here α is a real parameter, which determined by lattice calculation. Then we obtain,

$$\lim_{m\to 0}\frac{1}{V}\frac{\partial^n \log(Z)}{\partial m^n}\bigg|^{\mathrm{qlc}} \sim -\int d\lambda|\lambda|^{\alpha-n}+\cdots. \tag{4.13}$$

Consider $\alpha<n$ case. In this case, right hand side of (4.13) is diverged. On the other hand, $\log(Z)$ is a regular function above the critical temperature. Then we obtain $\alpha\geq n$. This means, if there are only connected diagrams contribution, $\rho(\lambda)$ dumps faster than arbitrary power n. In other words, $\rho(\lambda)$ is extremely flat. This situation can be realize by existence of the gap in the Dirac spectrum (Fig. 5).

Next, we prove $\rho(\lambda)$ starts at least quadratic order above the critical temperature[14],

$$\frac{\partial\rho}{\partial\lambda}\bigg|_{\lambda=0} = 0. \tag{4.14}$$

We start from the pion susceptibility,

$$\chi_\pi = -\int d^4x\langle\pi(x)\pi(0)\rangle. \tag{4.15}$$

Using Banks-Casher's argument,

$$\chi_\pi = \int d\lambda\frac{\rho(\lambda)}{\lambda^2+m^2} = \frac{\langle\bar{\psi}\psi\rangle}{m}. \tag{4.16}$$

Here we assume $\rho(\lambda)=c|\lambda|^\alpha$, where α is a real parameter ($\alpha\leq 1$). c is a real parameter, which has mass dimension 2. Additionally, we assume that this form holds also at the quark mass vanishing limit *i.e.* c does not vanish at $m\to 0$,

$$\chi_\pi = \int d\lambda\frac{c|\lambda|^\alpha}{\lambda^2+m^2} = \frac{c\pi}{2m^{1-\alpha}\cos(\pi\alpha/2)}. \tag{4.17}$$

[13]See Appendix D

[14]Note that, constant term is inconsistent with the Banks-Casher relation.

If $\alpha \leq 1$, right hand side diverges at the quark mass vanishing limit[15]. This contradicts to analyticity of the partition function above the critical temperature. Therefore, we obtain $\alpha > 1$.

4.2.2 U(1) anomaly on disconnected diagram

In this subsection we discuss disconnected diagram contribution when we assume the gap in the spectrum based on [6]. SU(2) chiral symmetry is restored above the QCD critical temperature for massless QCD, this means,

$$\langle \bar{\psi}\psi \rangle = 0, \tag{4.18}$$

where $\langle \cdots \rangle$ means thermal and quantum average of the operators, as same as previous sections. This implies,

$$\langle \rho(\lambda) \rangle = 0, \tag{4.19}$$

because of the Banks-Casher relation. This gives stronger constraint to $\rho_A(0)$, which can be seen from the path integral representation of (4.19),

$$0 = \frac{1}{Z}\int [\mathcal{D}A] e^{-S_{\rm YM}} \mathrm{Det}\,[\not{D} - m] \rho_A(0). \tag{4.20}$$

In the integral, $e^{-S_{\rm YM}}\mathrm{Det}\,[\not{D} - m]$ is positive[16], and $\rho_A(\lambda)$ is non-negative because it is a number density. Therefore $\rho_A(0) = 0$ for all gauge configuration to realize (4.18). This means, there are no near zero-modes on all of the gauge configuration.

He argued also the difference between the correlator of σ and the correlator of η, which are in pair on $\mathrm{U(1)_A}$ and SU(2) chiral symmetry,

$$\Pi_\sigma(x) - \Pi_\delta(x) = \frac{1}{Z}\int [\mathcal{D}A] e^{-S_{\rm YM}} \mathrm{Det}\,[\not{D} - m] \left[\mathrm{Tr}\,[G(x,x)]\mathrm{Tr}\,[G(0,0)]\right], \tag{4.21}$$

where $G(x,y)$ is a quark propagator[17] in the presence of a background gauge field A_μ. Here we use isospin symmetry. Note that, this quantity only comes from disconnected diagram in terms of quark line. If $\mathrm{Tr}\,[G(x,x)] \sim \mathcal{O}(m)$ is verified for all possible configuration, this leads,

$$\Pi_\sigma(x) - \Pi_\delta(x) \sim \mathcal{O}(m^2). \tag{4.22}$$

In which case, we can conclude $\Pi_\sigma(x) - \Pi_\delta(x) = 0$ at the quark mass vanishing limit.

[15] For $\alpha = 1$, the formula diverge logarithmically.

[16] The determinant is real and positive. This is because,

$$\mathrm{Det}\,[\not{D} - m] = \prod_n [i\lambda_n - m] = \prod_{\lambda_n > 0} [\lambda_n^2 + m^2] > 0.$$

Here we ignore zero-modes.

[17] This is a matrix in flavor space.

In order to verify $\mathrm{Tr}\,[G(x,x)] \sim \mathcal{O}(m)$, we rewrite the quark propagator in terms of the Dirac spectrum. The quark propagator can be expressed as,

$$\mathrm{Tr}\,[G(x,x)] = \sum_j \frac{-m\psi_j^\dagger(x)\psi_j(x)}{\lambda_j^2+m^2}, \tag{4.23}$$

$$= \int d\lambda \frac{-m\rho_A(\lambda)}{\lambda^2+m^2}. \tag{4.24}$$

This means, the quark propagator is negative semi-definite for any gauge configurations.

The chiral condensate vanishes above the critical temperature at the quark mass vanishing limit, and is represented by the path integral,

$$\langle\bar{\psi}\psi\rangle = \frac{1}{Z}\int [\mathcal{D}A] e^{-S_{\mathrm{YM}}} \mathrm{Det}\,[\not{D}-m]\mathrm{Tr}\,[G(x,x)], \tag{4.25}$$

$$\sim -\mathcal{O}(m). \tag{4.26}$$

In the quark mass vanishing limit, this gives,

$$0 = \frac{1}{Z}\int [\mathcal{D}A] e^{-S_{\mathrm{YM}}} \mathrm{Det}\,[\not{D}-m]\mathrm{Tr}\,[G(x,x)]. \tag{4.27}$$

The integrant in (4.27) is negative semi-definite, then we can conclude,

$$e^{-S_{\mathrm{YM}}} \mathrm{Det}\,[\not{D}-m]\mathrm{tr}\,[G(x,x)] = 0, \tag{4.28}$$

for all configuration. This leads $\mathrm{tr}\,[G(x,x)] = 0$ and $e^{-S_{\mathrm{YM}}}\mathrm{Det}\,[\not{D}-m]\mathrm{Tr}\,[G(x,x)]\mathrm{Tr}\,[G(0,0)] = 0$. Therefore we obtain, $\Pi_\sigma(x) = \Pi_\delta(x)$. This means $\langle\sigma(x)\sigma(0)\rangle$ and $\langle\delta(x)\delta(0)\rangle$ are identical above the critical temperature at the quark mass vanishing limit.

Next we prove $\Pi_\eta = \Pi_\pi$. The difference between them is given by,

$$\Pi_\eta - \Pi_\pi = \frac{1}{Z}\int [\mathcal{D}A] e^{-S_{\mathrm{YM}}} \mathrm{Det}\,[\not{D}-m]\left[\mathrm{Tr}\,[G(x,x)\gamma_5]\mathrm{Tr}\,[G(0,0)\gamma_5]\right]. \tag{4.29}$$

In order to evaluate this integral, first we prove $|\mathrm{Tr}\,[G(x,x)\gamma_5]| \le |\mathrm{Tr}\,[G(x,x)]|$. This comes from $\psi_j^\dagger(1-\gamma_5)^2\psi_j \ge 0$[18]. Then we conclude $\Pi_\eta = \Pi_\pi$ at the quark mass vanihing limit.

[18]Evaluate $\psi_j^\dagger(1-\gamma_5)^2\psi_j$ in two different ways,

$$\psi_j^\dagger(1-\gamma_5)^2\psi_j = |(1-\gamma_5)\psi_j|^2 \ge 0, \tag{4.30}$$

$$\psi_j^\dagger(1-\gamma_5)^2\psi_j = 2\psi_j^\dagger\psi_j - 2\psi_j^\dagger\gamma_5\psi_j. \tag{4.31}$$

Expand $\psi_j^\dagger(1-\gamma_5)^2\psi_j$,

$$|\psi_j^\dagger\psi_j| \ge |\psi_j^\dagger\gamma_5\psi_j|. \tag{4.32}$$

We multiply $\frac{1}{|i\lambda_j - m|}$ both side, and sum over j, we obtain

$$\mathrm{Tr}\,[G(x,x)] \ge \mathrm{Tr}\,[G(x,x)\gamma_5] \tag{4.33}$$

Summing up all of results in this subsection, we conclude that all of mesons in the multiplet in U(2) ×U(2) are identical above the critical temperature at the quark mass vanishing limit.

See (4.24), if there is a gap in the spectrum (Fig. 5), all correlators in U(2) multiplet are identical. In other words, the appearing of the gap in the spectrum at the quark mass vanishing and thermodynamical limit is sufficient condition for $\mathrm{U}(1)_\mathrm{A}$ restoration.

4.3 Correlator and Dirac spectrum on the lattice

Aoki, Fukaya and Taniguchi improved in the treatment of UV structure of the Dirac spectrum which does not treat accurate in Cohen's argument. They used overlap fermion, which defined in following section, as a regularization description of the fermion. Thanks to the regularization, treatment of zero-modes is clear. They assume some plausible assumptions, they obtained stronger constraints on $\rho(\lambda)$,

$$\lim_{m\to 0}\lim_{V\to\infty}\langle\rho_A(\lambda)\rangle_m = \lim_{m\to 0}\lim_{V\to\infty}\left[\frac{N_f}{V}\langle N_{R+L}\rangle_m + c_0 + c_1\lambda + c_2\lambda^2 + c_3\lambda^3 + \mathcal{O}(\lambda^4)\right], \tag{4.34}$$

$$= c_3\lambda^3 + \mathcal{O}(\lambda^4). \tag{4.35}$$

This c_i is a real coefficient, which is constrained by the Ward-Takahashi identities for SU(2) chiral symmetry. N_{R+L} is a total number of zero-modes for given gauge field. Important point is, topological zero-modes vanish in the thermodynamic and the quark mass vanishing limit.

They also discuss possible effect on the $\mathrm{U}(1)_\mathrm{A}$ restoration/violation by lattice artifacts. The Lattice artifact is a discretization (regularization) effect, which vanishes at the continuum limit. We will mention in next section, lattice regularization of fermion is essentially not unique. Here we focus on the explicit SU(2) chiral symmetry violating lattice artifact, which is called m_{break} by them. The m_{break} vanishes in the continuum limit, it is natural to estimate $m_{\mathrm{break}} \sim \Lambda_{\mathrm{QCD}}a^2$. Here a is a lattice spacing and Λ_{QCD} is the dynamical scale of QCD. At finite temperature, we have another scale temperature T. However the lattice artifact is mild at weak coupling regime, which corresponds to high temperature, it is unlikely to include T to m_{break}. Here, we assume, T_c is not essentially different from Λ_{QCD}. They derive following relation,

$$\langle\rho_A(\lambda)\rangle_m = c_1' m_{\mathrm{break}}\Lambda_{\mathrm{QCD}}\lambda + c_2' m_{\mathrm{break}}\lambda^2 + \left(c_3 + c_3'\frac{m_{\mathrm{break}}}{\Lambda_{\mathrm{QCD}}}\right)\frac{\lambda^3}{3!} + \cdots, \tag{4.36}$$

where c_i' is unknown dimensionless order one constant. Oppose to previous case, $\mathrm{U}(1)_\mathrm{A}$ breaking effect as $\langle N_{R+L}\rangle/V$, is order m_{break}. In this case, there is no reason to restore the $\mathrm{U}(1)_\mathrm{A}$ symmetry even in the quark mass vanishing limit.

Let us summarize this section. We have discussed SU(2) and $\mathrm{U}(1)_\mathrm{A}$ symmetry from the view point of the spectral density $\rho(\lambda)$. Cohen argued, if SU(2) is restored, $\rho(\lambda)$ may have a gap. In such case, a signal of $\mathrm{U}(1)_\mathrm{A}$ violation is disappeared from meson correlators. In order to check his argument, we will introduce lattice QCD in next section.

5 Chiral symmetry on a lattice

In earlier section, we have analyzed SU(2) chiral symmetry and $\mathrm{U}(1)_\mathrm{A}$ symmetry on meson correlators. Cohen pointed out, when SU(2) chiral symmetry is restored, $\mathrm{U}(1)_\mathrm{A}$ symmetry

may be restored. The chiral symmetry, which includes $\mathrm{U}(1)_{\mathrm{A}}$, is essentially important in the analysis.

Since QCD is strongly coupled at low energy regime, non-perturbative approach is needed. Most rigorous way is lattice gauge theory [14]. Lattice gauge theory is gauge theory defined on discrete space-time. As a result of the discretization, degrees of freedom of fields reduct to countable infinity, moreover system put in the finite box, degrees of freedom of fields reduct to finite. By definition, lattice gauge theory is a regularized theory, there are no ultraviolet divergence *i.e.* no ambiguity. This enables us to evaluate the path integral by computers [15]. A gauge field on the discretized space-time is described by infinitesimally small Wilson loop called plaquette. Thank to the gauge invariance of the Wilson loop, the gauge invariance of the gauge action is preserved even the space-time is discretized. Note that, If the theory is asymptotically free, we can take continuum limit.

On the other hand, discretization (regularization) of fermion is not unique. If we discretize the covariant derivative for 1 flavor in a naive way, we will encounter unwanted extra 15 flavors called doublers. Actually, there is a no-go theorem. As we will see in following section, that theorem claims, if the action has chiral symmetries, doublers must emerge.

Ginsparg and Wilson gave a breakthrough of the problem. They re-defined chiral symmetry on the lattice. They allow small violation of the symmetry relation which preserve "chiral symmetry" relation under the block spin transformation. The modified relation is called the Ginsparg-Wilson relation. Thanks to the relation, chiral fermion can be defined on the lattice, which approach to the chiral fermion in the continuum theory along the continuum limit.

In following subsections, we review how do we define fermions on the discretized space-time with chiral symmetries.

5.1 Chiral symmetry and lattice fermions

In this subsection, we briefly review the chiral symmetry and the lattice formulation of fermions. Let us recall chiral symmetry in the continuum theory (3.9),

$$\gamma_5 \not{D} + \not{D}\gamma_5 = 0.$$

As we see below, if we maintain this chiral symmetry and discretize the covariant derivative and then, extra 15 flavors called *doublers* is automatically generated. This fact called Nielsen-Ninomya theorem. Precisely speaking, doublers cannot be avoid *if* the Dirac operator satisfy,

1. translational invariance on the lattice,
2. chiral symmetry (3.9),
3. hermiticity,
4. bilinear form,
5. locality

In order to perform 1-15 flavors simulation, we must give up at least one of them. For example, Wilson fermion and staggered gives up 2, Domain-wall fermion with Pauli-Villers regulator and overlap fermion gives up 2 and 5. However overlap fermion has another exact "chiral symmetry" as follows. In next subsection we briefly review generation of doubler modes, in order to motivate to introduce the overlap-Dirac operator.

5.1.1 Naive discretization of the Dirac operator

In order to see doublers generation, first, consider massless free Dirac action for one flavor fermion in the Euclidean continuum space-time,

$$S = \int d^4x \bar{\psi}(x) \not{\partial} \psi(x). \tag{5.1}$$

Next, discretize the covariant derivatve naïve way *i.e.* partial derivative replace to difference with lattice spacing a,

$$\frac{\partial}{\partial x^\mu}\psi(x) \to \frac{\psi(x + a\hat{\mu}) - \psi(x - a\hat{\mu})}{2a}, \tag{5.2}$$

where $\hat{\mu}$ is a unit vector along with μ direction. Using lattice spacing a, fermion field ψ to dimensionless field $\psi'_n = a^{3/2}\psi(na)$, where $na = x$, $(n \in \boldsymbol{Z})$,

$$S^{\text{lat}} = \frac{1}{2}\sum_{n,\mu} \bar{\psi}'_n \gamma_\mu [\psi'_{n+\mu} - \psi'_{n-\mu}]. \tag{5.3}$$

After here, we use dimensionless notation and does not denote prime as ψ_n. Summation of μ is over 1 to 4 in this case. This is called naïve lattice fermion. In order to see emergence of doublers, we move to momentum space[19]. Institute $\psi_n = \int_D \frac{d^4p}{(2\pi)^4} e^{ipn}\psi(p)$, $D = \{p_\mu | -\pi/a < p_\mu \leq \pi/a, 1 \leq \mu \leq 4\}$, and we obtain the action in the momentum space,

$$S^{\text{lat}} = \int_D \frac{d^4p}{(2\pi)^4} \bar{\psi}(-p)[i\gamma_\mu \sin p_\mu]\psi(p). \tag{5.4}$$

Propagator is inverse of the Dirac operator in the momentum space,

$$G_F(p) = \frac{1}{i\gamma_\mu \sin p_\mu}, \tag{5.5}$$

and pole of the propagator represents physical particle. In the continuum theory, we have pole at $(0,0,0,0)$ only. However, now we have other poles located at $(\frac{\pi}{a},0,0,0)$, $(\frac{\pi}{a},\frac{\pi}{a},0,0)$ and so on. These are doublers, which contribute to physics same way.

In order to introduce gauge interaction, only have to do is introducing link variable as,

$$S^{\text{lat}} = \frac{1}{2}\sum_{n,\mu} \left[\bar{\psi}_n \gamma_\mu U_{n,\mu} \psi_{n+\hat{\mu}} - \bar{\psi}_{n+\hat{\mu}} \gamma_\mu U^\dagger_{n,\mu} \psi_n\right], \tag{5.6}$$

where $U_{n,\mu}$ is a link variable which is a function value on $SU(3)$ group[20]. At weak coupling limit, $U_{n,\mu}$ is given by $U_{n,\mu} = \exp[iaA_\mu(x)]$. When we quantize the system, the path integral is taken over link variables instead of A_μ. Note that, gauge fixing term is not necessary because gauge fields take a value on compact group manifold on the contrary to A_μ.

In summary, naïvely discretized fermion action preserve chiral symmetry as in continuum theory, however doublers contribute to low energy physics as same as pole at $(0,0,0,0)$. Note that, if take into account gauge interaction, doublers cannot be removed. In following subsections we give a prescription of this issue.

[19]Here we consider non-compact *i.e.* infinitely large, space-time for simplicity.

[20]Precisely speaking, $U_{n,\mu}$ is a unitary representation of the gauge group.

5.1.2 Wilson fermion

The Wilson fermion includes second derivative term in order to eliminate doublers from physical space[21],

$$\begin{aligned} S_{\mathrm{W}} &= \frac{1}{2}\sum_{n,\mu}\left[\bar{\psi}_n\gamma_\mu U_{n,\mu}\psi_{n+\hat{\mu}} - \bar{\psi}_{n+\hat{\mu}}\gamma_\mu U^\dagger_{n,\mu}\psi_n\right] + M\sum_n \bar{\psi}_n\psi_n \\ &\quad - \frac{r}{2}\sum_{n,\mu}\left[\bar{\psi}_n U_{n,\mu}\psi_{n+\hat{\mu}} + \bar{\psi}_{n+\hat{\mu}}U^\dagger_{n,\mu}\psi_n - 2\bar{\psi}_n\psi_n\right], \qquad (5.7) \\ &\equiv \bar{\psi}D_W(M)\psi, \qquad (5.8) \end{aligned}$$

where M is a dimensionless quark mass ma. After here, the Wilson parameter r taken to be 1. The last term in (5.7) is called the Wilson term, which is introduced in order to remove the doublers from physical space. However, the Wilson term breaks all chiral symmetries, which includes $\mathrm{U}(1)_{\mathrm{A}}$, simultaneously.

Here we mention to γ_5 hermiticity of the Wilson-Dirac operator. the Wilson-Dirac operator satisfy $\gamma_5 D_W \gamma_5 = D_W^\dagger$, this is called γ_5 hermiticity. In Appendix F, we use this property.

5.1.3 Overlap fermion

The overlap-Dirac operator is one of the chiral fermion on a lattice, which is given by,

$$D_{\mathrm{ov}}(m) = \frac{1+m}{2} + \frac{1-m}{2}\gamma_5 \mathrm{sgn}(H_M), \quad H_M = \gamma_5 \frac{bD_W(-M)}{2+cD_W(-M)}, \qquad (5.9)$$

where $D_W(-M)$ is the Wilson-Dirac operator with negative mass $-M < 0$ which around cut-off scale ($= 1/a$). Conventional overlap fermion case, H_M is taken to be H_W ($b = 2$, $c = 0$). $\mathrm{sgn}(x)$ is a sign function $\mathrm{sgn}(x) \equiv \frac{x}{\sqrt{x^2}}$. Normalization of the overlap-Dirac operator is discussed in Appendix F.5.

The overlap fermion describe chiral fermion[22], and since doublers are decoupled from infra-red (IR) physics. Thus we can regard this fermion as one flavor Dirac fermion. The overlap-Dirac operator at quark mass vanishing limit satisfies,

$$\gamma_5 D + D\gamma_5 = aDR\gamma_5 D, \qquad (5.10)$$

where R is an arbitral operator commute with γ_5, instead of usual chiral symmetry relation (3.9). Here a is appeared in order to emphasize the dimension, after here it will be dropped. This is the Ginsparg-Wilson relation [29].

If multiply D^{-1} from both left and right, one can immediately understand that the violation of chiral symmetry is local in terms of the propagator. M. Lüsher pointed out, the Dirac operator which satisfy the Ginsparg-Wilson relation has an exact chiral symmetry on the lattice[23],

$$\psi(x) \to \psi'(x) = \exp[i\theta\gamma_5(1-RD)]\psi(x), \quad \bar{\psi} \to \bar{\psi}'(x) = \bar{\psi}(x)e^{i\theta\gamma_5}, \qquad (5.11)$$

[21]Here D means the Dirac operator on the lattice and $\not{D}$ is one on the continuum space-time.

[22]Appendix F.1.3

[23]This relation is satisfied not only for the overlap fermion. If other Dirac operator which satisfy the Ginsparg-Wilson relation, its also has such exact chiral symmetry.

This can be checked directly as follows. We start from the massless overlap-Dirac action,

$$S = \bar{\psi} D \psi, \tag{5.12}$$

here integral (summation) of the space-time is suppressed. Infinitesimal chiral rotation is given by,

$$\delta\psi = \gamma_5[1 - RD]\psi, \quad \delta\bar{\psi} = \bar{\psi}\gamma_5. \tag{5.13}$$

Substitute the transformation, the variation of the action is,

$$\delta S = (\delta\bar{\psi})D\psi + \bar{\psi}D(\delta\psi) = \bar{\psi}\gamma_5 D\psi + \bar{\psi}D\gamma_5[1 - RD]\psi, \tag{5.14}$$

$$= \bar{\psi}[\gamma_5 D + D\gamma_5 - D\gamma_5 RD]\psi = 0. \tag{5.15}$$

In this sense, we can treat the overlap fermion as a chiral fermion. As we will see following section, $\mathrm{U}(1)_\mathrm{A}$ anomaly arises from the Jacobian of the path integral measure as same as in the continuum theory[24].

The overlap-Dirac operator (5.9) has the exact chiral symmetry on the lattice, which prohibits additive mass renormalization. However, numerical simulations are difficult for practical reasons. All causes is the sign function and there are two difficulties. First is the approximation of the sign function. We have to pay best effort for approximation of the sign function to preserve the Ginsparg-Wilson relation within numerical precision. Second is a difficulty of molecular dynamics. In practical lattice QCD calculation, we need to calculate a derivative of the action in molecular dynamics step. If H_M has zero-modes, we have to take a derivative of the sign function around zero. Thus, we cannot perform simulation practically[25]. This happens when the topology of gauge configuration is changed.

5.1.4 Domain-wall type fermion

As we mentioned above, the treatment of the sign function in the overlap-Dirac operator is difficult in practice. To avoid such a difficulty, one can introduce approximation for the sign function[26]. Such approximated Dirac operator is exactly same as 4 dimensional effective operator of generalized domain-wall fermion action,

$$D_{\mathrm{DW}}^{4D}(m) = \frac{1+m}{2} + \frac{1-m}{2}\gamma_5 \mathrm{sgn}_{\mathrm{rat}}(H_M), \quad \mathrm{sgn}_{\mathrm{rat}}(H_M) = \frac{1 - \prod_s^{Ls} T_s(H_M)}{1 + \prod_s^{Ls} T_s(H_M)}, \tag{5.16}$$

$$T_s(H_M) = \frac{1 - \omega_s H_M}{1 + \omega_s H_M}, \quad H_M = \gamma_5 \frac{bD_W}{2 + cD_W}. \tag{5.17}$$

Note that, domain-wall type fermion approaches to the overlap fermion when $L_s \to \infty$. In this limit, domain-wall type fermion satisfy Ginsparg-Wilson relation exactly. Figure. 6 shows the "sign function" behavior of several approximations. Black, blue and red line corresponds to exact sign function, hyperbolic tangent approximation with Möbius kernel and hyperbolic tangent approximation with conventional Shamir kernel, respectively. As we mention in following section, these sign function is used in previous JLQCD study, this work and BNL/LLNL study, respectively.

[24] See Appendix F.3.

[25] Precisely speaking, if we have enough precision to tame this singular behavior, we can perform simulation. However, numerical cost is too expensive to perform realistic simulation.

[26] Historical order is different. See [16] or other modern text book of lattice gauge theory.

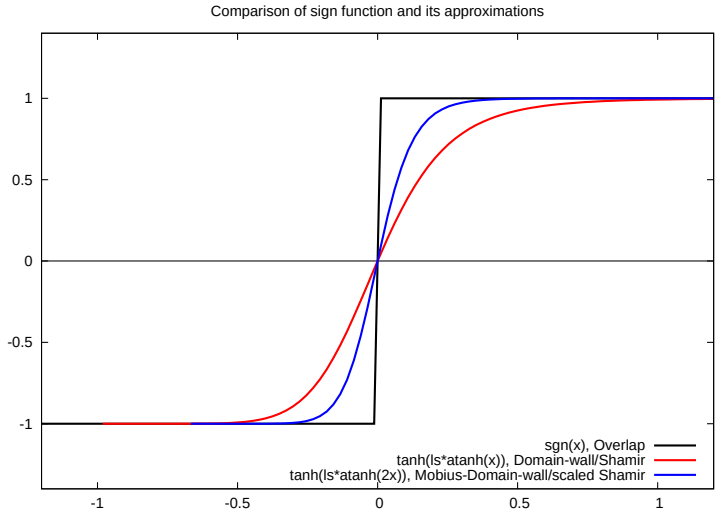

Figure 6: Several approximation of the sign function.

5.2 Summary of previous works

In this subsection, we review known 4 results which is obtained using "chiral fermion" on the lattice. First is obtained using staggered fermion[27] which preserve partial chiral symmetry. Other results are obtained using overlap/domain-wall type fermions. As we have mentioned before, domain-wall type fermions are approximation of the overlap fermion. However results are different from each other. Of course, at after taking quark mass vanishing, thermodynamic and continuum limit, all lattice fermion should give same result. In order to clarify and understand these difference, We are starting from briefly review of previous studies.

Ohno's group studied $\mathrm{U}(1)_\mathrm{A}$ symmetry with the improved staggered fermion called HISQ (Highly Improved Staggered Quark) [21][22]. They observed a peak in the spectrum $\rho(\lambda)$ around $\lambda \sim 0$ at two volume at $T \sim 300$ MeV. In their setup, the QCD critical temperature is around $T \sim 150$ MeV. They concluded $\mathrm{U}(1)_\mathrm{A}$ symmetry might not be restored above the critical temperate.

Hot QCD and LLNL/BNL studied $\mathrm{U}(1)_\mathrm{A}$ symmetry with conventional domain-wall fermion in 5-dimensional description [19][20]. They observed a peak in the spectrum $\rho(\lambda)$ around $\lambda \sim 0$ at two volume at $T \sim T_c \sim 170$ MeV. They also investigated degeneracy between several correlators. They observed degeneration of only for SU(2) multiplet, not for $\mathrm{U}(1)_\mathrm{A}$ at the critical temperature. So they concluded $\mathrm{U}(1)_\mathrm{A}$ symmetry might not be restored just above the critical temperate. Conventional domain-wall fermion which they used can be understood in terms of 4-dimensional effective operator of Möbius domain-wall operator. Their Dirac operator corresponds to $b = 2$, $c = 0$, and $\omega_s = 1$ for (5.16) (5.17). This choice of ω_s corresponds to hyperbolic tangent approximation of the sign function.

TWQCD studied $\mathrm{U}(1)_\mathrm{A}$ symmetry with the optimal domain-wall fermion in 4-dimensional description [18]. They did not observe clear gap in the spectrum $\rho(\lambda)$ around $\lambda \sim 0$ at $T \sim 180$ MeV. However results are constant with the constraint of the result of Aoki *et al.* [13]. They also investigated several correlators. They observed degeneration of both of SU(2) multiplet and $\mathrm{U}(1)_\mathrm{A}$. They concluded that $\mathrm{U}(1)_\mathrm{A}$ symmetry were likely to be

[27] See Appendix F.1.1.

restored at nearby the critical temperature. Their optimized domain-wall can be understood in terms of 4-dimensional effective operator of Möbius domain-wall operator, $b = 2$, $c = 0$ (*i.e.*, $H = H_W$), and ω_s taken $\mathrm{sgn}_{\mathrm{rat}}(x)$ to be Chebyshev-Zolotarev approximation of the exact sign function.

JLQCD studied $\mathrm{U}(1)_{\mathrm{A}}$ symmetry with overlap fermion (5.9) with topology fixing term to avoid difficulty of HMC [17]. They observed a gap in the spectrum $\rho(\lambda)$ around $\lambda \sim 0$ at $T \sim 180$ MeV. They also investigated several correlators and they observed degeneracy for all correlators. They concluded that $\mathrm{U}(1)_{\mathrm{A}}$ symmetry were restored above the critical temperate.

Table 1 is a summary of previous works.

Group	Fermion	Spacial size (fm)	Existence of gap	Correlator	$\mathrm{U}(1)_{\mathrm{A}}$
JLQCD	OV (Q_{fix})	2	Yes	Degenerated	Restored
TWQCD	ODW	3	No ($\rho \sim \lambda^3 + \cdots$)	Degenerated	Restored?
Hot QCD	DW	2, 4	No ($\rho \sim \delta$)	No degeneracy	Violated
Ohno *et.al.*	HISQ	4, 5	No	-	Violated

Table 1: OV, ODW, DW, HISQ, means overlap, optimized domain-wall, domain-wall, highly-improved-staggered-quark, respectively. Q_{fix} means simulation with topology-fixing term. Hot QCD represent Hot QCD and BNL/LLNL collaboration. Here "Correlator" means degeneracy of a set of correlators in $\mathrm{U}(1)_{\mathrm{A}}$ multiplet just above the critical temperature.

6 Lattice analysis

In previous section, we have reviewed previous works. It is obvious that, ideal simulation is, simulation with the overlap fermion without topology fixing in large volume. However as we have mentioned above, the overlap fermion is not good at for the Monte Carlo simulation. On the other hand, the domain-wall fermion is good for the calculation but it does not have exact chiral symmetry. We somehow attempt to perform ideal simulation. Firstly, we generate gauge configuration using domain-wall-type fermion, and next, we use the reweighting technique in order to change the fermion determinant from the domain-wall type fermion to the overlap fermion.

If we use reweighting technique, it needs, the original action is enough to similar to the action which we want to substitute. In our case, domain-wall type fermion must have enough accurate chiral symmetry. In order to realize such a situation, we employ improved domain-wall fermion called the Möbius domain-wall fermion. Since the Möbius domain-wall fermion has accurate chiral symmetry, reweighting should be work. However, the result is not for large volume simulation, thus we introduce an approximated reweighting factor for large volume simulation.

6.1 Simulation with dynamical Möbius domain-wall quarks

In this subsection we introduce our numerical setup. In the previous study of JLQCD, they employed the overlap-Dirac operator to realize exact chiral symmetry, however, there were

some difficulties of the sign function in the overlap-Dirac operator, as we have mentioned in earlier subsection. To overcome these problems, we introduce rational approximation for the sign function *i.e.* we employ the Möbius domain-wall fermion action [24, 25] for the quarks[28]. Its determinant is equivalent (except for overall constants) to that of a 4-dimensional effective Dirac operator:

$$D_{\rm DW}^{4D}(m) = \frac{1+m}{2} + \frac{1-m}{2}\gamma_5 {\rm sgn}_{\rm rat}(H_M), \quad {\rm sgn}_{\rm rat}(H_M) = \frac{1-(T(H_M))^{L_s}}{1+(T(H_M))^{L_s}}, \tag{6.1}$$

$$T(H_M) = \frac{1-H_M}{1+H_M}, \quad H_M = \gamma_5 \frac{2D_W}{2+D_W}, \tag{6.2}$$

We introduce three steps of the stout smearing for the gauge links. In order to evaluate explicit chiral symmetry breaking which comes from the approximation of the sign function, we introduce the residual mass, calculated as

$$m_{\rm res} = \frac{\langle {\rm tr}\, G^\dagger \Delta_L G\rangle}{\langle {\rm tr}\, G^\dagger G\rangle}, \ \ \Delta_L = \frac{1}{2}\gamma_5(\gamma_5 D_{\rm DW}^{4D} + D_{\rm DW}^{4D}\gamma_5 - 2a D_{\rm DW}^{4D}\gamma_5 D_{\rm DW}^{4D}), \tag{6.3}$$

where G is the contact-term-subtracted quark propagator. The residual mass is roughly 5-10 times smaller than that of the conventional domain-wall Dirac operator for a fixed L_s, the size of fifth direction.

The overlap Dirac operator is obtained by choosing a better approximation for the sign function in (6.1), while keeping the same kernel operator $H_M = \gamma_5\big(2D_W/(1+D_W)\big)$. On the generated configurations, we compute the lowest eigenmodes of the kernel operator $2H_T$, and exactly treat the sign function for them. Namely, we use

$$D_{\rm ov}(0) = \frac{1}{2}\sum_{\lambda_i<|\lambda_{\rm th}|}(1+\gamma_5 {\rm sgn}\lambda_i)|\lambda_i\rangle\langle\lambda_i| + D_{\rm DW}^{\rm 4D}(0)(1-\sum_{\lambda_i<|\lambda_{\rm th}|}|\lambda_i\rangle\langle\lambda_i|), \tag{6.4}$$

where λ_i is the i-th eigenvalue of H_M and $\lambda_{\rm th}$ is a certain threshold, gives a good numerical definition for the overlap Dirac operator. This is because the difference between sign function in the overlap-Dirac operator and the approximated sign function in Möbius domain-wall fermion is near-zero point for the argument. With our choice $\lambda_{\rm th} = 0.35$ (for $L = 16$) and 0.24 (for $L = 32$) the residual mass is negligible, *i.e.* $< 4 \times 10^{-3}$ MeV.

6.2 Reweightng and low-mode reweighting

In this work, one of out aims is to understand the difference between the domain-wall type fermions and the overlap fermions. For this purpose, we perform the reweighting of the dynamical Möbius domain-wall ensembles to those with the overlap Dirac operator determinant. Derivation of conventional reweighting technique is following. We start from thermal

[28] A derivation is in Appendix F.4.

and quantum average of operator $\mathcal{O}$ with overlap-Dirac action,

$$\langle \mathcal{O} \rangle_{\rm ov} = \int \mathcal{D}\bar{\psi}\mathcal{D}\psi\mathcal{D}A_\mu \; \mathcal{O} \; e^{-S_{\rm gauge}} e^{-\bar{\psi}[D_{\rm OV}(m)]\psi}, \tag{6.5}$$

$$= \int \mathcal{D}A_\mu \; \mathcal{O} \; e^{-S_{\rm gauge}} {\rm Det}[D^2_{\rm OV}(m)], \tag{6.6}$$

$$= \int \mathcal{D}A_\mu \; \mathcal{O} \; e^{-S_{\rm gauge}} {\rm Det}[D^2_{\rm OV}(m)] \frac{{\rm Det}[D^2_{\rm DW}(m)]}{{\rm Det}[D^2_{\rm DW}(m)]}, \tag{6.7}$$

$$= \int \mathcal{D}\bar{\psi}\mathcal{D}\psi\mathcal{D}A_\mu \; \mathcal{O}R(A) \; e^{-S_{\rm gauge}} e^{-\bar{\psi}[D_{\rm DW}(m)]\psi}, \tag{6.8}$$

$$= \langle \mathcal{O}R(A) \rangle_{\rm DW}, \tag{6.9}$$

In the first line is the definition of expectation value with overlap-Dirac kernel. In the second line, we perform fermion path integral. In the third line, we insert functional determinant of domain-wall Dirac operator. In the fourth line, we define reweighting factor, which depends on the gauge configuration,

$$R(A) = \frac{{\rm Det}[D^2_{\rm ov}(m)]}{{\rm Det}[D^2_{\rm DW}(m)]}, \tag{6.10}$$

where the ratio of the determinants are stochastically estimated usually. In the last line, we use definition of the expectation value. However this definition of naive overlap/domain-wall reweighting factor does not converge efficiently. Instead of this, we employ,

$$R(A) = \frac{{\rm Det}\, D^2_{\rm ov}(m)}{{\rm Det}\, D^2_{\rm DW}(m)} \frac{{\rm Det}\, D^2_{\rm DW}(1/2a)}{{\rm Det}\, D^2_{\rm ov}(1/2a)}. \quad (\text{for } L = 16^3 \times 8) \tag{6.11}$$

for $L = 16^3 \times 8$ lattice, where the ratio of the determinants are stochastically estimated using $\mathcal{O}(10)$ noise samples for each configuration. Note that we have added an additional determinant of the quarks (and ghosts) with a cut-off scale mass $(1/2a)$, which are irrelevant for the low-energy physics but effective in reducing statistical fluctuation originating from the UV modes [27].

Even for stochastic reweighting factor with UV-suppression factor cannot be obtained for $L = 32^3 \times 8$. In order to calculate reweighting factor, we employ low-mode approximation, *i.e.* we approximate reweighting factor by multiplication of low-lying eigenvalues of Dirac operator as,

$$R(A) \sim \frac{\prod_i^{N_{th}} [(\lambda_{{\rm ov}_m}{}^i)^2]}{\prod_i^{N_{th}} [(\lambda_{{\rm DW}_m}{}^i)^2]} = R_{\rm low}(A), \quad (\text{for } L = 16^3 \times 8,\, 32^3 \times 8) \tag{6.12}$$

where $\lambda^i_{{\rm ov/DW}_m}$ is a eigenvalue for massive hermitian overlap/domain-wall Dirac operator. $N_{\rm th}$ is order 10 truncation level for the approximation. This is not a precise approximation of the determinant, but as we will discuss later, still gives information of the possible gap in the Dirac spectrum.

6.3 Ensambles

Our simulation set-up is summarized in Table 2. For the gauge action, we employ the tree-level-improved Symanzik gauge action with $\beta = 4.07$ and 4.10. The lattice spacing a

is estimated from the measurement of the Wilson flow at zero-temperature as 0.135 fm and 0.125 fm, respectively. For each value of β, we simulate on two volumes $L^3 \times L_t = 16^3 \times 8$ and $32^3 \times 8$, at the quark mass $am_{\rm ud} = 0.001$ (3.0 or 3.2 MeV). The size of the 5-th dimension L_s is chosen such that the residual mass is kept around 1 MeV. From the Polyakov loop and the chiral condensate, the simulated temperatures 180 MeV ($\beta = 4.07$) and 200 MeV ($\beta = 4.10$) are estimated to be slightly above T_c. For each ensemble, we sample 50-200 gauge configurations from 100-700 trajectories of the hybrid Monte Carlo updates.

$L^3 \times L_t$	β	$m_{\rm ud}$(MeV)	L_s	$m_{\rm res}$(MeV)	Temp.(MeV)
$16^3 \times 8$	4.07	30	12	2.5	180
$16^3 \times 8$	4.07	15^*	12	2.4	180
$16^3 \times 8$	4.07	3.0	24	1.4	180
$16^3 \times 8$	4.10	32	12	1.2	200
$16^3 \times 8$	4.10	16^*	12	1.2	200
$16^3 \times 8$	4.10	3.2	24	0.8	200
$32^3 \times 8$	4.07	3.0	24	1.3	180
$32^3 \times 8$	4.10	32	12	1.7	200
$32^3 \times 8$	4.10	16	24	1.7	200
$32^3 \times 8$	4.10	3.2	24	0.7	200

Table 2: Our lattice set-up. Those with $m^*_{\rm ud}$ are obtained by the stochastic reweighting of the Dirac operator determinant from the ensemble with the higher quark mass.

7 Results

In this section, we report our simulation results. We measure the Dirac spectrum $\rho(\lambda)$ for the overlap and the Möbius domain-wall fermion in 2 different volume at 2 different temperature. Physical system size corresponds to 2 and 4 fm, and temperature is 180 and 200 MeV.

Thermalization of the configuration and the history of reweighting factor are summarized in Appendix G.

7.1 Domain-wall and Overlap spectrum

First, we examine the effect of the residual violation of chiral symmetry by comparing the spectrum of low-lying eigenvalues of $\gamma_5 D_{DW}(m)$ and that of the reweighted $\gamma_5 D_{ov}(m)$ measured on the same configurations[29]. Using the ensembles on two different lattice volumes, we can check the volume scaling at the same time. Since the configurations are generated with the Möbius domain-wall quark action, the topology tunneling is active.

Figure 7 shows the eigenvalue spectrum $\rho(\lambda)$ calculated on the $T = 180$ MeV lattices.

[29]We measured eigenvalue of $\gamma_5 D$ instead of D itself. This is because, if D has γ_5 hermiticity, $\gamma_5 D$ is hermitian operator. Thus eigenvalue of $\gamma_5 D$ is real number. Note that, both of eigenvalue can be mapped each other.

Here, the i–th eigenvalue of massless Dirac operator λ_i is obtained by,

$$\lambda_i a \equiv \frac{\sqrt{a^2(\lambda_i^m)^2 - a^2 m_{\rm ud}^2}}{\sqrt{1 - a^2 m_{\rm ud}^2}}, \tag{7.1}$$

where λ_i^m is the i–th eigenvalue of massive hermitian Dirac operator $\gamma_5 D_{\rm DW}^{4D}(m)$ or $\gamma_5 D_{\rm ov}(m)$. When the quark mass is heavy, $m_{\rm ud} \sim 30$ MeV, our data show apparent difference between the Möbius domain-wall and overlap-Dirac eigenvalues near $\lambda \sim 0$ (Fig. 7, Yellow bars). The left panel shows the spectrum for $\gamma_5 D_{\rm DW}^{4D}(0)$, while the right panel is those of (reweighted) $\gamma_5 D_{\rm ov}(0)$. The overlap-Dirac spectrum (right panel) has a peak around $\lambda \sim 0$, while the Möbius Domain-wall does not. The peak in the overlap spectrum originates from chiral zero-modes, which are determined unambiguously thanks to the nearly exact chiral symmetry of the overlap Dirac operator. Above the peak region, *i.e.* $\lambda a \sim 0.02$, the spectral density for the overlap becomes lower than that of Möbius domain-wall.

On the other hand, for the smaller $m_{\rm ud}$ (~ 3 MeV) we do not find the peak after the reweighting, and the near-zero modes around $\lambda a \sim 0.01$ are washed out as shown in right panel of Figure 7, where we present the data for $L \sim 2$ fm (top) and $L \sim 4$ fm (bottom). For the reweighted overlap, a gap ~ 20 MeV is found on both volumes, while the Möbius domain-wall spectrum shows eigenmodes below $|a\lambda| \approx 0.01$. On the large volume, in particular, there is an eigenvalue in the lowest bin. This suggests that importance of the chiral symmetry of the fermion determinant. The data at $T \sim 200$ MeV are qualitatively similar (Figure 8).

The reweighted overlap Dirac spectrum shows a gap, which is apparently insensitive to the volume. Then, we may conclude that the difference from the Möbius domain-wall fermion is mainly due to the violation of the chiral symmetry, that we investigate detail below.

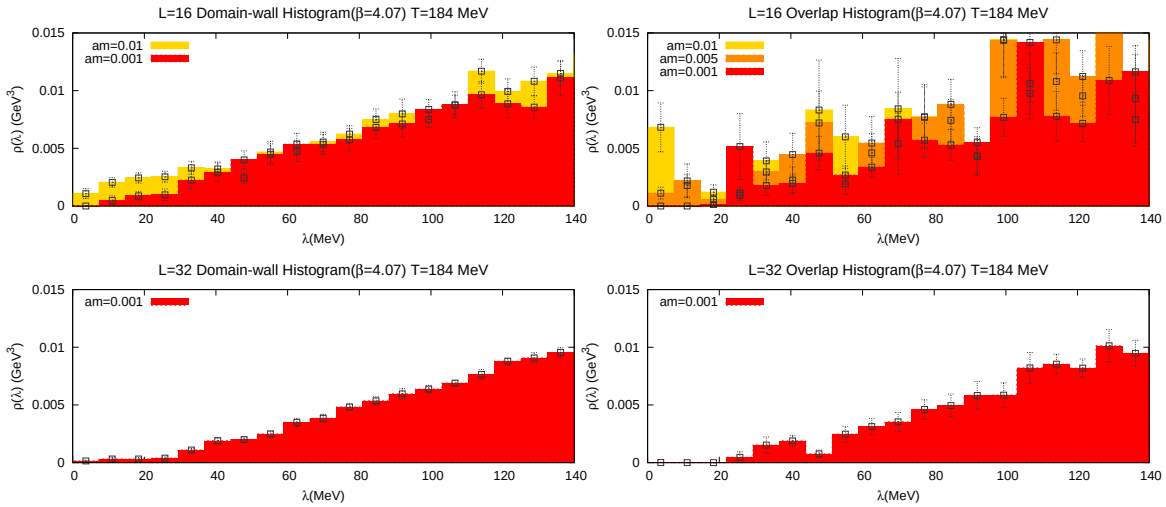

Figure 7: The eigenvalue histograms of the domain wall (left panels) and reweighted overlap (right) Dirac operators. The data for $T \sim 180$ MeV on $L^3 = 16^3$ (top panels) and $L^3 = 32^3$ (bottom) lattices are presented.

7.2 Ginsparg-Wilson relation violation

We measure the violation of the Ginsparg-Wilson relation on each eigenmode of the Hermitian Dirac operator $\gamma_5 D$ through

$$g_i \equiv \frac{\psi_i^\dagger \gamma_5 [D\gamma_5 + \gamma_5 D - 2aD\gamma_5 D]\psi_i}{\lambda_i^m} \left[\frac{(1 - am_{\rm ud})^2}{2(1 + am_{\rm ud})}\right], \tag{7.2}$$

where λ_i^m, ψ_i denotes the i–th eigenvalue/eigenvector of massive hermitian Dirac operator respectively. D is the domain-wall or overlap Dirac operator. Last factor in (7.2) comes from the normalization of the Dirac operator. Note that one can obtain the residual mass by an weighted average of g_i,

$$m_{\rm res} = \frac{\langle {\rm tr}\, G^\dagger \Delta_L G\rangle}{\langle {\rm tr}\, G^\dagger G\rangle} = \sum_i \frac{\lambda_i^m (1 + am_{\rm ud})}{(1 - am_{\rm ud})^2 (a\lambda_i^m)^2} g_i \Big/ \sum_i \frac{1}{(a\lambda_i^m)^2}. \tag{7.3}$$

where the sum runs over all eigenvalues.

Figure 9 shows $|g_i|$ for each eigenvalue on the configuration of $16^3 \times 8$ and $m_{\rm ud} \sim 3$ MeV. For the Möbius domain-wall fermion (crosses), the low-lying modes violate the chiral symmetry to the order of one, which means that the expectation value of $D\gamma_5 + \gamma_5 D - 2aD\gamma_5 D$ is of the same order of λ. The violation is of course negligible for the overlap fermion (stars). This result indicates that the low modes of the Möbius domain-wall Dirac operator contain substantial lattice artifact. Such lattice artifacts may also distort the eigenvalues, and explain the difference from the overlap operator.

7.3 Low mode reweighting

As mentioned above, the conventional stochastic reweighting does not work on the larger lattice. Instead, we introduce an approximation of using only the low-lying eigenvalues. This corresponds to a certain modification of the fermion action in the ultraviolet regime.

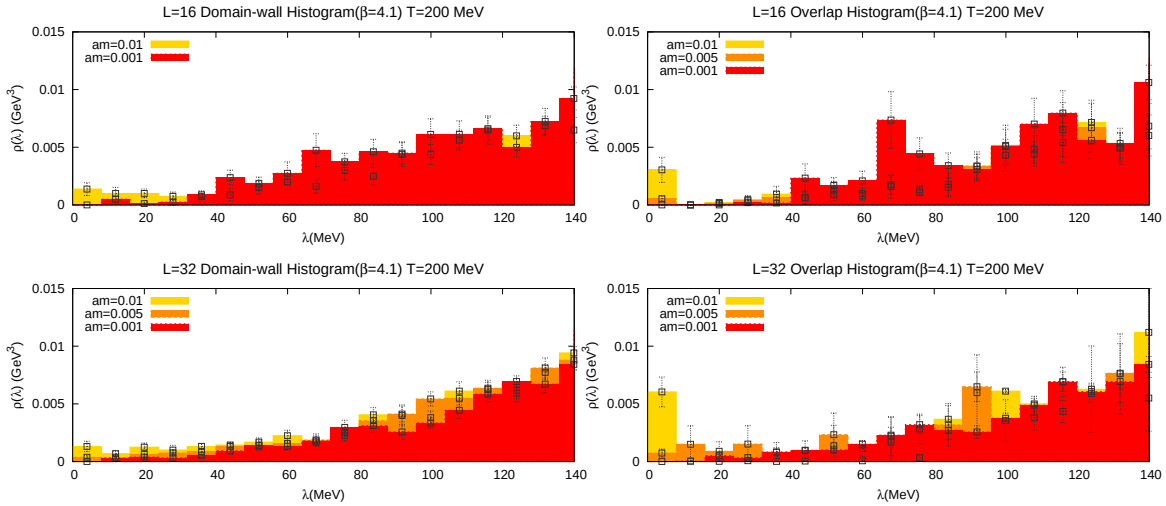

Figure 8: The eigenvalue histograms of the domain wall (left panels) and reweighted overlap (right) Dirac operators. The data for $T \sim 200$ MeV on $L^3 = 16^3$ (top panels) and $L^3 = 32^3$ (bottom) lattices are presented.

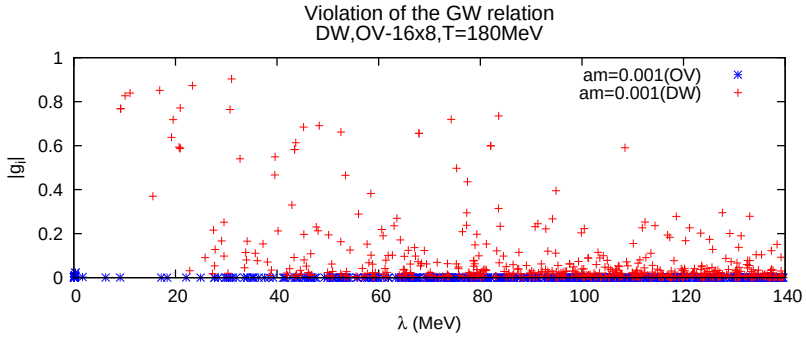

Figure 9: Violation of the Ginsparg-Wilson relation g_i for individual eigenmode. Pluses represent the Möbius domain-wall eigenvectors, while stars show the overlap eigenvectors, which are of course zero.

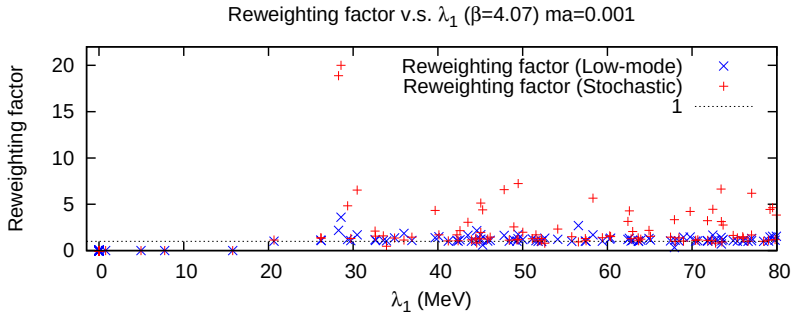

Figure 10: Reweighting factor with the low-mode reweighting (stars) and stochastic reweighting including all modes (pluses). The horizontal axis is the lowest eigenvalue of the overlap-Dirac operator for that gauge configuration. Data at $\beta = 4.07$ and $am_{\rm ud} = 0.001$ on the $16^3 \times 8$ lattice are plotted.

We incorporate all the eigenvalues below $\lambda \sim 100$ MeV. Here, we show that this low-mode reweighting can be used to study the gap in the Dirac spectrum.

On the smaller lattice, we compare the reweighting and the low-mode reweighting as shown in Fig. 10. Pluses and crosses represent the conventional stochastic reweighting factor and the low-mode reweighting factor, respectively. Each point represents a gauge configuration on which the reweighting factor is calculated. As the horizontal axis, we take the first eigenvalue λ_1. Below $\lambda_1 \sim 20$ MeV, both reweighting factors are consistent and essentially zero. Configurations having near-zero modes are strongly suppressed in both reweighting techniques, and we may therefore conclude that the non-existence of the gap in the Dirac spectrum does not depend on the details of the reweighting technique.

8 Summary and discussion

In this section, we summarize our result and discuss remnant issues. And following subsection, we note future perspective of this work.

8.1 Summary

We have studied the low-lying eigenvalue spectrum of the Möbius domain-wall and reweighted overlap Dirac operators slightly above the critical temperature, in order to judge that the $\mathrm{U}(1)_\mathrm{A}$ symmetry is restored or not. Our preliminary result at the lightest quark mass shows a significant difference between the overlap and Möbius domain-wall eigenvalue spectrum. This result points to a need for carefully treatment of chiral symmetry in the Lagrangian. The overlap-Dirac eigenvalue spectrum for the lightest quark mass shows a gap, which is insensitive to the volume, while that of the Möbius domain-wall has small but non-zero spectrum near $\lambda = 0$. The large violation of the Ginsparg-Wilson relation on the low-modes of the domain-wall Dirac operator may explain the difference.

In order to analyze accurately, we start configuration generation near to continuum limit. Such ensemble gives better stochastic reweighting factor, then we do not have to use low-mode approximation for the reweighting factor for such ensemble.

Further study is needed because we did not evaluate enough effects of finite volume and finite cut-off.

8.2 Future perspective

After confirm the restoration of $\mathrm{U}(1)_\mathrm{A}$ symmetry, we would like to try determination of the transition order of the QCD phase transition at quark mass vanishing limit. According to Pisarski and Wilczek, if anomaly disappear at critical temperature, this transition likely to be first order [28]. However their results obtained by using effective theory. More accurate treatment is needed. This is connected to the structure of the Columbia plot as mentioned in Introduction.

If transition order of massless two-flavor is first order, that affects to another area of nuclear and particle physics, and there are several applications. First application of the transition is the QCD phase diagram for $T - \mu$ plane. If realize the columbia plot in right panel in Fig.1, this may connected to the existence of critical end point. C. Bonati *et. al.* investigated the relation between the QCD critical end point and the columbia plot [31]. They extended the columbia plot with baryon chemical potential direction. They somehow related finite μ (real experiment) to $\mu = 0$ world. If the second order line shits $\mu = 0$ plane, it may give stronger constraint for existence of the critical end point in the QCD phase diagram. Second application is for baryogenesis via walking technicolor(WTC) theories [30]. WTC theories are theory for the beyond the standard model. The model may give a solution for fine-tuning problem, triviality problem and the origin of the generations. Typical WTC theories constructed by $SU(3)$ gauge field and $N_f \geq 8$ fermions in fundamental representation. Ejiri and Yamada argued low energy effective model of WTC theory. They use $N_f = 2$ QCD as a effective model for WTC theory. This is natural because in the WTC scenario, $N_f = 2$ fermions are generate 3 NG bosons by chiral symmetry breaking and they absorbed by gauge bosons. If the phase transition is strong first order, we can use this transition to the baryogenesis. Third application is strongly coupled hidden sector models [32]. Most of hidden sector model assume $\mathrm{U}(1)_\mathrm{A}$ violating term. However if we conclude the disappearance of $\mathrm{U}(1)_\mathrm{A}$ anomaly above the critical temperature, this assumption does not hold. This may affect to current constraint for those models.

Part II
Symmetry breaking caused by large $\mathcal{R}$-charge

9 Introduction

In part 1, we have discussed $\mathrm{U}(1)_\mathrm{A}$ symmetry in finite temperature QCD. Finite temperature QCD is gauge theory on 3+1 dimension with appropriate boundary condition for imaginary time (temperature) direction. Let us generalize boundary condition for the theory, in such a case, the system is not finite temperature system anymore. It can be regarded as a toy model for extra-dimension model *i.e.* gauge theory on 3+1 dimension. In such case, gauge symmetry in three dimension may be broken, in other words, gauge boson can acquire mass. In this part, we discuss this issue.

As we have seen in earlier part, gauge symmetry/principle is a method to introduce forces between matters in quantum field theory in quantum mechanically behaved way. The standard model is a good example for the gauge theory, which has $\mathrm{SU}(3)_\mathrm{c} \times \mathrm{SU}(2)_\mathrm{L} \times \mathrm{U}(1)_\mathrm{Y}$ gauge symmetries. $\mathrm{SU}(2)_\mathrm{L} \times \mathrm{U}(1)_\mathrm{Y}$ symmetry breaks down to $\mathrm{U}(1)_\mathrm{EM}$ by so-called Higgs mechanism. As a result, three of gauge bosons which corresponds $\mathrm{SU}(2)_\mathrm{L} \times \mathrm{U}(1)_\mathrm{Y}$ accrue the mass, and one of gauge boson remains massless, which is the photon. Simultaneously all the fermions obtain their masses and generate a Higgs boson which has been discovered by LHC experiments. Although the standard model is successful theory, it does not contain the dark matter and it has naturalness problem. Therefore we must construct the model for the beyond the standard model. An attractive model for the beyond the standard model is the gauge-Higgs unification model[33, 34, 35, 36, 37, 38, 39, 40]. In the model, gauge symmetry broken by the Wilson line phase which comes from non-simply connected structure of compactified extra dimensional space. If the expectation value of the Wilson line phase is non-zero, gauge bosons acquire the mass. The expectation can be evaluated by the 1PI effective potential which is constructed by the loop expansion of the theory. At the tree level, the effective potential is flat because the Wilson line phase is a solution of the equations of motion which are invariant under the gauge transformation *i.e.* gauge symmetry does not break. Surprisingly, although higher dimensional theories are non-renormalizable, this effective potential does not diverge on the Wilson line phase at 1 loop level. And the consequence, beyond the tree level, the gauge symmetry is spontaneously broken. This is called *the Hosotani mechanism* which has been studied as a electroweak symmetry breaking mechanism[41, 42, 43, 44, 45, 46, 47]. However, there is an unsatisfactory point with Hosotani mechanism : this mechanism for non-Abelian gauge theory has not been established by all order or non-perturvative way. In order to overcome this problem, it is necessary to study it with the non-perturvative method. The mechanism have been studied already by lattice gauge theories[48, 49, 50, 51, 52, 53]. For example, in [49, 50], they studied the SU(3) gauge symmetry in the 3+1 dimensional flat spacetime. In their analysis, SU(3) gauge theory with adjoint fermions has 4 phases, *confined phase, deconfined phase, split phase* and *reconfined phase*. By changing the mass of the adjoint fermions, these distinct phases emerge in a certain order. In terms of the Hosotani mechanism, they show that these phases correspond to SU(3), SU(3), $\mathrm{SU}(2) \times \mathrm{U}(1)$ and $\mathrm{U}(1) \times \mathrm{U}(1)$ global symmetries respectively. In addi-

tion to the adjoint fermions, they also considered the fundamental fermions, and checked *the Rogerge-Weiss (RW) transition*[54].

On the other hand, Supersymmetry (SUSY) which is a symmetry between fermions and bosons, enable to investigate non-perturbative properties of the theory in analytic way. Famous example is the Seiberg duality for $\mathcal{N} = 1$ gauge theories. This is a duality between different gauge theories, which are strongly/weakly coupled. Thanks to the duality, we can explore strongly coupled theory by using perturbation theory in dual theory. This couple of years, SUSY also defined on curved space-time, which has different characters compared with the usual theories on the flat space-time. By using the formulation, an exact way to perform the path integral so-called supersymmetric localization method have been developed [55, 56, 57, 58, 59]. A novel point for these recent developments is defining SUSY gauge theories on a compact manifold in order to regularize IR divergence naturally. For example, we can choose $M \times S^1$ as such a compact space. It turns out to be possible to construct supersymmetry on $M \times S^1$ for a certain M, and the exact results are known as so-called (superconformal) index [60, 61, 62, 63, 64, 65]. If we consider SUSY gauge theories by taking

$$M = \text{a flat spacetime},$$

the effective potential for the Wilson line phase turns to be totally flat because the fermionic contribution cancels the corresponding bosonic contribution. As a result, gauge symmetry is unbroken. However, we define SUSY gauge theories by taking

$$M = \text{a curved spacetime},$$

in this case, the boson only couples with the background scalar curvature and this makes difference between bosons and fermions. This fact may suggest a possibility towards a non-trivial and non-perturbative analysis of Hosotani mechanism based on SUSY gauge theories on a curved $M \times S^1$. As a first step to move on more realistic studies, we analyze gauge theory on $S^2 \times S^1$ in this thesis for simplicity.

A formal argument In usual argument, a minimum of the effective potential is selected because of the large volume in the following sense. Suppose we have a partition function as

$$Z = \sum_{v \in \text{vacua}} e^{-\text{Vol} \cdot V_{\text{eff}}(v)}. \tag{9.1}$$

When we take Vol$\to \infty$, the steepest decent v_0 will dominate Z. It means the vacuum which satisfies

$$V'_{\text{eff}}(v_0) = 0, \tag{9.2}$$

$$V''_{\text{eff}}(v_0) > 0, \tag{9.3}$$

is selected automatically as a true vacuum. In this thesis, we use $\mathcal{N} = 2$ superconformal field theories. Intuitively, we have no volume dependence with these theories because of the conformal symmetry. However, as we noted above, once we turn on the matter fields into the theory on a certain curved space, the matter couples with the scalar curvature R via $\mathcal{R}$*-charge* Δ_Φ. Our discussion on the symmetry breaking is based on *large* $\mathcal{R}$*-charge limit* $\Delta_\Phi \to \infty$. Schematically, in our case, the partition function takes the following form

$$Z = \sum_{v \in \text{vacua}} e^{-\Delta_\Phi \cdot V_{\text{eff}}(v)}. \tag{9.4}$$

Through the same argument presented above, when we take $\Delta_\Phi \to \infty$, a vacuum corresponds to (9.2), (9.3) is selected. Actually, large $\mathcal{R}$-charge limit is same as the thermodynamic limit. We will argue this issue in Section 14.

This part is organized as follows. Next section, we explain localization principle briefly. In Section 11, we summarize results of exact calculation for super Yang-Mills (SYM) theory with two matters on $S^2 \times S^1$. And we discuss large $\mathcal{R}$-charge limit which causes the symmetry breaking. In Section 12, we investigate *the finite size effects* via the effective potential with the small $\mathcal{R}$-charge. In Section 13, we show phase structures of the broken vacua at large $\mathcal{R}$-charge limit. Section 14 contains results and comments on our method. In Appendix I we summarize our localization calculous.

10 Localization principle

In this section, we briefly review localization technique symbolically. The "localization" is a mathematical phenomena, which is a reduction of (path) integral. If localization of path integral occurs, we can evaluate it by the Gaussian integral, even in interacting case. A sufficient condition of the localization is, the action has nilpotency. If the action has nilpotency, the partition function independent of the coupling constant, in other wards, path integral can be evaluated weak coupling limit. In the weak coupling limit, the action takes quadratic form, then we obtain functional determinant of Laplacian or Dirac operator. The determinant can be evaluated by expanding appropriate basis, in our case, spherical harmonics. In following section, we briefly review localization phenomena.

We start from the partition function,

$$Z(\beta) = \int \mathcal{D}\Phi e^{-\beta S(\Phi)} \tag{10.1}$$

where Φ represents all of field in SUSY multiplets. If $S(\Phi)$ is supersymmetric exact, *i.e.* $S(\Phi) = \delta V(\Phi)$, actually $Z(\beta)$ is not depend on β. Here δ is a nilpotent supersymmetric operator and $V(\Phi)$ is a function of given field. This can be prove as follows.

$$\begin{aligned}
\frac{d}{d\beta} Z(\beta) &= \frac{d}{d\beta} \int \mathcal{D}\Phi e^{-\beta S(\Phi)} && (10.2)\\
&= \int \mathcal{D}\Phi \frac{d}{d\beta} e^{-\beta S(\Phi)} && (10.3)\\
&= \int \mathcal{D}\Phi [-S(\Phi)] e^{-\beta S(\Phi)} && (10.4)\\
&= \int \mathcal{D}\Phi [-\delta V(\Phi)] e^{-\beta S(\Phi)} && (10.5)\\
&= \int \mathcal{D}\Phi \delta [-V(\Phi) e^{-\beta S(\Phi)}]. && (10.6)
\end{aligned}$$

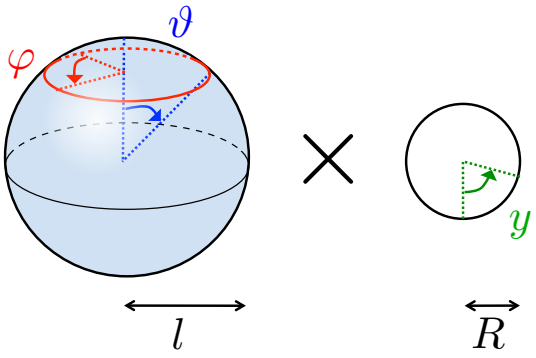

Figure 11: $S^2 \times S^1$, l is the radius of S^2, and R is the radius of S^1.

Here we rewrite integrant as $f(\Phi) = -V(\Phi)e^{-\beta S(\Phi)}$,

$$\frac{d}{d\beta}Z(\beta) = \int \mathcal{D}\Phi\delta f(\Phi) \tag{10.7}$$

$$= \int \mathcal{D}\Phi[f(\Phi') - f(\Phi)] \tag{10.8}$$

$$= \int \mathcal{D}\Phi f(\Phi') - \int \mathcal{D}\Phi f(\Phi) \tag{10.9}$$

$$= \int \mathcal{D}\Phi' f(\Phi') - \int \mathcal{D}\Phi f(\Phi) = 0. \tag{10.10}$$

Here we assume no anomaly on the supersymmetric transformation. This result means, if $V(\Phi)$ which satisfy $S(\Phi) = \delta V(\Phi)$ is found, one can evaluate the path integral at $\beta = \infty$. In such parameter region, steepest decent method is exact.

11 Preliminaries

11.1 Basic concepts

11.1.1 Our spacetime

We consider Euclidean $S^2 \times S^1$ space-time (Fig. 11) for following 3 reasons. First reason is, if dimension is equal or lower than 2, continuous symmetry does not break. In order to discuss spontaneous symmetry breaking, we need dimension higher than 2. For simplicity we choose a theory on three dimensional space-time. Second reason is, we would like to discuss is the symmetry breaking via the Wilson line phase. In order to the wilson line phase effect to the physics, we need compactified direction, S^1. Third reason is, we want to take nontrivial $\mathcal{R}$-charge contribution into account via the coupling with the scalar curvature R. If we employ, say T^2 space-time, curvature is zero. Thus, the simplest model is a theory on $S^2 \times S^1$. We use the following metric and coordinates of the $S^2 \times S^1$,

$$ds^2 = l^2(d\vartheta^2 + \sin^2\vartheta d\varphi^2) + dy^2, \qquad \vartheta \in [0, \pi], \quad \varphi \in [0, 2\pi], \quad y \in [0, 2\pi R]. \tag{11.1}$$

As reported in [60, 61, 62], even on such a curved space, we can construct supersymmetric field theories[30]. Note that we have 3 distinct "R" s,

[30]See more details in Appendix I.

$\mathcal{R}$ - charge : curly $\mathcal{R}$, S^1- radius : Itaric R, scalar curvature : normal R.

11.1.2 Possible fields and theories

We construct two distinct irreducible field representations of $\mathcal{N}=2$ off-shell supersymmetry on $S^2\times S^1$,

$$\text{vector multiplet}: V=(A_\mu,\sigma,\bar\lambda,\lambda,D)\in \text{Ad}, \tag{11.2}$$

$$\text{matter multiplet}: \Phi=(\phi,\psi,F)\in \text{Rep}, \tag{11.3}$$

where the σ, D, F are scalar fields, $\bar\lambda,\lambda,\psi$ are spinors and A_μ is a gauge field. In the flat case, one can obtain these supermultiplets in 3 dimensional space by the dimensional reduction from 4 dimensional $\mathcal{N}=1$ vector and matter multiplets, respectively. By using the off-shell components, following supersymmetric Lagrangians[31] is constructed,

$$\mathcal{L}_{\text{SYM}}=\text{Tr}\left(\frac{1}{2}F_{\mu\nu}F^{\mu\nu}+D^2+\mathcal{D}_\mu\sigma\mathcal{D}^\mu\sigma+\frac{1}{l}\epsilon^{3\rho\sigma}\sigma F_{\rho\sigma}+\frac{\sigma^2}{l^2}+i\bar\lambda\gamma^\mu\mathcal{D}_\mu\lambda-i\bar\lambda[\lambda,\sigma]-\frac{i}{2l}\bar\lambda\gamma_3\lambda\right), \tag{11.4}$$

$$\begin{aligned}\mathcal{L}_\Phi=&-i(\overline{\psi}\gamma^\mu\mathcal{D}_\mu\psi)+i(\overline{\psi}\sigma\psi)-i\overline{\phi}(\bar\lambda\psi)-\frac{i(2\Delta_\Phi-1)}{2l}(\overline{\psi}\gamma_3\psi)+\overline{F}F\\&+i(\overline{\psi}\lambda)\phi+\mathcal{D}_\mu\overline{\phi}\mathcal{D}^\mu\phi+\overline{\phi}\sigma^2\phi+i\overline{\phi}D\phi\ -\frac{2\Delta_\Phi-1}{l}\overline{\phi}\mathcal{D}_3\phi-\frac{\Delta_\Phi(2\Delta_\Phi-1)}{2l^2}\overline{\phi}\phi+\frac{\Delta_\Phi}{4}\text{R}\overline{\phi}\phi,\end{aligned} \tag{11.5}$$

where R is the scalar curvature calculated from (11.1) and Δ_Φ is the $\mathcal{R}$-charge[32] of the matter multiplet Φ. Note that, we can take arbitrary Δ_Φ without breaking supersymmetry. In addition, we define the covariant derivative $\mathcal{D}_\mu$ as

$$\mathcal{D}_\mu=\nabla_\mu-iA_\mu, \tag{11.7}$$

where ∇_μ is the covariant derivative with respect to the spin connection:

$$\nabla_\mu(\text{scalar})=\partial_\mu(\text{scalar}),\qquad \nabla_\mu(\text{spinor})=(\partial_\mu-\frac{1}{4}\omega_\mu{}^{ab}\gamma_{ab})(\text{spinor}). \tag{11.8}$$

11.2 Our model and the vacua

11.2.1 Field contents

We focus on the SU(3) gauge theory in order to compare results in [49] by using lattice calculation. Our model is constructed by

$$\begin{aligned}&1\text{ vector}: V,\\&2\text{ matters}: \begin{cases}\Phi_1 & \text{represented by } +\rho\\ \Phi_2 & \text{represented by } -\rho\end{cases}.\end{aligned} \tag{11.9}$$

[31] We can also take the supersymmetric *Chern-Simons* (CS) term. However it will cause a sign problem. Therefore, we discard the CS term in this study for simplicity.

[32] $\mathcal{R}$-charge is an "electric charge" for $U(1)_R$ symmetry. $U(1)_R$ transformation is a transformation for the fields Φ,

$$\Phi\to e^{i\alpha\mathcal{R}}\Phi, \tag{11.6}$$

where α is a real parameter. $\mathcal{R}$ charge for each field is given in Table 3. If the Lagrangian is invariant under this transformation, this transformation called $U(1)_R$ symmetry.

The reason why we need 2 matters, is in Appendix I.

11.2.2 The $\mathcal{R}$-charge and chemical potential for matters

In addition, in order to simplify the exact calculations by the supersymmetric localization method, we assign identical $\mathcal{R}$-charges Δ with these matters:

$$\Delta_{\Phi_1} = \Delta_{\Phi_2} = \Delta, \tag{11.10}$$

and turn on opposite imaginary chemical potentials

$$\mu_{\Phi_1} = -\mu_{\Phi_2} = i\alpha. \tag{11.11}$$

The simplifications caused by this choice of quantities will be explained in Appendix I. For later use, we comment on the boundary conditions of the component fields in the matter multiplets. We have many fields which satisfy the boundary conditions (I.12)-(I.17). For example, the scalars $\phi_1, \overline{\phi}_1, \phi_2, \overline{\phi}_2$ satisfy[33]

$$\phi_1(\vartheta, \varphi, y + 2\pi R) = e^{-\Delta \frac{\pi R}{l}} e^{+i\alpha} \phi_1(\vartheta, \varphi, y), \tag{11.12}$$

$$\overline{\phi}_1(\vartheta, \varphi, y + 2\pi R) = e^{+\Delta \frac{\pi R}{l}} e^{-i\alpha} \overline{\phi}_1(\vartheta, \varphi, y), \tag{11.13}$$

$$\phi_2(\vartheta, \varphi, y + 2\pi R) = e^{-\Delta \frac{\pi R}{l}} e^{-i\alpha} \phi_2(\vartheta, \varphi, y), \tag{11.14}$$

$$\overline{\phi}_2(\vartheta, \varphi, y + 2\pi R) = e^{+\Delta \frac{\pi R}{l}} e^{+i\alpha} \overline{\phi}_2(\vartheta, \varphi, y). \tag{11.15}$$

Note that the factors $e^{\pm\Delta\frac{\pi R}{l}}$ are necessary in order to maintain the supersymmetry[34]. This constraint comes from compactification of S^1 direction. Note that, if we employ this boundary condition, the Lagrangian is still single-valued.

11.2.3 Our Lagrangian and the vacua

We have introduced SYM Lagrangian $\mathcal{L}_{\text{SYM}}$ in (11.4) and matter Lagrangian $\mathcal{L}_\Phi$ in (11.5). Throughout this part, we consider the following Lagrangian on $S^2 \times S^1$:

$$\mathcal{L} = \mathcal{L}_{\text{SYM}} + \mathcal{L}_{\Phi_1} + \mathcal{L}_{\Phi_2}. \tag{11.16}$$

This Lagrangian gives the following vacua [60, 61, 62], in other words, *the locus* :

$$\begin{aligned} &A = mA_{\text{mon}} + \frac{\theta}{2\pi R} dy, \quad \sigma = -\frac{m}{2l}, \\ &m = \text{diag}(m_1, m_2, -m_1 - m_2), \quad \theta = \text{diag}(\theta_1, \theta_2, -\theta_1 - \theta_2), \end{aligned}$$

other fields are zero. A_{mon} is the Dirac monopole configration:

$$A_{\text{mon}} = \frac{1}{2}(\kappa - \cos\vartheta) d\varphi, \quad \kappa = \begin{cases} +1 & \vartheta \in [0, \frac{\pi}{2}] \\ -1 & \vartheta \in [\frac{\pi}{2}, \pi] \end{cases} . \tag{11.17}$$

The m is so-called GNO charge [66], and θ represent the Wilson line phase.

[33] Boundary conditions for fields are appeared in Appendix I

[34] See Appendix H

11.3 An exact result, large $\mathcal{R}$-charge limit and the symmetry breaking

Via so-called localization method [60, 61, 62], we can calculate the path integral on the $S^2 \times S^1$ exactly. Finally one can obtain the result in the form of a summation over the locus:

$$\int \mathcal{D}V\mathcal{D}\Phi_1\mathcal{D}\overline{\Phi}_1\mathcal{D}\Phi_2\mathcal{D}\overline{\Phi}_2\ e^{-\int d^3x\sqrt{g}\mathcal{L}} = \sum_{m_1,m_2=-\infty}^{\infty} \frac{1}{\text{sym}} \int_{-\pi}^{\pi} \frac{d\theta_1}{2\pi R}\frac{d\theta_2}{2\pi R}\ \mathcal{Z}_{\text{1-loop}}^{vec(reg)} \times \mathcal{Z}_{\text{1-loop}}^{mat1,2(reg)}. \tag{11.18}$$

The 'sym' represents symmetric factors for the configurations of m_1, m_2. The summation $\sum_{m_1,m_2}$ comes from the GNO monopoles' quantization condition on S^2 which can be regarded as one of *the finite size effects*. In the following section, we discuss on the finite size effects. The integral $\int d\theta_1 d\theta_2$ is caused by the Wilson line phase. The domain $[-\pi, \pi]$ is a consequence of the gauge symmetry of $\mathcal{L}$. Let us forcus to the integrands. The first one is the contribution from the vector multiplet :

$$\mathcal{Z}_{\text{1-loop}}^{vec(reg)} = \prod_{i>j} \Big| 2\sin\Big(\frac{\theta_i - \theta_j}{2} + i\frac{\pi R}{l}\frac{m_i - m_j}{2}\Big)\Big|^2. \tag{11.19}$$

The second one is the contribution from the two matter multiplets :

$$\mathcal{Z}_{\text{1-loop}}^{mat1,2(reg)} = \prod_{\rho\in R}\prod_{J=1-\frac{\Delta}{2}}^{\frac{\Delta}{2}-1} \Big| 2\sin\Big(\frac{\rho(\theta)-\alpha}{2} + i\frac{\pi R}{l}\big(|\frac{\rho(m)}{2}| + J\big)\Big)\Big|^2, \tag{11.20}$$

where we have assumed $\Delta - 1 \in \mathbb{N}$. Of course there is no Δ dependence on the contribution from the vector multiplet $\mathcal{Z}_{\text{1-loop}}^{vec(reg)}$, but the contribution from the two matter multiplets $\mathcal{Z}_{\text{1-loop}}^{mat1,2(reg)}$. We can rewrite this $\mathcal{Z}_{\text{1-loop}}^{mat1,2(reg)}$ into a more useful form

$$\mathcal{Z}_{\text{1-loop}}^{mat1,2(reg)} = \exp\Big(-\Delta V_{\text{eff}}(\theta, m)\Big), \tag{11.21}$$

where

$$V_{\text{eff}}(\theta, m) = -\sum_{\rho\in R} 2\text{Re}\sum_{J=1-\frac{\Delta}{2}}^{\frac{\Delta}{2}-1} \frac{1}{\Delta}\log 2\sin\Big(\frac{\rho(\theta)-\alpha}{2} + i\frac{\pi R}{l}\big(|\frac{\rho(m)}{2}| + J\big)\Big). \tag{11.22}$$

Roughly speaking, $V_{\text{eff}} \sim \sum_J \frac{1}{\Delta} \sim \Delta\frac{1}{\Delta} = 1$. Therefore, this definition is meaningful for any integer Δ.

11.3.1 Large $\mathcal{R}$-charge limit

In order to break the symmetry, we take $\Delta \to \infty$ as we noted in the introduction[35]. However there is one problem. See boundary conditions (11.12) - (11.15). These conditions include

[35] In the original the Hosotani mechanism, we decompose gauge fields to the dynamical modes and the Wilson line phase. And after the decomposition, the Wilson line phase is determined by using the 1-loop effective potential constructed by dynamical fields. However we integrate over all of field first, so we cannot construct effective potential in terms of the fields. In this study, we regard the integrants of (11.18) as a effective potential for the θ. Similar situation occurred in lattice calculation [49]. In practical lattice calculation, the field component cannot be decomposed. They reconstructed the effective potential from the histogram of Polyakov loop.

the following factor

$$\Delta\frac{\pi R}{l} =: c. \tag{11.23}$$

The naive $\Delta \to \infty$ limit defines pathological behaviors for Φ_1, Φ_2 because $c \to \infty$. Therefore, we have to take $\Delta \to \infty$ with fixing c in order to avoid such ill defined S^1 boundary conditions for Φ_1, Φ_2. This means, we have to take $l \to \infty$ simultaneously. It corresponds to the large volume limit. Note that $R \to +0$ is different from $l \to \infty$ because of the presence of R in (11.18). Once we take $\Delta \to \infty$, we can replace $\sum_J \frac{1}{\Delta}$ to the corresponding integral over $-1/2$ to $1/2$ in the sense of Riemann sum:

$$\sum_{J=1-\frac{\Delta}{2}}^{\frac{\Delta}{2}-1} \frac{1}{\Delta} = \sum_{J=1-\frac{\Delta}{2}}^{\frac{\Delta}{2}-1} \frac{\delta J}{\Delta} \to \int_{-1/2}^{+1/2} dj, \tag{11.24}$$

where we define a continuous parameter j as

$$j := \frac{J}{\Delta}. \tag{11.25}$$

In addition, we can simplify

$$\frac{\rho(\theta)-\alpha}{2} + ic\big(|\frac{\rho(m)}{2\Delta}| + j\big) \quad \to \quad \frac{\rho(\theta)-\alpha}{2} + icj, \tag{11.26}$$

by using (11.23) and $\Delta \to \infty$. In (11.26), the m dependence vanishes. This is natural because m dependence can be regarded as the finite size effect of S^2 which comes from the nontrivial Dirac monopole configuration[36]. In summary, our effective potential for the Wilson line phase is constructed by

$$\begin{aligned} V_{\text{eff}}(\theta, m) \to \mathcal{V}_{\text{eff}}(\theta) &= -\sum_{\rho\in R} 2\text{Re}\int_{-1/2}^{+1/2} dj \ \log\sin\big(\frac{\rho(\theta)-\alpha}{2} + icj\big) \\ &= -\sum_{\rho\in R} \text{Re}\Big[\frac{1}{c}\text{Li}_2\Big(e^{-i\left(\rho(\theta)-\alpha\right)-2cj}\Big)\Big]_{-1/2}^{+1/2}, \end{aligned} \tag{11.27}$$

where Li_2 is the dilogarithmic function[37]. In the following section, we discuss the phases of SU(3) gauge theory based on this dilogarithmic potential.

11.3.2 Contribution from the vector multiplet

After large $\mathcal{R}$-charge procedure $\Delta \to \infty$, we have

$$\mathcal{Z}_{\text{1-loop}}^{vec(reg)} \to \prod_{i>j} |2\sin\frac{\theta_i - \theta_j}{2}|^2. \tag{11.28}$$

This is *the Haar measure*. As commented in [49], this is not the dynamical contribution but the Jacobian caused by diagonalizing the Wilson line phase θ, and we should not take it into account. It means we cannot break the gauge symmetry only with SYM. This interpretation does not conflict with the known results based on the perturbative calculation [67].

[36]This corresponds to exchange the order of large $\mathcal{R}$ limit and summation over m. This may affect to the result. We comment on this issue in later section.

[37]In general, multilogarithmic function is defined by $\text{Li}_n(z) = \sum_{k=1} \frac{z^k}{k^n}$.

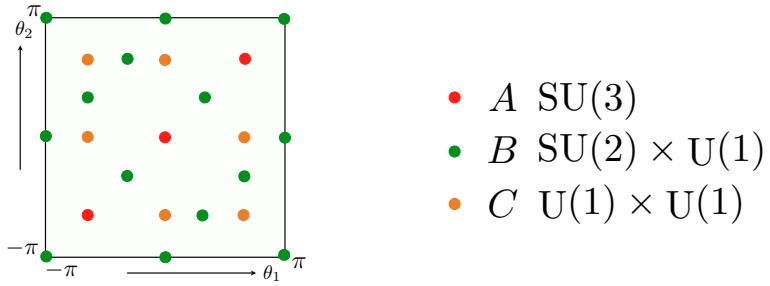

Figure 12: Names for each configuration

11.4 Notations of SU(3) phases

According to [50], we use the conventional names for particular combination of (θ_1, θ_2). We use the following names :

$$\text{SU(3) symmetric configurations} \begin{cases} A_1 : (\theta_1, \theta_2) = (0, 0) \\ A_2 : (\theta_1, \theta_2) = (\frac{2}{3}\pi, \frac{2}{3}\pi) \\ A_3 : (\theta_1, \theta_2) = (-\frac{2}{3}\pi, -\frac{2}{3}\pi) \end{cases}, \tag{11.29}$$

$$\text{SU(2)} \times \text{U(1)} \text{ symmetric configurations} \begin{cases} B_1 : (\theta_1, \theta_2) = (0, \pi) \\ B_2 : (\theta_1, \theta_2) = (\frac{2}{3}\pi, -\frac{1}{3}\pi) \\ B_3 : (\theta_1, \theta_2) = (-\frac{2}{3}\pi, \frac{1}{3}\pi) \end{cases}, \tag{11.30}$$

$$\text{U(1)} \times \text{U(1)} \text{ symmetric configurations} \begin{cases} C : (\theta_1, \theta_2) = (0, \frac{2}{3}\pi) \end{cases}. \tag{11.31}$$

Figure 12 explains the positions for phases A, B, C, in the (θ_1, θ_2) plane. The symmetries SU(3), SU(2) × U(1) and U(1) × U(1) in (11.29), (11.30) and (11.31) correspond to the remaining gauge symmetry in the context of the Hosotani mechanism.

12 Finite Δ and the finite size effects

Here, we do not intend to discuss the symmetry breaking, but *the finite size effects* caused by GNO charge. Small l corresponds to the small S^2. As we commented in Section 2, we consider fixed $c = \Delta\pi R/l$ (11.23). Combining small l and fixed c, we expect that the finite size effect emerges with small Δ. For small Δ, we should not use the dilogarithmic effective potential (11.27) but (11.22) which depends on GNO charge. One may wonder how we should determine the precise values of GNO charges (m_1, m_2). However, it is clear from (11.22) that the effects of GNO charge will be dropped when we take large l. We assume this ambiguity for choosing (m_1, m_2) values itself is also one of the finite size effects. In this section, we observe what happens when we take $\Delta = 2$ and $(m_1, m_2) = (1, 1)$ as an examination of the finite size effects.

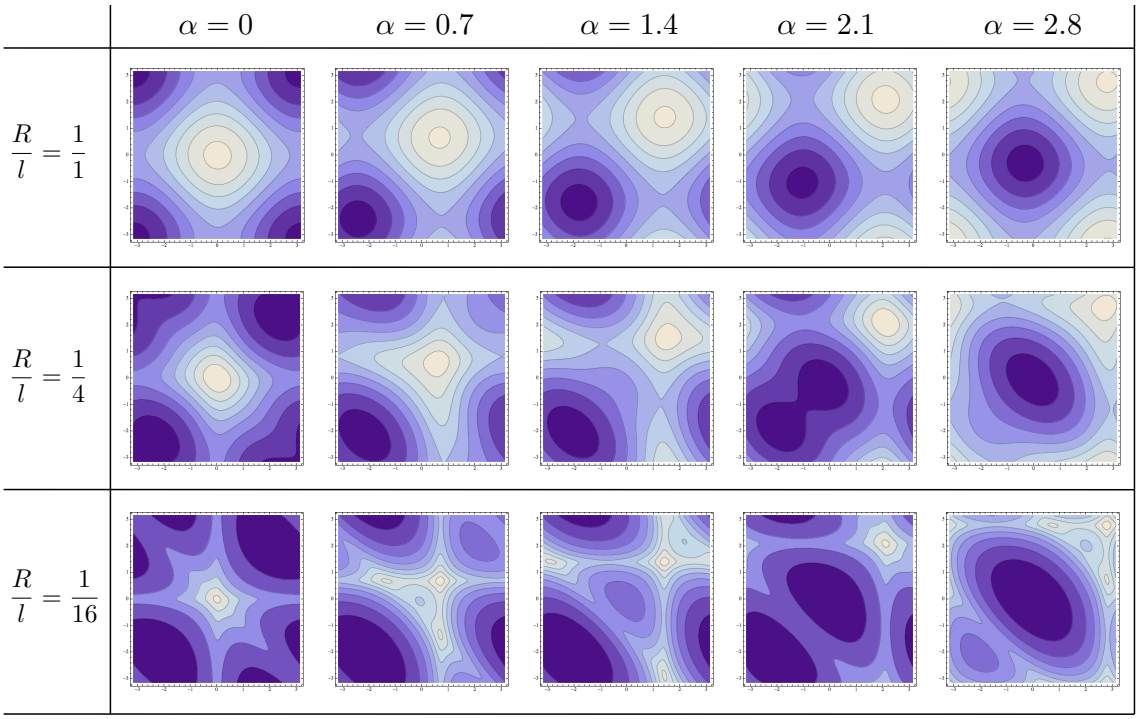

Figure 13: Contour plots of the effective potential for the fundamental matter, $\rho = fd$. Smaller values of the effective potential correspond to darker colors. The column corresponds to R/l =(the size of S^1)/(the size of S^2). The row corresponds to the imaginary chemical potential α.

12.1 Fundamental matter

See Figure 13. We plot the effective potentials for the fundamental matter, $\rho = fd$, with various ratios R/l (the column) and imaginary chemical potentials $\alpha \in [0, 2.8]$ (the low). There are two important things we shall explain.

12.1.1 Splitting locations of minima

The first row ($R/l = 1$) in Figure 13 shows false minima for (θ_1, θ_2). For example, when the imaginary chemical potential $\alpha = 0$, $(\theta_1, \theta_2) = (0, 0)$ looks the minimum. However, this false vacuum is caused by the non-zero values $(m_1, m_2) = (1, 1)$, and splits into two true vacua when we take large l. It is easier to observe this splitting with $\alpha = 2.1$ column.

12.1.2 RW transition with fundamental matter

Once we turn on the imaginary chemical potential α, an interesting phenomena occur as shown in the lows of Figure 13. In the $R/l = 1/16$ low, we can see discrete change of the locations of the minima at $\alpha = 2.1$ which is known so-called RW transition [54]. On the other hand, in the $R/l = 1$ low, the minimum looks moving continuously along the line $\theta_2 = \theta_1$. In the intermediate region *i.e.* the $R/l = 1/4$ low, we observe continuous move of the minimum in $0 \leq \alpha \leq 1.4$. However, a very quick transition of the minimum occurs around $\alpha = 2.1$.

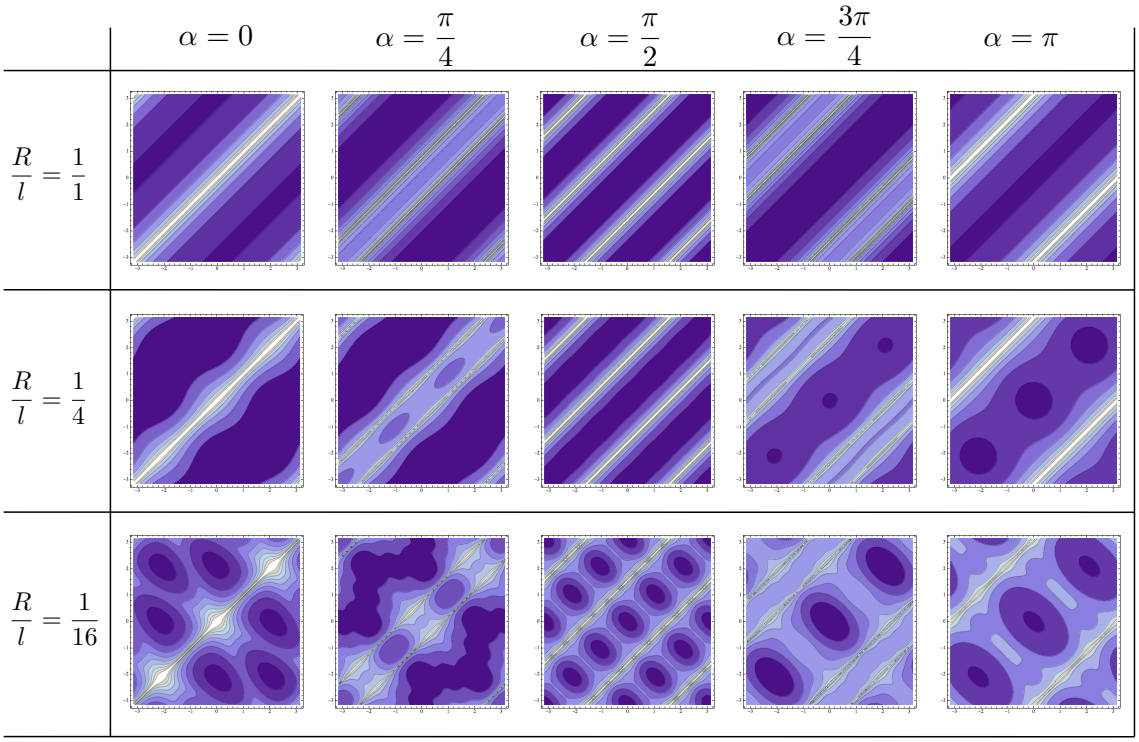

Figure 14: Contour plots of the effective potential for adjoint matter, $\rho = ad$. Smaller values of the effective potential correspond to darker colors. The column corresponds to R/l =(the size of S^1)/(the size of S^2). The row corresponds to the imaginary chemical potential α.

12.2 Adjoint matter

See Figure 14. We plot the effective potentials for the adjoint matter, $\rho = ad$, with various ratios R/l (the column) and imaginary chemical potentials $\alpha \in [0, \pi]$ (the low). There are also two important things we shall explain.

12.2.1 Degenerated minima

The first row ($R/l = 1$) in Figure 14 shows false *degenerated* minima for (θ_1, θ_2). Rigorously, the potential is not degenerated but has very slight depth around the minima. The degeneracy is truly realized in $l \to +0$ limit. Such a ill behavior of the minima is also caused by the presence of (m_1, m_2). In fact, such behavior vanishes as we take large l. Therefore this is caused by the finite size effect. For example, with $\alpha = \pi$, one can see that the degeneracy becomes weaker as l, the radius of S^2, becomes larger.

12.2.2 RW-like transition with adjoint matter

We have "jumps" of the location of degenerated vacua. With $\alpha \sim 0$, the vacua around C, B phases are preferred. On the other hand, when we turn $\alpha \sim \pi$, the vacua around A phase is preferred. This jumping structure is observed both in the region $R \sim l$ and the region $R \gg l$. This means such phenomena are not caused by the finite size, but come from universal structure of the SU(3) gauge theory with adjoint matters. We will see later that this structure emerges even in large $\mathcal{R}$-charge limit.

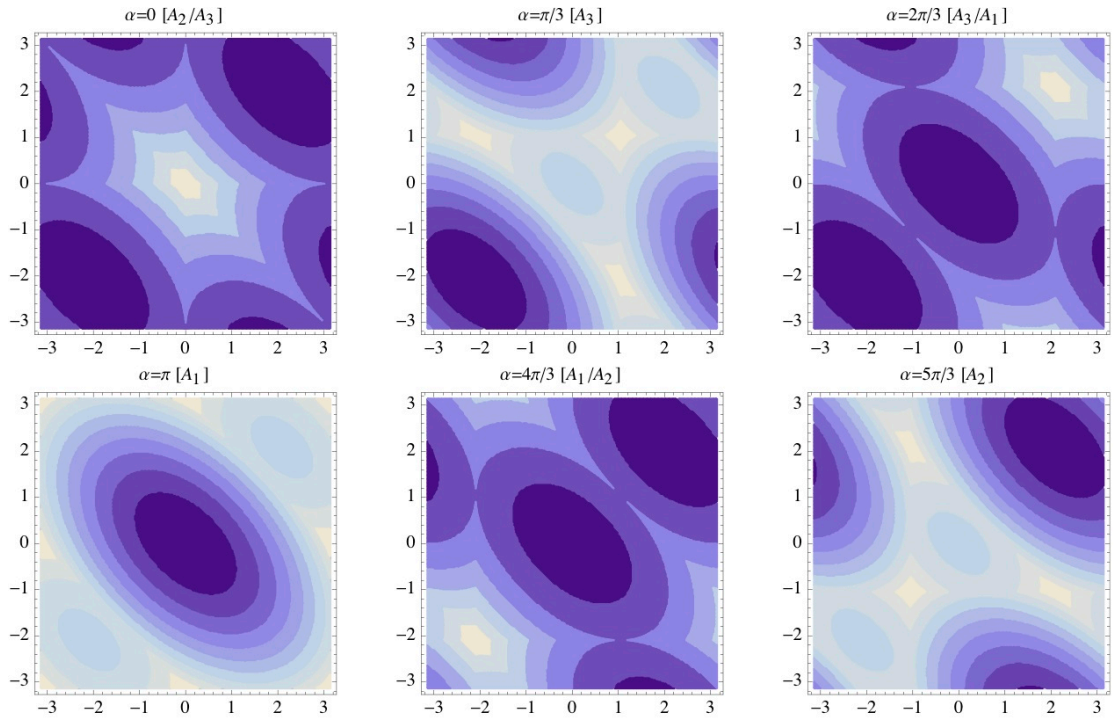

Figure 15: Contour plots of the effective potential for the fundamental matter, $\rho = fd$. Smaller values of the effective potential correspond to darker colors. From top left to top right are $\alpha = 0, \pi/3, 2\pi/3$ and bottom lines are $\alpha = \pi, 4\pi/3, 5\pi/3$. Vertical and horizontal axis are θ_1 and θ_2 in each figure. From left top to right bottom panels correspond to A_2/A_3, A_3, A_3/A_1, A_1, A_1/A_2 and A_2 phase respectively.

13 Large Δ and the symmetry breaking

13.1 Analysis method

In earlier Section, we obtain the effective potential (11.27). The effective potential has free parameter c. In principle we can take an arbitrary value of c. We check the c dependence of our effective potential. As a result, locations of minima of our effective potential do not change qualitatively for $c = 50,\ 500,\ 5000$. In this section, we show contour plots of the effective potential with $c = 5000$ (Figure 15, Figure 16).

By the way, there exists another non-perturbative result for the phase structure based on the lattice gauge theory [49]. They measured the Polyakov loop and reconstruct the effective potential from configurations of the Polyakov loop. In our method we can see non-perturbative exact effective potential directly. We do not see the Polyakov loop nor other physical quantities.

13.2 Fundamental matter

First, we investigate α dependence of minima for the effective potential with the fundamental matter (Figure 15). This is one of our main results. Darker regions correspond to deeper

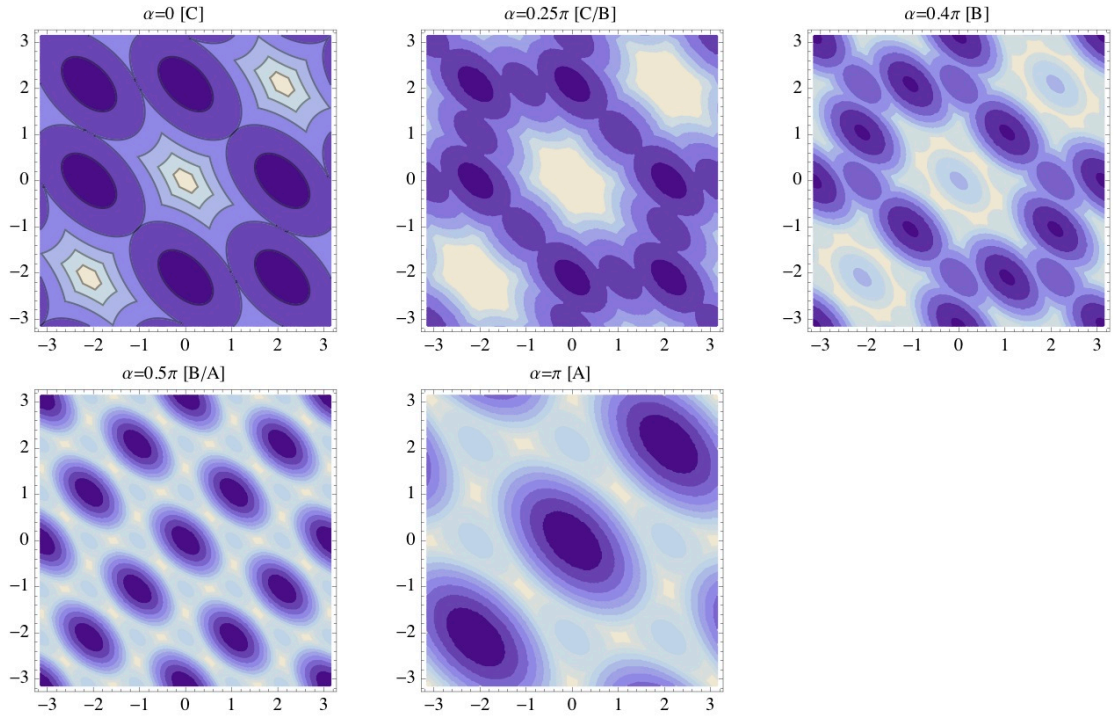

Figure 16: Contour plots of the effective potential for adjoint matter, $\rho = ad$. Smaller values of the effective potential correspond to darker colors. From top left to top right are $\alpha = 0, 0.25\pi, 0.4\pi$ and bottom lines are $\alpha = 0.5\pi$ and π. Vertical and horizontal axis are θ. From left top to right bottom panels correspond to C, C/B, B, B/A and A phase respectively.

regions of our effective potential. As we said before, a minimum of the effective potential is selected in large $\mathcal{R}$-charge limit. Phases appear in the order of A_3, A_1, A_2 as α moves from $\pi/3$ to $5\pi/3$ with discrete transition. This means we obtain RW transition in exact way.

Compared with the perturbative result for non-supersymmetric 4 dimensional theory in [49], appearing order of $A_{1,2,3}$ phases is inverted. This is because we use the opposite sign convention of the gauge coupling through the covariant derivative (11.7). In this sense, our result is similar to their result. However our effective potential does not depend on any coupling constant. This fact indicates there is no difference between the strong coupling limit and the weak coupling limit. We comment on this issue later.

13.3 Adjoint matter

Next, we investigate α dependence of minima for the effective potential with the adjoint matter. Figure 16 is our second main result. These contour plots show discrete phase transitions. Phases appear in the order of C, B, A as α moves from 0 to π. When we increase α from π to 2π, the phases move to A, B and go back to C.

Again we get the similar result via non-perturbative method. Compared with the perturbative result for non-supersymmetric 4 dimensional theory in [49], they have shown critical points for the boundary condition. The global minima of the effective potential with $c = 0$

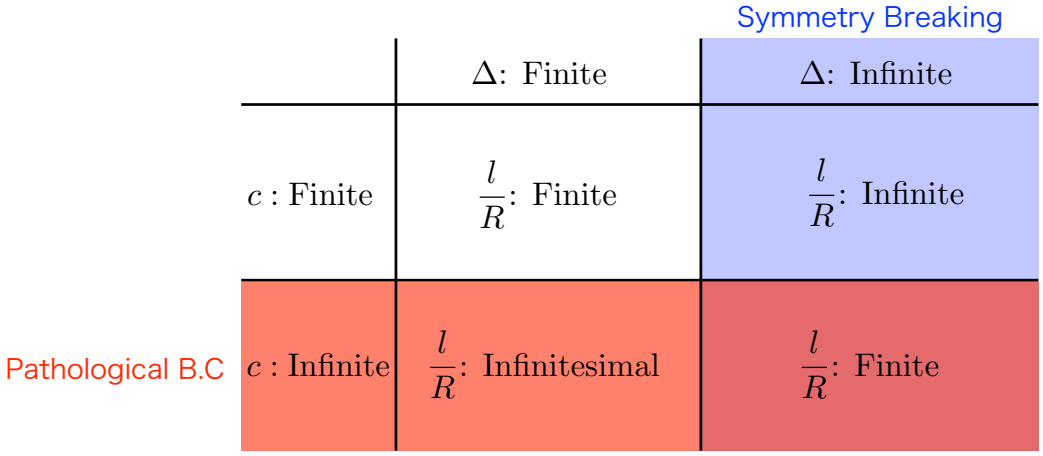

Figure 17: l is the radius of S^2. R is the radius of S^1. Red colored region defines the pathological boundary conditions with matters, and we do not consider in this paper. In blue colored region, the symmetry breaks due to large Δ.

are located at

$$\begin{aligned} A_{1,2,3} \quad &\text{for} \quad 0.5\pi \leq \alpha \leq \pi, \\ B_{1,2,3} \quad &\text{for} \quad 0.3\pi \leq \alpha \leq 0.5\pi, \\ C \quad &\text{for} \quad \alpha \leq 0.3\pi. \end{aligned} \tag{13.1}$$

We determine the critical values for the imaginary chemical potential $\alpha = 0.3\pi,\ 0.5\pi$ in numerical calculation. We expect that these values are determined analytically for $c \neq 0$.

14 Conclusion and Discussion

14.1 Summary and Conclusion

We calculated the effective potential of the Wilson line phase for SYM theory with two matters on $S^2 \times S^1$ via the localization technique. See Figure 17. Red colored region defines the pathological boundary conditions with matters, and we do not consider in this paper. In blue colored region, the symmetry breaks due to large Δ.Our main target region is the one with finite c and infinite Δ. In this region, the volume is also infinite because l is infinite. So as a result, we have not only the large $\mathcal{R}$-charge limit but also the thermodynamic limit as noted in Introduction.

We checked the finite size effects for our effective potential in Section 12. For finite Δ, the effective potential (11.22) is affected by the existence of the GNO monopole on S^2. The GNO monopole exists only on S^2, such a deformation of the effective potential is naturally understood as a finite size effect. This is because the effect disappears by taking large l limit.

On the other hand, the effective potential is written by the dilogarithmic function (11.27) for large Δ. We investigated this effective potential for matter fields in fundamental representation and adjoint representation at large $\mathcal{R}$-charge limit. We found the phase transition had occurred in this SUSY gauge theory non-perturbatively both with the fundamental matter

and the adjoint matter. In general, this phenomenon for the fundamental matter is called RW transition [54]. This fact supports our analysis.

In the fundamental matter case, phases appear in the order of A_3, A_1, A_2 as α moves from $\pi/3$ to $5\pi/3$. The critical αs coincide with the ones in the perturbative one-loop effective potential for non-supersymmetric theory on $R^3 \times S^1$ [49].

Phases with the adjoint matter appear in the order of C, B, A as α moves from 0 to π. When we increase α from π to 2π, the phases move to A, B and go back to C. The critical values for the imaginary chemical potential $\alpha = 0.3\pi$, 0.5π are determined by numerical calculation.

14.2 Discussion

We have 2 open questions for this model. First, in usual flat supersymmetric theories, contributions from bosons and fermions are canceled out completely. Therefore this effective potential for such models becomes flat(trivial). However, in our case, the potential is nontrivial. We guess this kind of a phenomenon caused by non-zero curvature effect. We need to investigate why the potential becomes nontrivial. Second, several previous works for RW transition had coupling constant dependence. However our model has no coupling constant after using the localization technique. In other words, our effective potential has no sensitivity for coupling constant. It is interesting to use other localization results which do depend on coupling constants.

14.3 Some issues

We would like to point out 2 issues of our analysis. First, we *assume* infinite volume limit is not spoiled by the GNO monopoles. In other words, we just dropped the contribution of m when we take large $\mathcal{R}$-charge limit. This assumption may be problematic because there are always monopoles with arbitrary large $|m|$, and in this case, the dropping of m becomes subtle. The second issue is related to the large $\mathcal{R}$-charge limit itself. In order to cause the symmetry breaking, we argue that the large Δ is necessary. However, Δ looks bounded in certain region. This restriction comes, naively speaking, from the sign of the quadratic potential for ϕ in the matter Lagrangian (11.5). If one wants to overcome this undesirable situation, it may be possible to recover it by adding certain SUSY-exact terms. Another way to recover it is taking $c = 0$. In this case, we have $\Delta \ll l$ and this condition makes the quadratic potential for ϕ to be zero. However these remedies are somewhat subtle. And these problems look very crucial. So we have to find better solutions.

14.4 Future direction

There are some extensions. One direction is to change background geometries. For example there are localization calculation results on D^2 [68, 69, 70] and $D^2 \times S^1$ [68]. As more phenomenological setup, we should consider theory on $M \times S^1/Z_2$ or Randall-Sundram spacetime. The Wilson line phase comes from these S^1 and S^1/Z_2. Another direction is the localization method in higher dimensional theories. For instance, we could apply results on $S^3 \times S^1$ [63] and $CP^2 \times S^1$ [64] to the exact calculation of the effective potential for the Wilson line phase.

Part III
APPENDIX

A Hermiticity of the Dirac operator in continuum theory

The continuum Dirac action in Minkowski space-time is given by

$$S_{\text{Minkowski}} = \int d^4x \bar{\psi}[i\gamma^\mu \partial_\mu - m]\psi. \tag{A.1}$$

We have two options to obtain the euclidian version of the gamma matrices.

1. All of gamma matrices taking as anti-hermitian.
2. All of gamma matrices taking as hermitian.

In this thesis use both of them. Following, we note the Dirac operator for both cases.

A.1 Anti-ermitian gamma matrices (Section 1)

In section 1, we employ anti-hermitian gamma matrices. These can be obtained by the definitions,

$$\gamma_E^4 = i\gamma^0, \tag{A.2}$$
$$\gamma_E^i = \gamma^i. \tag{A.3}$$

We let x^0 become pure imaginary ($dx^0 = -id\tau$, $i\partial_4 = \partial_0$), and use these definitions,

$$S_{\text{Minkowski}} \to +i \int d^4x_E \bar{\psi}[i\not{\partial} - m]\psi = iS_{\text{Euclid}}. \tag{A.4}$$

Here we changed variable $\psi \to \gamma_5\psi$ in order to flip the sign of the mass term. In this case, $\not{\partial}$ is an hermitian operator.

A.2 Hermitian gamma matrices (Other sections)

Except section1, we employ hermitian gamma matrices. These can be obtained by the definitions,

$$\gamma_E^4 = \gamma^0, \tag{A.5}$$
$$\gamma_E^i = -i\gamma^i \tag{A.6}$$

Use these definitions and same coordinate changing as first case,

$$S_{\text{Minkowski}} \to +i \int d^4x_E \bar{\psi}[\not{\partial} + m]\psi = iS_{\text{Euclid}}. \tag{A.7}$$

In this case, $\not{\partial}$ is an anti-hermitian operator. This corresponds to conventional notation used in literatures.

B Anomaly calculation in continuum theory

In this appendix, we derive anomaly term as a Jacobian for the path integral [5]. In order to clarify the meaning of path integral measure for fermions, we expand fermion fields to eigenfunction for Dirac operator[38] $\not{D}$,

$$\psi(x) = \sum_n a_n \phi_n(x) = \sum_n a_n \langle x|n\rangle, \tag{B.1}$$

$$\bar{\psi}(x) = \sum_n \bar{b}_n \phi_n^\dagger(x) = \sum_n \bar{b}_n \langle n|x\rangle, \tag{B.2}$$

where $\phi_n(x)$ is the eigenfunction which satisfy,

$$\not{D}\phi_n(x) = \lambda_n \phi_n(x), \tag{B.3}$$

$$\int d^4x \phi_n^\dagger(x)\phi_l(x) = \delta_{n,l}. \tag{B.4}$$

Perform $U(1)$ chiral transformation to fermion fields,

$$\psi(x) \to \psi'(x) = e^{i\alpha(x)\gamma_5}\psi(x) = \psi(x) + i\alpha(x)\gamma_5\psi(x), \tag{B.5}$$

$$\bar{\psi}(x) \to \bar{\psi}'(x) = \bar{\psi}(x)e^{i\alpha(x)\gamma_5} = \bar{\psi}(x) + \bar{\psi}(x)i\alpha(x)\gamma_5. \tag{B.6}$$

$$\psi'(x) \equiv \sum_n a'_n \phi_n(x), \tag{B.7}$$

$$= \sum_n a_n \phi_n(x) + i\alpha(x)\gamma_5 \sum_n a_n \phi_n(x), \tag{B.8}$$

multiply $\phi_m^\dagger(x)$ on the left and integrate over coordinate, we obtain,

$$a'_n = a_n + \sum_m i \int d^4x \phi_n^\dagger(x)\alpha(x)\gamma_5\phi_m(x)a_m. \tag{B.9}$$

In same way,

$$\bar{\psi}'(x) \equiv \sum_n \bar{b}'_n \phi_n^\dagger(x) \tag{B.10}$$

$$= \sum_n \bar{b}_n \phi_n^\dagger(x) + \sum_n \bar{b}_n \phi_n^\dagger(x) i\alpha(x)\gamma_5 \tag{B.11}$$

$$\bar{b}'_n = \bar{b}_n + \sum_m i\bar{b}_m \int d^4x \phi_n^\dagger(x)\alpha(x)\gamma_5\phi_m(x) \tag{B.12}$$

[38] In this section, we employ hermitian Dirac operator which same as Section 2.

$$\mathcal{D}\bar{\psi}\mathcal{D}\psi = [\det\langle n|x\rangle \det\langle x|n\rangle]^{-1} \lim_{N\to\infty}\prod_{n=1}^{N} d\bar{b}_n da_n \tag{B.13}$$

$$= [\det \int d^4x \langle n|x\rangle\langle x|n\rangle]^{-1} \lim_{N\to\infty}\prod_{n=1}^{N} d\bar{b}_n da_n \tag{B.14}$$

$$= (\delta_{n,m})^{-1} \lim_{N\to\infty}\prod_{n=1}^{N} d\bar{b}_n da_n \tag{B.15}$$

$$= \lim_{N\to\infty}\prod_{n=1}^{N} d\bar{b}_n da_n \tag{B.16}$$

Then, the Jacobian of the path integral can be expressed in terms of eigenmodes of the Dirac operator,

$$\mathcal{D}\bar{\psi}'\mathcal{D}\psi' = \lim_{N\to\infty}\prod_{n=1}^{N} d\bar{b}'_n da'_n, \tag{B.17}$$

where,

$$\prod_{n=1}^{N} d\bar{b}'_n da'_n = \det[\delta_{n,m} + i\int d^4x \phi_n^\dagger(x)\alpha(x)\gamma_5\phi_m(x)]^{-1}\prod_{n=1}^{N} d\bar{b}_n \tag{B.18}$$

$$\times \det[\delta_{n,m} + i\int d^4x \phi_n^\dagger(x)\alpha(x)\gamma_5\phi_m(x)]^{-1}\prod_{n=1}^{N} da_n. \tag{B.19}$$

Thus, the Jacobian for the path integral is expressed as,

$$\det[\delta_{n,m} + i\int d^4x \phi_n^\dagger(x)\alpha(x)\gamma_5\phi_m(x)]^{-2} = \exp\left[-2i\sum_n \int d^4x \phi_n^\dagger(x)\alpha(x)\gamma_5\phi_m(x)\right] \tag{B.20}$$

Here we note the path integral and the Jacobian symbolically,

$$\mathcal{D}\bar{\psi}'\mathcal{D}\psi' = J\mathcal{D}\bar{\psi}\mathcal{D}\psi, \tag{B.21}$$

$$J \equiv \exp[-2i \lim_{N\to\infty}\sum_{n=1}^{N}\int d^4x \phi_n^\dagger(x)\alpha(x)\gamma_5\phi_m(x)]. \tag{B.22}$$

Now we can evaluate the Jacobian for the path integral as,

$$\sum_{n=1}^{N}\int d^4x\alpha(x)\phi_n^\dagger(x)\gamma_5\phi_m(x) \equiv \lim_{M\to\infty}\sum_{n=1}^{\infty}\int d^4x\alpha(x)\phi_n^\dagger(x) f((\lambda_n)^2/M^2)\gamma_5\phi_m(x) \tag{B.23}$$

$$= \lim_{M\to\infty}\sum_{n=1}^{\infty}\int d^4x\alpha(x)\phi_n^\dagger(x) f(\not{D}^2/M^2)\gamma_5\phi_m(x) \tag{B.24}$$

$$\equiv \lim_{M\to\infty} \mathrm{Tr}\,[\alpha(x)\gamma_5 f(\not{D}^2/M^2)] \tag{B.25}$$

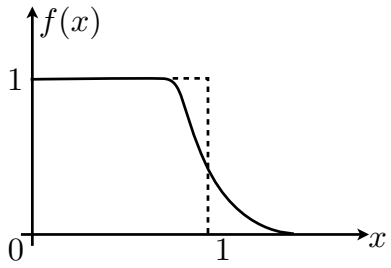

Figure 18: Typical behavior of the regulator function $f(x)$.

Where $f(x)$ is arbitrary cut-of function which satisfies,

$$f(0) = 1, \quad f(\infty) = 0, \quad xf'(x)|_{x=0} = xf'(x)|_{x=\infty} = 0. \tag{B.26}$$

This function is typically take a shape as in Fig. 18.

Now the functional trace is well regularized *i.e.* there are no ambiguity, we can expand in the plane wave basis for each position x.

$$\lim_{M\to\infty} \mathrm{tr}\,[\gamma_5 f(\not{D}^2/M^2)] = \mathrm{tr}\,[\int \frac{d^4k}{(2\pi)^4} e^{-ikx}\gamma_5 f(\not{D}^2/M^2)e^{ikx}] \tag{B.27}$$

The covariant derivative can be decomposed into two parts,

$$\not{D}^2 = \frac{1}{2}\{\gamma_\mu, \gamma_\nu\}D_\mu D_\nu + \frac{1}{2}[\gamma_\mu, \gamma_\nu]D_\mu D_\nu, \tag{B.28}$$

$$= D_\mu D^\mu - \frac{ig}{4}[\gamma^\mu, \gamma^\nu]F_{\mu,\nu}. \tag{B.29}$$

In addition, cut-off function with the covariant derivative is evaluated by,

$$e^{-ikx} f(\not{D}^2/M^2)e^{ikx} = e^{-ikx} f[(D_\mu D^\mu - \frac{ig}{4}[\gamma^\mu, \gamma^\nu]F_{\mu,\nu})/M^2]e^{ikx}, \tag{B.30}$$

$$= f\left(\frac{1}{M^2}(D_\mu + ik_\mu)(D^\mu + ik^\mu) - \frac{ig}{4}\frac{1}{M^2}[\gamma^\mu, \gamma^\nu]F_{\mu,\nu}\right). \tag{B.31}$$

Now our integral is well-defined because of the cut-off function, we can rescale $k_\mu \to Mk_\mu$,

$$\to f\left(-k_\mu k^\mu + \frac{2ik^\mu D_\mu}{M} + \frac{D_\mu D^\mu}{M^2} - \frac{ig}{4}\frac{1}{M^2}[\gamma^\mu, \gamma^\nu]F_{\mu,\nu}\right). \tag{B.32}$$

expand $f(x)$ around $x_0 = -k_\mu k^\mu = |k^2|$

$$f\left(-k_\mu k^\mu + \frac{2ik^\mu D_\mu}{M} + \frac{D_\mu D^\mu}{M^2} - \frac{ig}{4}\frac{1}{M^2}[\gamma^\mu, \gamma^\nu]F_{\mu,\nu}\right) \tag{B.33}$$

$$= f(-k_\mu k^\mu) + f'(-k_\mu k^\mu)\left(\frac{2ik^\mu D_\mu}{M} + \frac{D_\mu D^\mu}{M^2} - \frac{ig}{4}\frac{1}{M^2}[\gamma^\mu, \gamma^\nu]F_{\mu,\nu}\right) \tag{B.34}$$

$$+ f''(-k_\mu k^\mu)\left(\frac{2ik^\mu D_\mu}{M} + \frac{D_\mu D^\mu}{M^2} - \frac{ig}{4}\frac{1}{M^2}[\gamma^\mu, \gamma^\nu]F_{\mu,\nu}\right)^2 + \cdots \tag{B.35}$$

for spinor trace, most of gamma matrices vanish. The remnant corresponds to tr $\left[\gamma_5[\gamma^\mu,\gamma^\nu][\gamma^\alpha,\gamma^\beta]\right] = -16\epsilon^{\mu\nu\alpha\beta}$, we obtain,

$$\lim_{M\to\infty} \mathrm{tr}\,[\gamma_5 f(\not{D}^2/M^2)] = \mathrm{tr}\,[\gamma_5 \frac{1}{2!}(\frac{1}{4}[\gamma^\mu,\gamma^\nu]F_{\mu\nu})^2] \int \frac{d^4k}{(2\pi)^4} f''(-k_\mu k^\mu). \tag{B.36}$$

The integral in the final line can be calculated by using property of cut-off function $f(x)$,

$$\int \frac{d^4k}{(2\pi)^4} f''(-k_\mu k^\mu) = \frac{\pi^2}{16\pi^4}\int_0^\infty dr f''(r) \tag{B.37}$$

$$= \frac{1}{16\pi^2} r f'(r)|_0^\infty - \frac{1}{16\pi^2}\int_0^\infty dr f'(r) \tag{B.38}$$

$$= \frac{1}{16\pi^2} \tag{B.39}$$

We finally obtain following expression,

$$\lim_{M\to\infty} \mathrm{tr}\,[\gamma_5 f(\not{D}^2/M^2)] = \frac{N_f g^2}{32\pi^2}\mathrm{tr}\,[\epsilon^{\mu\nu\alpha\beta}F_{\mu\nu}F_{\alpha\beta}], \tag{B.40}$$

where N_f is the number of flavor which come from flavor trace. Therefore, the Jacobian for the path integral,

$$J = \exp\left[-2i\int d^4x \alpha(x)\frac{N_f g^2}{32\pi^2}\mathrm{tr}\,[\epsilon^{\mu\nu\alpha\beta}F_{\mu\nu}F_{\alpha\beta}]\right]. \tag{B.41}$$

This is the Jacobian for $U(1)$ chiral transformation *i.e.* $U(1)_A$ anomaly.

C Proof of Nambu-Goldstone theorem

We review a proof of Nambu-Goldstone theorem from the point of view of the Green function [73]. Here we consider only scaler field for simplicity. One of merit of this method is proof is independent of the order parameter is elementary or composite field in the Lagrangian. In this section, we use operator formalism in the Minkowski space. We start from classical argument. Consider action of relativistic scaler fields, $S = \int d^4x \mathcal{L}(\phi, \partial\phi)$. If a transformation δ^A preserve the form of the action *i.e.* $\delta^A S = 0$, we can define the current which satisfies conservation law $\partial^\mu J^A_\mu = 0$. This fact is called Nöther theorem. In this case, we may define conserved charge operator $Q^A = \int d^3x J^A_\mu$. In the quantum field theory, previous charge leads a infinitesimal transformation for the scaler field,

$$\phi(x) \to \phi'(x) = e^{i\epsilon_A Q^A}\phi(x)e^{-i\epsilon_A Q^A} \tag{C.1}$$

or samely,

$$\delta^A\phi(x) = [iQ^A, \phi(x)]. \tag{C.2}$$

n–point Green function is defined by, $G_n(x_1, x_2, \ldots, x_n) = \langle 0|T\phi_1(x_1)\phi_2(x_2)\cdots\phi_n(x_n)|0\rangle$. And this transformed as,

$$G_n \to G'_n = \langle 0|T\phi'_1(x_1)\phi'_2(x_2)\cdots\phi'_n(x_n)|0\rangle = \langle 0'|T\phi_1(x_1)\phi_2(x_2)\cdots\phi_n(x_n)|0'\rangle \tag{C.3}$$

$|0'\rangle = e^{-i\epsilon_A Q^A}|0\rangle$.

$$\delta G_n \equiv G'_n - G_n = \epsilon_A \delta^A G_n \tag{C.4}$$

Here we assume symmetry breaking *i.e.* $|0'\rangle = e^{-i\epsilon_A Q^A}|0\rangle \neq |0\rangle$

Variation $\delta^A G_n$ called an order parameter. Oder parameters are not local in general but could be local if all arguments taken to identical limit, $x_1 = \cdots = x_n$. Local composite operator are called condensates[39].

$$\begin{aligned}\delta^A G_n(x_1,\ldots,x_n) &= \langle 0|[iQ^A, T\phi_1(x_1)\phi_2(x_2)\cdots\phi_n(x_n)]|0\rangle &\text{(C.5)}\\ &= \langle 0|[iQ^A, T\phi_1(x_1)]\phi_2(x_2)\cdots\phi_n(x_n)|0\rangle \\ &\quad + \langle 0|T\phi_1(x_1)[iQ^A,\phi_2(x_2)]\cdots\phi_n(x_n)|0\rangle + \cdots \\ &\quad + \langle 0|T\phi_1(x_1)\phi_2(x_2)\cdots[iQ^A,\phi_n(x_n)]|0\rangle &\text{(C.6)}\end{aligned}$$

Here we define current matrix element with momentum q_μ,

$$M^A_\mu(q,x_1,\ldots,x_n) \equiv \int d^4z e^{iqz}\langle 0|TJ^A_\mu\phi_1(x_1)\cdots\phi_n(x_n)|0\rangle \tag{C.7}$$

,

$$\begin{aligned}\lim_{q_\mu\to 0} q^\mu M^A_\mu &= \lim_{q_\mu\to 0}\int d^z e^{iqz}(i\partial^\mu_z)\langle 0|TJ^A_\mu\phi_1(x_1)\cdots\phi_n(x_n)|0\rangle &\text{(C.8)}\\ &= \langle 0|T[iQ^A,\phi_1(x_1)]\phi_2(x_2)\cdots\phi_n(x_n)|0\rangle + \cdots + \langle 0|T\phi_1(x_1)\cdots[iQ^A,\phi_n(x_n)]|0\rangle &\text{(C.9)}\\ &= \delta^A G_n(x_1,\ldots,x_n) &\text{(C.10)}\end{aligned}$$

here we assumed current conservation $\partial^\mu J^A_\mu = 0$ in quantum level[40] and $\partial^\mu_z T\partial^A_\mu(z)\phi(x) = [J^A_0,\phi(x)]\delta(z^0-x^0)$.
Thus, if we have at least one oder parameter is non-zero *i.e.* $\delta^A G_n \neq 0$, corresponding M^A_μ has a pole at $q^2 = 0$:

$$M^A_\mu(q,x_1,\ldots,x_n) \sim \frac{q_\mu}{q^2}\delta^A G_n(x_1,\ldots,x_n) \tag{C.11}$$

Thus, if we have a conservation current and corresponding order parameter $\neq 0$, we obtain massless particle (pole) in the S-matrix[41].

D Quark line diagram

In this subsection, briefly review quark line diagram with some examples. Our notation of braket is summarized in Appendix E. We use expectation value defined by (E.2) (E.1).

[39] In QCD case, the oder parameter for $SU(2)$ chiral symmetry is called chiral condensation, which defined by, $\langle\bar\psi\psi\rangle = \lim_{m\to 0}\lim_{V\to\infty}\lim_{x\to 0}\langle T\bar\psi(x)\psi(0)\rangle = -\lim_{m\to 0}\lim_{V\to\infty}\lim_{x\to 0}\frac{i}{N_f}\mathrm{tr}\,G(x)$ [74].

[40] If there is an anomaly, this assumption does not hold.

[41] If S-matrix has a single pole, the pole corresponds to an elementary/composite particle (See Chapter 10 in [75]). In the case of QCD, this massless pole corresponds to π mesons, which are the composite particles of quarks.

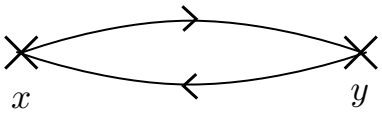

Figure 19: Connected part of the quark line diagram.

Consider correlator of π^+ and π^-,

$$\langle \pi^+(x)\pi^-(y)\rangle_{\rm QCD} = \langle [\bar\psi(x)\tau^+\gamma_5\psi(x)][\bar\psi(y)\tau^-\gamma_5\psi(y)]\rangle_{\rm QCD} \tag{D.1}$$
$$= \langle [\bar u(x)\gamma_5 d(x)][\bar d(y)\gamma_5 u(y)]\rangle_{\rm QCD} \tag{D.2}$$

Apply Wick contraction.

$$\langle \pi^+(x)\pi^-(y)\rangle_{\rm QCD} = -\langle {\rm tr}\,\gamma_5 \not{D}^{-1}_{xy}\gamma_5 \not{D}^{-1}_{yx}\rangle_A \tag{D.3}$$

This can be drown by diagrammatically in Fig. 19. Solid lines represents background field dependent quark propagator $\not{D}^{-1}_{xy}$. This graphical representation similar to Feynman diagram. The difference is, this representation only the quark lines directly connected to the external courses are visible. Final line of last equation can be represent in terms of the path integral,

$$\langle {\rm tr}\,\gamma_5 \not{D}^{-1}_{xy}\gamma_5 \not{D}^{-1}_{yx}\rangle_A = \int [\mathcal{D}A_\mu] {\rm Det}\,[\not{D}(A_\mu)+m]{\rm tr}\,[\gamma_5 \not{D}^{-1}_{xy}\gamma_5 \not{D}^{-1}_{yx}]\exp\left[-S_{\rm YM}[A_\mu]\right] \tag{D.4}$$

Here, Let us analyze derivative of ${\rm Det}\,[\not{D}(A_\mu)+m]$ with respect to mass m as we mentioned in Section 4. First, functional determinant is given by,

$${\rm Det}\,[\not{D}(A_\mu)+m] = \int \mathcal{D}\bar\psi\mathcal{D}\psi e^{\int d^4x\bar\psi[\not{D}_{(A_\mu)}+m]\psi}. \tag{D.5}$$

Take a derivative with respect to m, we obtain bilinear term of fermion fields,

$$\frac{\partial}{\partial m}{\rm Det}\,[\not{D}(A_\mu)+m] = \int \mathcal{D}\bar\psi\mathcal{D}\psi \frac{\partial}{\partial m} e^{\int d^4x\bar\psi[\not{D}_{(A_\mu)}+m]\psi}, \tag{D.6}$$
$$= \bar\psi\psi. \tag{D.7}$$

If we integrate over gauge configuration,

$$\int [\mathcal{D}A_\mu]\frac{\partial}{\partial m}{\rm Det}\,[\not{D}(A_\mu)+m] = \langle\bar\psi\psi\rangle_m \tag{D.8}$$

Right hand side is a one point function, thus this contribution is called disconnected in the context of the quark line diagram. In the first Cohen's argument, he ignored this contribution as we reviewed in Section 4.

E Banks-Chaser-like relations

Meson correlators are defined by (3.42),

$$\pi^a(x) = i\bar\psi(x)\gamma_5\tau^a\psi(x), \quad \sigma(x) = \bar\psi(x)\psi(x),$$
$$\delta^a(x) = \bar\psi(x)\tau^a\psi(x), \quad \eta(x) = i\bar\psi(x)\gamma_5\psi(x).$$

Here we write $SU(2)$ index explicitly[42]. In this section we employ following notation to clarify the meaning of bra-kets for the expectation value for an operator $\mathcal{O}$,

$$\langle \mathcal{O} \rangle_{\rm QCD} = \int [\mathcal{D}A_\mu] \mathcal{D}\bar{\psi} \mathcal{D}\psi \mathcal{O} \exp\left[-S_{\rm YM}[A_\mu] - \int d^4x \bar{\psi} [\not{D} + m] \psi \right], \tag{E.1}$$

$$\langle \mathcal{O} \rangle_A = \int [\mathcal{D}A_\mu] {\rm Det}\left[\not{D}(A_\mu) + m \right] \mathcal{O} \exp\left[-S_{\rm YM}[A_\mu] \right] \tag{E.2}$$

where the volume of integration domain of the action is taken to be V. After here, we suppress the gauge field dependence on $\not{D}(A_\mu)$.

Note that, every physical quantity which we are interested in is a physical quantity at infinite volume, especially order parameters of symmetry breaking. However we can not start from infinite volume because of existence of infrared divergence. Therefore we have to start from field theory in compact space-time. In the compact space-time, any symmetries do not break spontaneously, we need to introduce source term in order to break symmetry. The oder of limit is essential for discussion of symmetry breaking. Thus, to discuss symmetry breaking, firstly we start from quantum field theory in compact space-time, secondly we introduce source term, thirdly we take thermodynamic limit, finally we take source term vanishing limit. For example, we are interested in chiral condensate at infinite volume limit, which is an order parameter of chital symmetry breaking. Then, we should define chiral condensate as,

$$\langle \bar{\psi}\psi \rangle \equiv \lim_{m \to 0} \lim_{V \to \infty} \langle \bar{\psi}\psi \rangle_{\rm QCD}, \tag{E.3}$$

where bra-ket in left hand side is defined by right hand side. If we first take a quark mass vanishing limit in right hand side, chiral condensate is zero. In practical numerical calculation, we have to take care about the order of limits.

The eigenvector (function) and eigenvalue for the Dirac operator in the continuum Euclidian space-time is given by,

$$\not{D}\psi_j(x) = i\lambda_j \psi_j(x), \tag{E.4}$$

where λ_j is a real number. $\psi_j(x)$ has spinor and color indices, and which is orthogonalized and normalized as,

$$\int d^4x \psi_j^\dagger(x) \psi_k(x) = \delta_{jk}. \tag{E.5}$$

The spectral density or the Dirac spectrum $\rho(\lambda)$ is defined by[43],

$$\rho_A(\lambda) = \frac{1}{V} \sum_j \delta(\lambda - \lambda_j) \tag{E.6}$$

$$\rho(\lambda) = \langle \rho_A(\lambda) \rangle_A. \tag{E.7}$$

Following, we derive relations between the spectral density and mesonic observables.

[42] In the quantum field theory, composite operators should be defined by normal ordering. In this thesis, all of composite operators taken normal ordering implicitly.

[43] $\rho(\lambda)$ actually has the volume dependence. However we do not note volume dependence for simplicity.

E.1 Banks-Casher relation

Here we review derivation of the Banks-Casher relation. We start from chiral condensation at finite volume with finite quark mass.

$$\langle\bar{\psi}\psi\rangle_{\rm QCD} = -\langle\frac{1}{V}\int d^4x \ \ {\rm tr}\,[\frac{1}{\not{D}+m}]\rangle_A \tag{E.8}$$

$$= -\langle\frac{1}{V}\int d^4x \ \ \sum_j \psi_j^\dagger(x)[\frac{1}{\not{D}+m}]\psi_j(x)\rangle_A \tag{E.9}$$

$$= -\langle\frac{1}{V}\sum_j[\frac{1}{i\lambda_j+m}]\rangle_A \tag{E.10}$$

in the first line, we integrated out all of Grassmannian variables by using Matthew's formula, next line, we expanded trace in the Dirac eigen function, in the final line, we used orthogonality of the Dirac eigen function.

$$\langle\bar{\psi}\psi\rangle_{\rm QCD} = -\int_{-\infty}^{\infty}d\lambda\frac{\rho(\lambda)}{i\lambda+m} \tag{E.11}$$

$$= -\frac{1}{i}\int_{-\infty}^{\infty}d\lambda\frac{\rho(\lambda)}{\lambda-im} \tag{E.12}$$

$$\langle\bar{\psi}\psi\rangle = \lim_{m\to 0}\lim_{V\to\infty}\langle\bar{\psi}\psi\rangle_{\rm QCD} \tag{E.13}$$

$$= -\lim_{m\to 0}\frac{1}{i}\int_{-\infty}^{\infty}d\lambda\frac{\rho(\lambda)}{\lambda-im} \tag{E.14}$$

Here we use following formula,

$$\frac{1}{x\pm i\epsilon} = \mathcal{P}[\frac{1}{x}] \mp i\pi\delta(x). \tag{E.15}$$

We assume $\rho(-\lambda)=\rho(\lambda)$ as mentioned before,

$$\langle\bar{\psi}\psi\rangle = \frac{1}{-i}\int_{-\infty}^{\infty}d\lambda\rho(\lambda)[\mathcal{P}[\frac{1}{\lambda}+i\pi\delta(\lambda)] \tag{E.16}$$

$$= -\pi\rho(0) \tag{E.17}$$

This is the Banks-Casher relation. The relative signature of this relation corresponds to signature of mass term in the Lagrangian. Another representation of Banks-Casher relation is obtained from (E.12),

$$\langle\bar{\psi}\psi\rangle_{\rm QCD} = -\frac{1}{i}\int_{-\infty}^{\infty}d\lambda\rho(\lambda)\frac{1}{\lambda-im}\frac{\lambda+im}{\lambda+im} \tag{E.18}$$

$$= \frac{1}{-i}\int_{-\infty}^{\infty}d\lambda\rho(\lambda)\frac{\lambda+im}{\lambda^2+m^2} \tag{E.19}$$

$$= -\int_{-\infty}^{\infty}d\lambda\rho(\lambda)\frac{m}{\lambda^2+m^2} \tag{E.20}$$

$$= -\int_{0}^{\infty}d\lambda\rho(\lambda)\frac{2m}{\lambda^2+m^2} \tag{E.21}$$

Finally we obtain the relation between $\rho(\lambda)$ and chiral condensate as mentioned in main body,

$$|\langle\bar{\psi}\psi\rangle| = \lim_{m\to 0}\int_0^\infty d\lambda\rho(\lambda)\frac{2m}{\lambda^2+m^2}. \tag{E.22}$$

E.2 Spectral representation of $\chi_{U(1)_A}$

Here we start from the definition of the $\mathrm{U(1)_A}$ susceptibility $\chi_{U(1)_A}$,

$$\chi_{U(1)_A} = \int d^4x\langle\pi^a(x)\pi^a(0) - \delta^a(x)\delta^a(0)\rangle_{\mathrm{QCD}}. \tag{E.23}$$

Pion correlator can be expressed by using the Dirac operator,

$$\langle\pi^a(x)\pi^b(y)\rangle_{\mathrm{QCD}} = \langle\mathrm{tr}\,[\gamma_5\left[\frac{1}{\not{D}+m}\right]_{yx}\tau^a\gamma_5\left[\frac{1}{\not{D}+m}\right]_{xy}\tau^b]\rangle_A \tag{E.24}$$

$$-\langle\mathrm{tr}\,[\left[\frac{1}{\not{D}+m}\right]_{xx}\tau^a]\rangle_A\langle\mathrm{tr}\,[\left[\frac{1}{\not{D}+m}\right]_{yy}\tau^b]\rangle_A. \tag{E.25}$$

Now we can evaluate the trace of the Dirac operator in terms of its eigenmodes,

$$\int d^4x\langle\pi^a(x)\pi^a(0)\rangle_{\mathrm{QCD}} = \langle\mathrm{Tr}\,[\gamma_5\frac{1}{\not{D}+m}\gamma_5\frac{1}{\not{D}+m}]\rangle_A \tag{E.26}$$

$$= \langle\mathrm{Tr}\,[\frac{1}{\not{D}^\dagger+m}\frac{1}{\not{D}+m}]\rangle_A \tag{E.27}$$

$$= \int_{-\infty}^\infty d\lambda\rho(\lambda)\frac{1}{-i\lambda+m}\frac{1}{i\lambda+m}. \tag{E.28}$$

Similarly, δ correlator is evaluated as,

$$\int d^4x\langle\delta^a(x)\delta^a(0)\rangle_{\mathrm{QCD}} = -\langle\mathrm{Tr}\,[\frac{1}{\not{D}+m}\frac{1}{\not{D}+m}]\rangle_A \tag{E.29}$$

$$= -\int_{-\infty}^\infty d\lambda\rho(\lambda)\frac{1}{i\lambda+m}\frac{1}{i\lambda+m}. \tag{E.30}$$

Finally, we institute concrete expression into the definition of the $\mathrm{U(1)_A}$ susceptibility,

$$\chi_{U(1)_A} = \int_{-\infty}^\infty d\lambda\rho(\lambda)\frac{1}{i\lambda+m}[\frac{1}{-i\lambda+m}+\frac{1}{i\lambda+m}] \tag{E.31}$$

$$= \int_{-\infty}^\infty d\lambda\rho(\lambda)\frac{1}{i\lambda+m}\frac{2m}{\lambda^2+m^2} \tag{E.32}$$

$$= \int_{-\infty}^\infty d\lambda\rho(\lambda)\frac{1}{i\lambda+m}\frac{-i\lambda+m}{-i\lambda+m}\frac{2m}{\lambda^2+m^2} \tag{E.33}$$

$$= \int_{-\infty}^\infty d\lambda\rho(\lambda)\frac{-i\lambda+m}{\lambda^2+m^2}\frac{2m}{\lambda^2+m^2} \tag{E.34}$$

$$= \int_0^\infty d\lambda\rho(\lambda)\frac{4m^2}{(\lambda^2+m^2)^2}. \tag{E.35}$$

The final line is the expression as we seen in the main body.

F Realization of chiral symmetry on the lattice

In this appendix, we discuss properties of chiral fermion on a lattice. This section is based on [5, 16]

F.1 Properties of lattice fermions

F.1.1 Properties of staggered fermion

In this subsection we briefly summarize another "chiral" fermion called staggered fermion. Staggered fermion action describe 4 flavor fermion[44] simultaneously, which has remnant $U(1)$ chiral symmetry. In order to perform two flavor simulation, one must use rooting technique. Staggered fermion action is given by,

$$S_{\rm ks} \equiv \bar{\psi} D_{\rm ks}(M)\psi \tag{F.1}$$

$$= \bar{\psi}\left[(\gamma_\mu \otimes \mathbf{1})\frac{\nabla_\mu}{2} + (\gamma_5 \otimes t_\mu t_5)\frac{\nabla_\mu^2}{2} + M(\mathbf{1}\otimes\mathbf{1})\right]\psi, \tag{F.2}$$

where ∇_μ corresponds to first derivative on the lattice (difference). t_μ, t_5 are gamma matrices which describe flavor structure. The staggered fermion is invariant under the chiral transformation,

$$\psi \to e^{i\theta(\gamma_5\otimes t_5)}\psi, \quad \bar{\psi} \to \bar{\psi}e^{i\theta(\gamma_5\otimes t_5)}. \tag{F.3}$$

If gauge interaction into account, flavor symmetry breaks down. This causes breaking of degeneracy of the pions. HISQ is one of improved staggered fermion, which has better flavor symmetry. However flavor symmetry is still violated.

F.1.2 Proof of the overlap-Dirac operator satisfy Ginsparg-Wilson relation

Here we change variable in the massless overlap-Dirac operator with Wilson kernel[45],

$$D_{\rm ov} = \frac{1}{R}(1+V), \tag{F.4}$$

where

$$V = A(A^\dagger A)^{-1/2}, \quad A = -M + D_W(m=0) \tag{F.5}$$

where $-M < 0$ is a negative mass term with cutoff scale ($\sim 1/a$). V satisfy following property,

$$\gamma_5 V \gamma_5 = V^\dagger, \tag{F.6}$$

$$VV^\dagger = 1, \tag{F.7}$$

[44] The flavor symmetry for staggered fermion called taste symmetry.

[45] Here we use another notation for Willson-Dirac operator for simplicity *i.e.* $A = D_W(-M)$, $V = \mathrm{sgn}$.

because,

$$\gamma_5 V \gamma_5 = \gamma_5 A (A^\dagger A)^{-1/2} \gamma_5 \tag{F.8}$$
$$= \gamma_5 A \gamma_5 \gamma_5 (A^\dagger \gamma_5 \gamma_5 A)^{-1/2} \gamma_5 \tag{F.9}$$
$$= A^\dagger \gamma_5 (A^\dagger \gamma_5 \gamma_5 A)^{-1/2} \gamma_5 \tag{F.10}$$
$$= A^\dagger (A A^\dagger)^{-1/2} \tag{F.11}$$
$$= \sum_n a_n A^\dagger (A A^\dagger)^n \tag{F.12}$$
$$= \sum_n a_n (A^\dagger A)^n A^\dagger \tag{F.13}$$
$$= (A^\dagger A)^{-1/2} A^\dagger = V^\dagger. \tag{F.14}$$

Then we can calculate following equation,

$$\gamma_5 \frac{1}{R D_{\rm ov}} \gamma_5 = \frac{1}{1 + \gamma_5 V \gamma_5} = \frac{V}{V+1} = 1 - \frac{1}{1+V}. \tag{F.15}$$

From this explosion, one can derive Ginsparg-Wilson relation. Note that, if we employ approximation for the sign function V, *i.e.* in the case of domain-wall fermion, Eq. (F.7) does not establish.

F.1.3 Massless chiral fermion in the overlap fermion

Here we review how the overlap fermion describe massless chiral fermion. In the free case, Wilson-Dirac operator in the overlap-Dirac operator is given by,

$$A = -M + \sum_\mu \gamma_\mu \sin p_\mu + \sum_\mu (1 - \cos p_\mu). \tag{F.16}$$

Thus, we obtain following relation,

$$A^\dagger A = s^2 + M(p), \tag{F.17}$$

and here we define $s^2 = \sum_\mu (\sin(p_\mu))^2$, $M(p) = -M + \sum_\mu (1 - \cos(p_\mu))$.

In IR physics, low-lying modes is relevant. Expand $M(p)$ for modes with $p_\mu \sim 0$,

$$M(p) = -M + \mathcal{O}(a^2), \tag{F.18}$$

and institute the definition of the overlap operator,

$$D_{\rm ov} = \frac{1}{R}\left[1 + \frac{i\not{p} - M}{M}\right]. \tag{F.19}$$
$$= \frac{1}{RM} i\not{p} \tag{F.20}$$

In this way overlap-Dirac operator describe massless fermion. In other words, overlap fermion is a infinitely tuned Wilson fermion thorough the fraction term.

For doubler modes, which momentum around boundary of the Brillouin zone, $p_\mu \sim \pi$. Expand $M(p)$ around $p_\mu \sim \pi$,

$$M(p) = -M + 2n + \mathcal{O}(a^2), \tag{F.21}$$

where n is the number of π. If we assume $0 < M < 2$, the overlap-Dirac operator becomes,

$$D_{\rm ov} = \frac{1}{R}\left[1 + \frac{i\not{p} - M + 2n}{2n - M}\right] \tag{F.22}$$

$$= \frac{1}{R(2n-M)}\left[i\not{p} + 2(2n - M)\right]. \tag{F.23}$$

Thus, doubler modes have cut-off scale mass. In this way overlap-Dirac operator suppress doubler modes.

F.2 Properties of eigenvalues of Ginsparg-Wilson Dirac operator

In this sub sub section, we summarize properties of eigenvalues of Dirac operator which satisfy Ginsparg-Wilson relation. Following, we take operator R is local, *i.e.* $R\delta_{nm}$ for simplicity. Let us assume gamma 5 hermiticity for D, *i.e.* $\gamma_5 D\gamma_5 = D^\dagger$, then $H \equiv \gamma_5 D$ becomes a hermitian operator. After here we focus on this hermitian Dirac operator H.

Modified gamma 5 operator $\hat{\gamma}_5 = \gamma_5(1 - \frac{R}{2}D)$ is anti-commute with H,

$$H\hat{\gamma}_5 + \hat{\gamma}_5 H = \gamma_5(D\gamma_5 - D\gamma_5 RD + \gamma_5 D) = 0. \tag{F.24}$$

Here Ginsparg-Wilson relation is used. Then, eigenvalues of H can be described as,

$$H\phi_n = \lambda_n \phi_n \tag{F.25}$$

$$H(\hat{\gamma}_5\phi_n) = -\lambda_n(\hat{\gamma}_5\phi_n), \tag{F.26}$$

where ϕ_n is eigenfunction(vector), and λ_n is real eigenvalue. As we show below, eigenmodes are paired except for zero modes and $\lambda_n = \pm\frac{2}{R}$ modes (Doubler modes, $\hat{\gamma}_5\phi_n = 0$).

Property of zero-modes $\lambda_n = 0$

Zero modes are eigenmodes of the γ_5,

$$\gamma_5\phi = \pm\phi \tag{F.27}$$

In main body of this thesis, we use this fact to distinguish exact zero modes from other near zero modes.

Property of bulk modes

$$H\phi_n = \lambda_n\phi_n \tag{F.28}$$

$$H\hat{\gamma}_5\phi_n = -\lambda_n\hat{\gamma}_5\phi_n. \tag{F.29}$$

Here we multiply $\phi^\dagger$ from left, and ϕ from right,

$$\phi^\dagger\hat{\gamma}_5\phi = 0 \tag{F.30}$$

$$\phi^\dagger\gamma_5\phi = \frac{R}{2}\lambda_n \tag{F.31}$$

$$|\frac{R}{2}\lambda_n| = |\phi^\dagger\gamma_5\phi| \le |\phi^\dagger||\gamma_5\phi| = 1. \tag{F.32}$$

$|\lambda_n| < \frac{2}{R}$

Property of doubler modes $\lambda_n = \pm\frac{2}{R}$

$$\hat{\gamma}_5\phi_n = 0 \tag{F.33}$$

$$H\phi_n = \pm\frac{2}{R}\phi_n, \quad \gamma_5\phi_n = \pm\phi_n \tag{F.34}$$

Atiyah-Singer index theorem on the lattice

The Dirac operator which satisfy the Gisparg-Wilson relation, also satisfy the index theorem,

$$\mathrm{Tr}\,\hat{\gamma}_5 = n_+ - n_-. \tag{F.35}$$

Proof of the index theorem is straightforward.

$$\begin{aligned}
\mathrm{Tr}\,\hat{\gamma}_5 &= \sum_n \psi_n^\dagger \hat{\gamma}_5 \phi_n && \text{(F.36)}\\
&= \sum_{\lambda_n=0} \psi_n^\dagger \hat{\gamma}_5 \phi_n + \sum_{0<|\lambda_n|<2/(Ra)} \psi_n^\dagger \hat{\gamma}_5 \phi_n + \sum_{\lambda_n=\pm 2/(Ra)} \psi_n^\dagger \hat{\gamma}_5 \phi_n && \text{(F.37)}\\
&= \sum_{\lambda_n=0} \psi_n^\dagger \gamma_5 \phi_n && \text{(F.38)}\\
&= n_+ - n_-. && \text{(F.39)}
\end{aligned}$$

Then, *r.h.s* of Eq. (F.35) can be regard as topological charge, and zero modes called exact zero modes or topological zero modes.

F.3 Anomaly arguments on the lattice via Ginsparg-Wilson relation

The chiral anomaly on the lattice can be define by using Ginsparg-Wilson relation. Details are in [5]. Here we start from following partition function,

$$Z_{\mathrm{ov}} = \int \mathcal{D}\bar{\psi}\mathcal{D}\psi \exp\left[\sum_{x,y} \bar{\psi}(x) D_{\mathrm{ov}}(x,y)\psi(y)\right]. \tag{F.40}$$

Here we assume $D_{\mathrm{ov}}(x,y)$ satisfies the Ginsparg-Wilson relation. This action is invariant under the transformation (5.13), then we obtain,

$$\int \mathcal{D}\bar{\psi}\mathcal{D}\psi \exp\left[\sum_{x,y} \bar{\psi}(x) D_{\mathrm{ov}}(x,y)\psi(y)\right] = \int \mathcal{D}\bar{\psi}\mathcal{D}\psi J \exp\left[\sum_{x,y} \bar{\psi}(x) D_{\mathrm{ov}}(x,y)\psi(y)\right], \tag{F.41}$$

where J is a Jacobian for this $U(1)$ chiral transformation,

$$J = \exp\left[-2i\mathrm{Tr}\,\hat{\gamma}_5\right] \tag{F.42}$$

After here we choose $R = 2$ in the Ginsparg-Wilson relation and explicitly note cut-off a,

$$\int \mathcal{D}\bar{\psi}\mathcal{D}\psi \exp\left[a^4 \sum_{x,y} \bar{\psi}(x) D_{\mathrm{ov}}(x,y)\psi(y)\right] \tag{F.43}$$

$$\delta\psi(y) = \sum_w i\alpha\gamma_5(1-2D_{\rm ov})\psi(w), \quad \delta\bar{\psi}(x) = \bar{\psi}i\alpha\gamma_5 \tag{F.44}$$

here α is a constant. Now we can evaluate the Jacobian as follows.

$$\begin{aligned} J &= \exp\left[-2i\alpha{\rm Tr}\left[\gamma_5(1-D_{\rm ov})\right]\right] && \text{(F.45)}\\ &= \exp\left[-2i\alpha{\rm Tr}\left[\hat{\gamma}_5\right]\right] && \text{(F.46)}\\ &= \exp\left[-2i\alpha N_f(n_+-n_-)\right] && \text{(F.47)} \end{aligned}$$

On the other hand, for $H=\gamma_5 D_{\rm ov}$, we can derive another expression for the Jacobian. In order to regulate the trace, we introduce heat kernel regularization factor for the trace,

$$\begin{aligned} \frac{1}{a^4}{\rm tr}\left[\hat{\gamma}_5 f(H^2/M^2)\right](x,x) &= \sum_n \phi_n^\dagger(x)\hat{\gamma}_5 f(H^2/M^2)\phi_n(x) && \text{(F.48)}\\ &= \frac{1}{a^4}{\rm tr}\left[(\gamma_5 - H)f(H^2/M^2)\right](x,x) && \text{(F.49)} \end{aligned}$$

The term includes $Hf(H^2/M^2)$ does not affect to the Jacobian near the continuum limit because,

$$\begin{aligned} \frac{1}{a^4}{\rm tr}\left[Hf(H^2/M^2)\right](x,x) &= \sum_n \phi_n^\dagger(x)Hf(H^2/M^2)\phi_n(x) && \text{(F.50)}\\ &\to 0. && \text{(F.51)} \end{aligned}$$

Thus, evaluation of $(\gamma_5)f(H^2/M^2)$ is enough to calculate the Jacobian,

$$\begin{aligned} \lim_{a\to 0}\frac{1}{a^4}{\rm tr}\left[\gamma_5 f(H^2/M^2)\right](x,x) &= \lim_{a\to 0}{\rm tr}\left[\int_{-\frac{\pi}{2a}}^{\frac{\pi}{2a}}\frac{d^4k}{(2\pi)^4}e^{ikx}\gamma_5 f(H^2/M^2)e^{-ikx}\right] && \text{(F.52)}\\ &= \lim_{\Lambda\to\infty}\lim_{a\to 0}{\rm tr}\left[\int_{-\Lambda}^{\Lambda}\frac{d^4k}{(2\pi)^4}e^{ikx}\gamma_5 f(H^2/M^2)e^{-ikx}\right] && \text{(F.53)}\\ &= \lim_{\Lambda\to\infty}{\rm tr}\left[\int_{-\Lambda}^{\Lambda}\frac{d^4k}{(2\pi)^4}e^{ikx}\gamma_5 f((i\gamma_5\not{D})^2/M^2)e^{-ikx}\right] && \text{(F.54)}\\ &= {\rm tr}\left[\gamma_5 f(\frac{\not{D}^2}{M^2})\right](x). && \text{(F.55)} \end{aligned}$$

Chase the equality, we finally obtain,

$$n_+ - n_- = {\rm Tr}\left[\gamma_5 f(\frac{\not{D}^2}{M^2})\right] = \int d^4x {\rm tr}\left[2\frac{N_f}{32\pi^2}\epsilon^{\mu\nu\alpha\beta}F_{\mu\nu}F_{\alpha\beta}\right]. \tag{F.56}$$

F.4 A Construction of chiral fermion on the lattice

To realize chiral symmetric fermion, we construct domain-wall fermion. The domain-wall fermion is one of 4 dimensional chiral fermion which constructed from 5 dimensional theory. In this subsection, we starting from continuum 5 dimensional theory to explain why 4 dimension chiral fermion arises from 5 dimensional theory and following sub subsection, we construct 4 dimensional effective action for (generalized) domain-wall fermion. In next subsection, taking appropriate limit for domain-wall fermion, we construct overlap fermion.

F.4.1 Continuum example for domain-wall fermion

Here we review how chiral fermion emerges from higher dimensional theory based on [16]. Consider free Dirac action in continuum 5-dimensional space,

$$S = \int d^4x ds \bar{\psi}(x,s) \left[\sum_{M=1}^{5} \gamma_M \partial_M - m(s) \right] \psi(x,s). \tag{F.57}$$

where $m(s)$ is a coordinate dependent mass term,

$$m(s) = \begin{cases} +m_0 & , \ s > 0 \\ 0 & , \ s = 0 \\ -m_0 & , \ s < 0 \ . \end{cases}$$

Solve equation of motion for this action to verify this action describe chiral fermion in 4 dimensional space.

$$\left[\sum_{M=1}^{5} \gamma_M \partial_M - m(s) \right] \psi(x,s) = 0. \tag{F.58}$$

Here we assume separation of variables type solution $\psi(x,s) = \phi(x)f(s)$, $\phi(x)$ contains all of spinor index and $f(s)$ is a scaler function. The action has translational invariance for 4 dimensional direction, so we can expand plain wave, then we obtain following explosion.

$$[\sum_{\mu=1}^{4} i\gamma_\mu p_\mu]u(p)f(s) + [\gamma_5 \partial_s f(s) - m(s)f(s)]u(p) = 0. \tag{F.59}$$

here $u(p)$ is a Fourier transformed wave function of $\phi(x)$. If $u(p)$ satisfy a Dirac equation for massless particle $[\sum_{\mu=1}^{4} i\gamma_\mu p_\mu]u(p) = 0$, *i.e.* last square bracket term needs to 0. Following condition is a sufficient condition.

$$\gamma_5 u(p) = \pm u(p) \tag{F.60}$$

$$\pm \partial_s f(s) - m(s)f(s) = 0. \tag{F.61}$$

One of a solution of second equation is $f(s) \propto \exp[\pm m_0|s|]$. If we start with $m_0 > 0$, $f(s) \propto \exp[-m_0 s]$ is the only normalizable solution. In this case, we obtain left handed fermion $\gamma_5 u(p) = -u(p)$ in 4 dimension. On the other hand, if we start with $m_0 < 0$, we obtain right handed fermion. Additionally, if taking $|m_0|$ large enough, $f(s)$ is localized on $s = 0$ hyper surface (4 dimensional space-time). In this way we can construct chiral fermion from five dimensional field theory.

Same construction can be done for compactified extra dimension with Dirichlet boundary condition. In this case, mass taken to be constant and then localized modes appears around $s = 0$ and $s = L_s$, left-handed mode and right handed mode, respectively. Here L_s is the size of compactified direction. Moreover, lattice version of domain-wall fermion can be define from Wilson fermion in 5-dimension. We will construct domain-wall fermion on the lattice in next subsection.

F.4.2 Construction of 4 dimensional effective operator generalized domain-wall fermion and the overlap fermion

Here, we construct 4-dimensional effective operator for generalized domain-wall fermion. First we start from slightly generalized 5-dimensional Wilson-Dirac action. Next we integrate out all fermions and Pauli-Villars regulator field, then we will obtain determinant of Dirac operator. Finally we express fermion determinant in terms of 4-dimensional fermion field. This construction based on private note written by S. Hahimoto.

The Wilson fermion with negative mass in 5 dimensional space-time can be represented as,

$$S^{5D}_{\mathrm{GDW}} = \sum_x \bar{\psi}(x) D^{5D}_{\mathrm{GDW}} \psi(x) \tag{F.62}$$

with

$$D^{5D}_{\mathrm{GDW}} = \begin{pmatrix} \tilde{D}^1 & -P_- & 0 & 0 & \cdots & mP_+ \\ -P_+ & \tilde{D}^2 & -P_- & 0 & & 0 \\ 0 & -P_+ & \tilde{D}^3 & -P_- & & \\ \vdots & & & \ddots & & \\ 0 & 0 & & & \tilde{D}^{L_s-1} & -P_- \\ mP_- & 0 & & \cdots & -P_+ & \tilde{D}^{L_s} \end{pmatrix} \tag{F.63}$$

where columns and rows means to 5-dimensional hopping. Here,

$$\tilde{D}^s = (D^s_-)^{-1} D^s_+ \tag{F.64}$$
$$D^s_+ = a_s(1 + b_s D_W(-M)) \tag{F.65}$$
$$D^s_- = a_s(1 - c_s D_W(-M)) \tag{F.66}$$

where, $D_{\mathrm{W}}(-M)$ is a 4 dimensional Wilson Dirac operator with negative mass ($M > 0$). s and L_s corresponds to coordinate of 5-dimensional direction and length of that direction, respectively. a_s, b_s and c_s are tunable real parameters, which depend on 5-dimensional coordinate. $P_\pm$ is a projection operator which given by[46],

$$P_\pm = \frac{1 \pm \gamma^5}{2}. \tag{F.67}$$

If b_s and c_s taken to be constant and 0, respectively, we will obtain conventional domain-wall fermion.

For practical reason, we multiply D^s_- to each row of D^{5D}_{GDW} from left,

$$D_- D^{5D}_{\mathrm{GDW}} = \begin{pmatrix} D^1_+ & -D^1_- P_- & 0 & 0 & \cdots & mD^1_- P_+ \\ -D^2_- P_+ & D^2_+ & -D^2_- P_- & 0 & & 0 \\ 0 & -D^3_- P_+ & D^3_+ & -D^3_- P_- & & \\ \vdots & & & \ddots & & \\ 0 & 0 & & & D^{L_s-1}_+ & -D^{L_s-1}_- P_- \\ mD^{L_s}_- P_- & 0 & & \cdots & -D^{L_s}_- P_+ & D^{L_s}_+ \end{pmatrix} \tag{F.68}$$

[46]This projection operator can be obtained only when we choose Wilson parameter $r = 1$.

with $D_- = \mathrm{diag}\,(D_-^1, D_-^2, \cdots, D_-^{L_s})$. Each element is,

$$(D_- D^{5D}_{\mathrm{GDW}})_{ss'} = \begin{cases} D_+^s \delta_{s,s'} - D_-^s P_- \delta_{s,s'-1} + m D_-^s P_+ \delta_{s',L_s} & , \ s = 1 \\ -D_-^s P_+ \delta_{s,s'+1} + D_+^s \delta_{s,s'} - D_-^s P_- \delta_{s,s'-1} & , \ 1 < s < L_s \\ m D_-^s P_- \delta_{s',1} - D_-^s P_+ \delta_{s,s'+1} + D_+^s \delta_{s,s'} & , \ s = L_s \ . \end{cases}$$

In order to obtain 4-dimensional effective action, we change basis, which decompose 4-dimensional degrees of freedom from 5-dimensional one.

$$S_{GDW} = \bar{\psi} D^{5D}_{\mathrm{GDW}} \psi = \bar{\chi} D^{5D}_{\chi} \chi \tag{F.69}$$

$$\chi = \mathcal{P}\psi, \quad \bar{\chi} = \bar{\psi}\gamma_5 Q_-, \tag{F.70}$$

$$D^{5D}_{\chi} = Q_-^{-1}\gamma_5 D^{5D}_{\mathrm{GDW}} \mathcal{P} \tag{F.71}$$

$$Q_- = \mathrm{diag}\,(Q_-^1, Q_-^2, Q_-^1, \cdots, Q_-^{L_s}) \tag{F.72}$$

$$Q_\pm^s = \tilde{D}^s P_\mp - P_\pm \tag{F.73}$$

$$\mathcal{P} = \begin{pmatrix} P_- & P_+ & 0 & \cdots & 0 \\ 0 & P_- & P_+ & 0 & \vdots \\ 0 & 0 & \ddots & \ddots & \vdots \\ \vdots & & \ddots & P_- & P_+ \\ P_+ & 0 & \cdots & 0 & P_- \end{pmatrix} \tag{F.74}$$

$T_s^{-1} = -(Q_-^s)^{-1} Q_+^s$ is a s dependent transfer matrix along with 5-dimensional direction.

$$D^{5D}_{\chi} = \left(\begin{array}{c|ccccc} P_- - mP_+ & -T_1^{-1} & 0 & \cdots & \cdots & 0 \\ \hline 0 & 1 & -T_2^{-1} & 0 & \cdots & 0 \\ \vdots & 0 & 1 & T_3^{-1} & \cdots & 0 \\ \vdots & \ddots & \ddots & \ddots & \ddots & \vdots \\ 0 & \cdots & \cdots & 0 & 1 & T_{L_s-1}^{-1} \\ -T^{-1}(P_+ - mP_-) & 0 & \cdots & \cdots & 0 & 1 \end{array}\right) \tag{F.75}$$

$$\equiv \begin{pmatrix} D & C \\ B & A \end{pmatrix} \tag{F.76}$$

Here we apply UDL decomposition to previous expression in order to obtain 4-dimensional effective Dirac operator. Decomposition is done following procedure,

$$\begin{pmatrix} D & C \\ B & A \end{pmatrix} = \begin{pmatrix} 1 & CA^{-1} \\ 0 & 1 \end{pmatrix} \begin{pmatrix} S_\chi & 0 \\ 0 & A \end{pmatrix} \begin{pmatrix} 1 & 0 \\ A^{-1}B & 1 \end{pmatrix} \tag{F.77}$$

with Schur component,

$$S_\chi = D - CA^{-1}B. \tag{F.78}$$

As a result, Schur component is,

$$S_\chi(m) = (P_- - mP_+) - T_1^{-1}T_2^{-1}\cdots T_{L_s}^{-1}(P_+ - mP_-) \tag{F.79}$$

$$= -(1 + T_1^{-1}T_2^{-1}\cdots T_{L_s}^{-1})\gamma_5 \left[\frac{1+m}{2} + \frac{1-m}{2}\gamma_5 \frac{T_1^{-1}T_2^{-1}\cdots T_{L_s}^{-1} - 1}{T_1^{-1}T_2^{-1}\cdots T_{L_s}^{-1} + 1}\right] \tag{F.80}$$

Here we introduce Pauli-Villars regulator $S_\chi(m=1)^{-1}$ in order to avoid infrared divergence at $L_s \to \infty$.

$$D_{\rm DW}^{4D}(m) = S_\chi(m=1)^{-1} S_\chi(m) \tag{F.81}$$

$$= \frac{1+m}{2} + \frac{1-m}{2}\gamma_5 \frac{T_1^{-1}T_2^{-1}\cdots T_{L_s}^{-1} - 1}{T_1^{-1}T_2^{-1}\cdots T_{L_s}^{-1} + 1} \tag{F.82}$$

Here we simplify transfer matrix T_s^{-1},

$$T_s^{-1} = -(Q_-^s)^{-1} Q_+^s \tag{F.83}$$

$$= \left[1 - \gamma_5 \frac{(b_s + c_s)D_W}{2 + (b_s - c_s)D_W}\right]^{-1} \left[1 + \gamma_5 \frac{(b_s + c_s)D_W}{2 + (b_s - c_s)D_W}\right] \tag{F.84}$$

$$= \frac{1 + \omega_s H_M}{1 - \omega_s H_M} \tag{F.85}$$

where

$$H_M = \gamma_5 \frac{bD_W}{2 + cD_W}, \tag{F.86}$$

and we determine s dependence on b_s and c_s as,

$$b_s + c_s = b\omega_s, \quad b_s - c_s = c. \tag{F.87}$$

Here we summarize final form of the generalized domain-wall fermion,

$$D_{\rm DW}^{4D}(m) = \frac{1+m}{2} + \frac{1-m}{2}\gamma_5 {\rm sgn}_{\rm rat}(H_M), \quad {\rm sgn}_{\rm rat}(H_M) = \frac{1 - \prod_s^{Ls} T_s(H_M)}{1 + \prod_s^{Ls} T_s(H_M)}, \tag{F.88}$$

$$T_s(H_M) = \frac{1 - \omega_s H_M}{1 + \omega_s H_M}, \quad H_M = \gamma_5 \frac{bD_W}{2 + cD_W}. \tag{F.89}$$

Choosing ω_s corresponds to choosing approximation of the sign function in the overlap Dirac operator.

Note that, L_s corresponds to approximation order of the sign function. Therefore, $L_s \to \infty$, the fraction term in the $\rm sgn_{rat}$ in (F.88) becomes exact sign function, then we obtain the overlap fermion,

$$D_{\rm ov}(m) = \frac{1+m}{2} + \frac{1-m}{2}\gamma_5 {\rm sgn}(H_M).$$

F.5 Normalization of overlap-Dirac operator

Overlap operator contains Wilson-Dirac operator,

$$D_W(-M) = D_W(0) - M \tag{F.90}$$

$D_W(0) \to \not{D}$ at $a \to 0$. Note that, higher derivative term disappear at continuum limit.

$$H_M = \gamma_5 \frac{bD_W(-M)}{2 + cD_W(-M)} \tag{F.91}$$

$$= \gamma_5 b \frac{D_W(0) - M}{2 + cD_W(0) - cM} \tag{F.92}$$

$$= \gamma_5 b (D_W(0) - M)[2 - Mc + cD_W(0)]^{-1} \tag{F.93}$$

$$= \gamma_5 \frac{b}{2 - Mc} (D_W(0) - M) \left[1 + \frac{cD_W(0)}{2 - Mc}\right]^{-1} \tag{F.94}$$

Expand final inverse term around near-zero modes[47].

$$H_M = \gamma_5 \frac{b}{2 - Mc} (D_W(0) - M) \left[1 - \left(\frac{cD_W(0)}{2 - Mc}\right) + \left(\frac{cD_W(0)}{2 - Mc}\right)^2 + \mathcal{O}(D_W^3)\right] \tag{F.95}$$

$$= \gamma_5 \frac{b}{2 - Mc} \left[(D_W(0) - M) - (D_W(0) - M)\frac{cD_W(0)}{2 - Mc} + \left(\frac{cD_W(0)}{2 - Mc}\right)^2 + \mathcal{O}(D_W^3)\right] \tag{F.96}$$

$$= \gamma_5 \frac{b}{2 - Mc} \left[D_W(0)\left(1 + \frac{Mc}{2 - Mc}\right) - M + \mathcal{O}(D_W^2)\right] \tag{F.97}$$

$\mathrm{sgn}(x) = \frac{x}{\sqrt{x^\dagger x}}$, For denominator, zero mode $D_W(0) \sim 0$, is important,

$$\sqrt{H_M^\dagger H_M} \to \frac{b}{2 - Mc} M \tag{F.98}$$

finally

$$\frac{1}{2}\gamma_5 \mathrm{sgn}(H_W) = \frac{1}{2}\gamma_5 \frac{H_M}{\sqrt{H_M^\dagger H_M}} = \frac{1}{2M}\left[D_W(0)\left(1 + \frac{Mc}{2 - Mc}\right) - M + \mathcal{O}(D_W^2)\right] \tag{F.99}$$

$$D_{\mathrm{ov}}(0) = \frac{1}{2} + \frac{1}{2}\gamma_5 \mathrm{sgn}(H_W) \tag{F.100}$$

$$= \frac{1}{2M}\left[D_W(0)\frac{2}{2 - Mc} + \mathcal{O}(D_W^2)\right] \tag{F.101}$$

Then, canonically normalized Dirac operator should be,

$$\not{D} = \lim_{a \to 0} 2M \left(1 - \frac{cM}{2}\right) D_{\mathrm{ov}}. \tag{F.102}$$

Our simulation parameters are $c = 1$ and $M = 1$, this normalization factor is 1.

[47] Indeed, this operation should be taken in the momentum space. In the momentum space, derivative become a momentum variable, then this operation is justified. However for simplicity, we use lazy notation

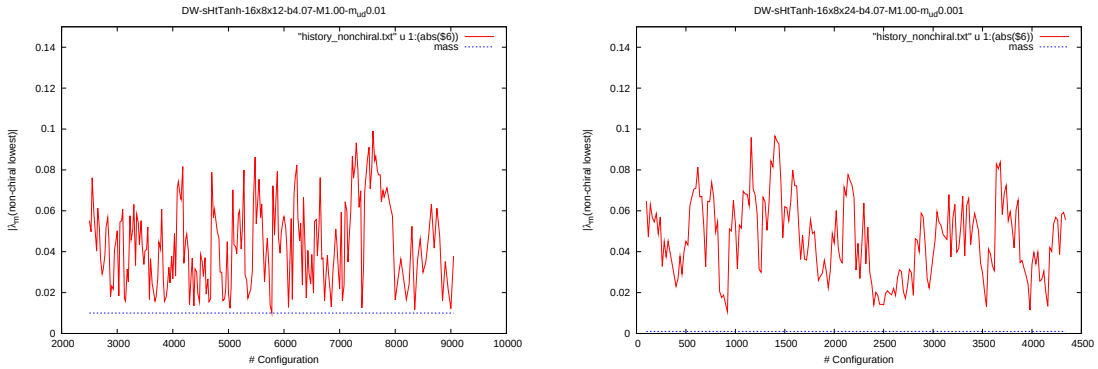

Figure 20: History of non-chiral lowest eigenvalue of the domain-wall Dirac operator for $\beta = 4.07$, $L = 16$. Left panel and right panel correspond to $m = 0.01$ and $m = 0.001$, respectively.

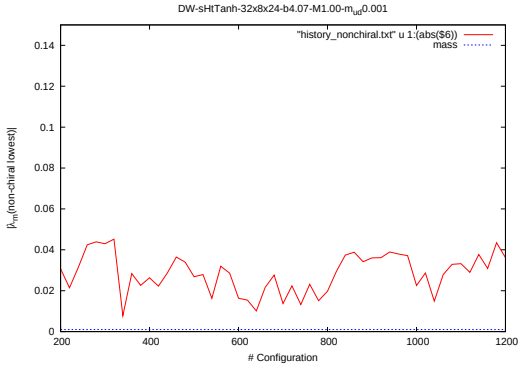

Figure 21: History of non-chiral lowest eigenvalue of the domain-wall Dirac operator for $\beta = 4.07$, $L = 32$, $m = 0.001$.

G Thermalization of our data

In this section we summarize thermalization for our measurement.

G.1 Thermalization

In this subsection we note our judgement of the thermalization. Our observable is the eigenvalue, so we check non-chiral lowest eigenvalue of the domain-wall Dirac operator. Chirality is determines by using information of eigenvector. Figure 20-23 are the result. It looks well fluctuate, thus all of data sets are thermalized.

G.2 Reweighting factors

In this subsection, we summarize the histories of reweighting factor. Figure 24 is the results for $\beta = 4.07$, $L = 16$ lattice. Reweighting factor fluctuate beyond 1 in the case of $m = 0.01$, however it does not relevant for the existence of the gap. On the other hand, for $m = 0.001$, reweighting factor fluctuates around 1, then we can use this information to judge the existence of the gap in the spectrum.

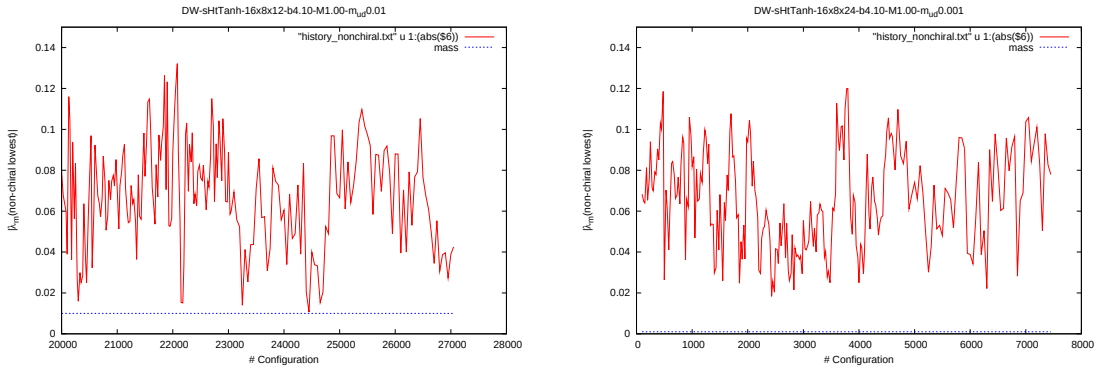

Figure 22: History of non-chiral lowest eigenvalue of the domain-wall Dirac operator for $\beta = 4.10$, $L = 16$. Left panel and right panel correspond to $m = 0.01$ and $m = 0.001$, respectively.

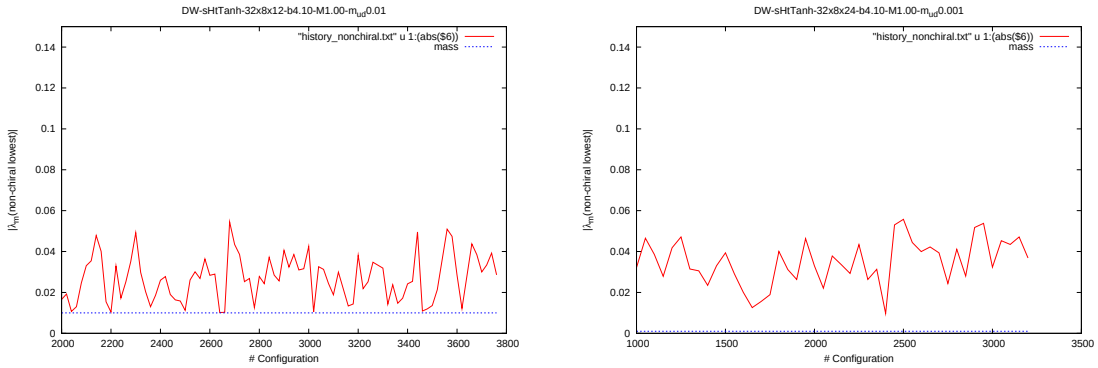

Figure 23: History of non-chiral lowest eigenvalue of the domain-wall Dirac operator for $\beta = 4.10$, $L = 32$. Left panel and right panel correspond to $m = 0.01$ and $m = 0.001$, respectively.

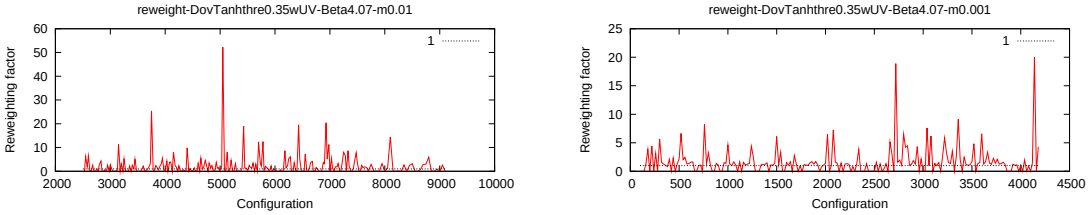

Figure 24: Reweighting factors for each configuration for $L = 16$, $\beta = 4.07$. Left panel and right panel correspond to $m = 0.01$ and $m = 0.001$ respectively.

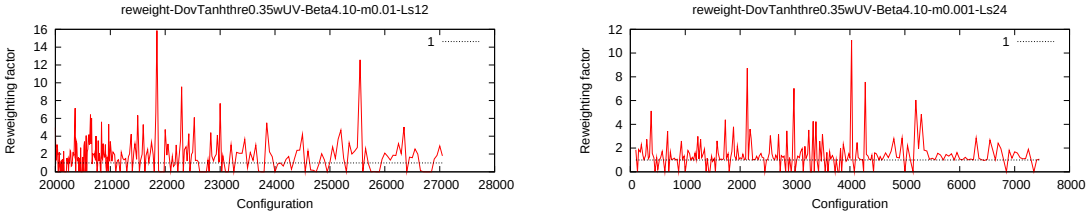

Figure 25: Reweighting factors for each configuration for $L = 16$, $\beta = 4.10$. Left panel and right panel correspond to $m = 0.01$ and $m = 0.001$ respectively.

Figure 25 is the results for $\beta = 4.10$, $L = 16$ lattice. Both of $m = 0.01$ and $m = 0.001$, reweighting factor fluctuates around 1, then we use this data in the analysis.

Figure 26 and Figure 27 are the history of low-mode reweighting factor for $L = 16$ lattice, $\beta = 4.07$ and $\beta = 4.10$, respectively. These data look different from Figure 24 and Figure 25, however, as we mentioned in section 7.3, the reweighting factor gives us believable information of the low-mode in the spectrum.

Figure 29 is the history of low-mode reweighting factor for $\beta = 4.10$, $L = 32$ lattice. Left panel, which is history for $m = 0.01$, shows lack of statistics, however the data does not show gap, so we does not increase statistics. Right panel is history for $m = 0.001$. The history is fluctuation around 1, so the data is used in the analysis.

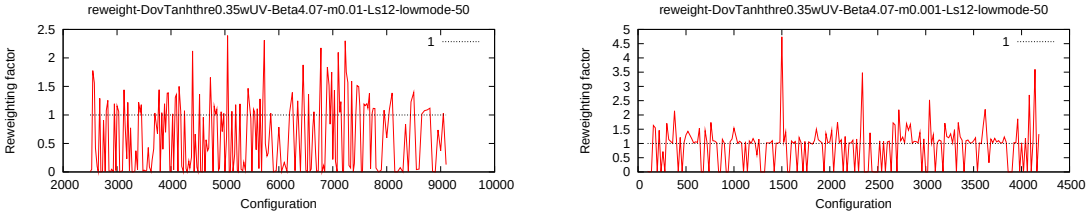

Figure 26: Low-mode reweighting factors for each configuration for $L = 16$, $\beta = 4.07$. Left panel and right panel correspond to $m = 0.01$ and $m = 0.001$ respectively.

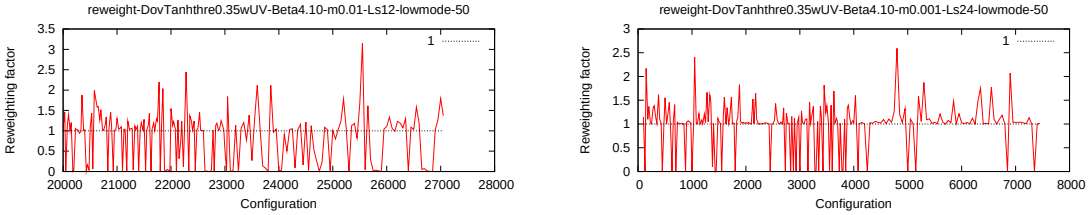

Figure 27: Low-mode reweighting factors for each configuration for $L = 16$, $\beta = 4.10$. Left panel and right panel correspond to $m = 0.01$ and $m = 0.001$ respectively.

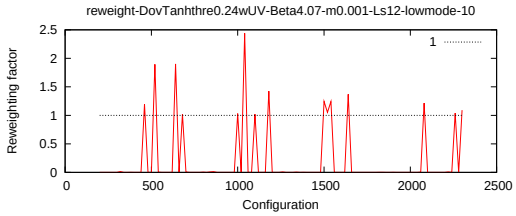

Figure 28: Low-mode reweighting factors for each configuration for $L = 32$, $\beta = 4.07$, $m = 0.001$.

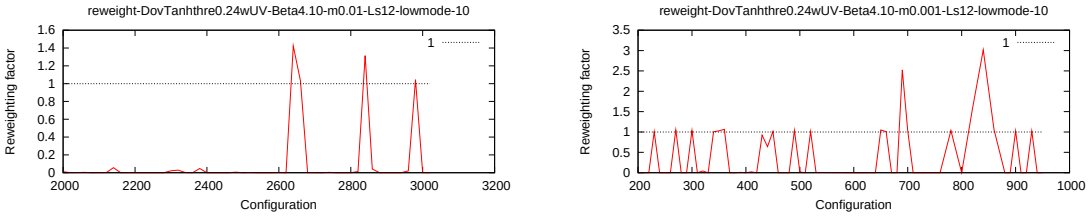

Figure 29: Low-mode reweighting factors for each configuration for $L = 32$, $\beta = 4.10$. Left panel and right panel correspond to $m = 0.01$ and $m = 0.001$ respectively.

H Boundary condition with supersymmetry

In this section, we briefly review why we have to impose special boundary condition as (11.12)-(11.15) (or generally, (I.12)-(I.17)) based on [76]. In general, it is difficult to construct supersymmetry on curved space-time. However, for some limited class of manifold, we can construct super symmetric field theory from flat space-time one, by using Weyl transformation. We can construct supersymmetry on $S^2 \times S^1$ from superymmetry on R^4 as following way.

First, construction of supersymmetry in 3-dimension flat space-time from 4-dimensional space-time is straightforward. Supersymmetric theory in flat three dimension is derived by using dimensional reduction, $\partial_4 \to 0$, and $A_4 =: \sigma$.

Second, we map the theory on flat space to the theory on curved manifold. If theory is covariant under the Weyl transformation, $g_{\mu\nu} \to f(x) g_{\mu\nu}$, we can construct theory on the mapped space consistently. Consider metric for n-dimensional flat space-time, $ds^2 = d\rho^2 + \rho^2 d\Omega_{n-1}^2$ (spherical coordinate), where $d\Omega_{n-1}^2$ corresponds to angular coordinate. Apply Weyl transformation, we obtain $ds^2 = \frac{l^2}{\rho^2} ds^2$, l is a constant, which will be radius of S^{n-1}. If we take time coordinate τ as $\frac{\rho}{l} = \exp[\frac{\tau}{l}]$, we obtain metric of $S^{n-1} \times R^1$,

$$ds'^2 = \frac{l^2}{\rho^2}(d\rho^2 + \rho^2 d\Omega_{n-1}^2), \tag{H.1}$$

$$= d\tau^2 + l^2 d\Omega_{n-1}^2. \tag{H.2}$$

In this way, we can construct theory on $S^2 \times R^1$. If we want to regard as this theory as theory on $S^2 \times R^1$, theory must be covariant under this transformation[48]. We have to modify the theory to covariant under the Weyl transformation. In fact, if the action is quadratic, the result is simple. Only have to do is, adding curvature coupling term to the scalar field[49]. In this way, we can construct theory on $S^2 \times R^1$.

Third, we construct global supersymmetric transformation on the curved space-time. Global supersymmetric transformation contains constant spinor ϵ, *i.e.* $\partial_\mu \epsilon = 0$. However this condition is not invariant under the Weyl transformation. We need to relax this condition in a consistent way. Since space-time is curved, we should switch to $\partial_\mu \to D_\mu$, where D_μ is a covariant derivative, and find covariant condition. We decompose irreducible component,

$$D_\mu \epsilon = [D_\mu \epsilon]_{3/2} + [D_\mu \epsilon]_{1/2}, \tag{H.3}$$

where,

$$[D_\mu \epsilon]_{1/2} = \frac{1}{d} \gamma_\mu \not{D} \epsilon, \tag{H.4}$$

$$[D_\mu \epsilon]_{3/2} = D_\mu \epsilon - \frac{1}{d} \gamma_\mu \not{D} \epsilon, \tag{H.5}$$

where d is a space-time dimension. If we apply Weyl transformation $\epsilon = e^{\frac{1}{2}\alpha(x)} \epsilon'$,

$$[D_\mu \epsilon]_{1/2} = e^{\frac{1}{2}\alpha} [D_\mu \epsilon']_{1/2} + \frac{1}{d} \gamma_\mu (\not{\partial} e^{\frac{1}{2}\alpha}) \epsilon' \tag{H.6}$$

$$[D_\mu \epsilon]_{3/2} = e^{\frac{1}{2}\alpha} [D_\mu \epsilon']_{3/2} \tag{H.7}$$

[48] If theory is not covariant under the transformation, the theory depends on which Weyl map is used. We would like to regard the theory as defined on $S^{n-1} \times R$ originally, this situation is unnatural.

[49] Details are in [76]

Only $[D_\mu \epsilon]_{3/2}$ is transformed in covariant way[50]. Then we should define the condition as,

$$[D_\mu \epsilon]_{3/2} = 0. \tag{H.8}$$

Or equivalently, this condition allow to exist spin 1/2 component in $D_\mu \epsilon$, *i.e.*,

$$D_\mu \epsilon = \gamma_\mu \kappa \tag{H.9}$$

where κ is a spinor which is allowed by the condition. This is the Killing spinor equation. If the solution is found, we can construct global supersymmetric transformation on the curved manifold[51]. As following section, we will give concrete form of the Killing spinor.

Finally we compactify R^1 direction consistent with the Killing spinor [62]. One of solution of Killing equation is given by[52],

$$\epsilon(y) = e^{\frac{1}{2}(\frac{y}{l}+i\varphi)} \begin{pmatrix} \cos\frac{\vartheta}{2} \\ \sin\frac{\vartheta}{2} \end{pmatrix}. \tag{H.10}$$

In previous expression, we note the argument of the Killing spinor in order to emphasize the dependence of S^1 coordinate, $y \in [0, 2\pi R]$. In order to consider boundary condition, we shift coordinate,

$$\epsilon(y + 2\pi R) = e^{\frac{1}{2}(\frac{y+2\pi R}{l}+i\varphi)} \begin{pmatrix} \cos\frac{\vartheta}{2} \\ \sin\frac{\vartheta}{2} \end{pmatrix} \tag{H.11}$$

$$= e^{\frac{\pi R}{l}} \epsilon(y) \tag{H.12}$$

This means, we need to multiply scale factor to preserve supersymmetry. By using the quantum numbers of Killing spinor, $\mathcal{R}$-charge $\mathcal{R}(\epsilon) = +1$, and flavor charge $F(\epsilon) = 0$, we can re-write the condition,

$$\epsilon(y + 2\pi R) = e^{\frac{\pi R}{l}\mathcal{R} + F\mu} \epsilon(y), \tag{H.13}$$

where μ is a real parameter. If we impose same boundary condition for all of fields Ψ,

$$\Psi(y + 2\pi R) = e^{\frac{\pi R}{l}\mathcal{R} + F\mu} \Psi(y), \tag{H.14}$$

this is enough to preserve supersymmetry. We summarize $\mathcal{R}$-charge and the flavor charge assignment of fields in Table 3. Note that, if we employ this boundary condition, fields are not single-valued, however, the Lagrangian (11.4) (11.5) are still single-valued.

	A_m	σ	λ	$\bar{\lambda}$	$\mathcal{D}$	ϕ	ψ	F	$\bar{\phi}$	$\bar{\psi}$	$\bar{F}$
$\mathcal{R}$	0	0	1	-1	0	$-\Delta_\Phi$	$-\Delta_\Phi + 1$	$-\Delta_\Phi + 2$	Δ_Φ	$\Delta_\Phi - 1$	$\Delta_\Phi - 2$
F	0	0	0	0	0	1	1	1	-1	-1	-1

Table 3: Charge assignment of fields. Δ_Φ is arbitrary real number at Lagrangian level.

[50] Here we use that D_μ is diagonal for spin index.

[51] However, now ϵ is not constant spinor. Here "global" means spin 3/2 components (gravitino) does not affect the dynamics.

[52] Our Killing spinor equation is (I.2).

I SUSY on $S^2 \times S^1$ and the exact results

Killing spinors As one can find in [61, 62, 65], it is sufficient for defining supersymmetric field theories on $S^2 \times S^1$ to find so-called Killing spinors[53]. We take the following 2 Killing spinors:

$$\epsilon = e^{\frac{1}{2}(\frac{y}{l}+i\varphi)} \begin{pmatrix} \cos\frac{\vartheta}{2} \\ \sin\frac{\vartheta}{2} \end{pmatrix}, \qquad \bar{\epsilon} = e^{\frac{-1}{2}(\frac{y}{l}+i\varphi)} \begin{pmatrix} \sin\frac{\vartheta}{2} \\ \cos\frac{\vartheta}{2} \end{pmatrix}. \tag{I.1}$$

These spinors satisfy the following equations,

$$\mathcal{D}_\mu \epsilon = \frac{1}{2l}\gamma_\mu\gamma_3\epsilon, \qquad \mathcal{D}_\mu \bar{\epsilon} = \frac{-1}{2l}\gamma_\mu\gamma_3\bar{\epsilon}, \tag{I.2}$$

where we take vielbein as

$$e^1 = l d\vartheta, \quad e^2 = l\sin\vartheta d\varphi, \quad e^3 = dy. \tag{I.3}$$

Vector multiplet We can construct the $\mathcal{N}=2$ vector multiplet $V = (A_\mu, \sigma, \bar{\lambda}, \lambda, D)$ on $S^2 \times S^1$ by using $\epsilon, \bar{\epsilon}$ defined in (I.1). We use SUSY transformation defined in [72]. Though their manifold is S^3, their SUSY construction is enough generic to use even on $S^2 \times S^1$. However, one cannot define SUSY invariant theory not only with the SUSY transformations, but also the S^1 boundary conditions for the component fields:

$$A_\mu(\vartheta, \varphi, y + 2\pi R) = A_\mu(\vartheta, \varphi, y), \tag{I.4}$$
$$\sigma(\vartheta, \varphi, y + 2\pi R) = \sigma(\vartheta, \varphi, y), \tag{I.5}$$
$$\lambda(\vartheta, \varphi, y + 2\pi R) = e^{\frac{\pi R}{l}}\lambda(\vartheta, \varphi, y), \tag{I.6}$$
$$\bar{\lambda}(\vartheta, \varphi, y + 2\pi R) = e^{-\frac{\pi R}{l}}\bar{\lambda}(\vartheta, \varphi, y), \tag{I.7}$$
$$D(\vartheta, \varphi, y + 2\pi R) = D(\vartheta, \varphi, y). \tag{I.8}$$

Note that the $\lambda, \bar{\lambda}$ have nontrivial scaling once they wrap the S^1. This scaling boundary condition comes from the y dependence of $\epsilon, \bar{\epsilon}$ in (I.1). One can guess that only $\mathcal{R}$-charged fields have the scaling. In fact, it becomes clear once we write down the definition of the *index* [60, 61, 62, 65]. Within these component fields and the Lagrangian (11.4), one can derive the following result [60, 61, 62],

$$\int \mathcal{D}V e^{-\frac{1}{g_{\rm YM}^2}\int\sqrt{g}\mathcal{L}_{\rm SYM}} = \sum_{m\in\mathbb{Z}} \frac{1}{\rm sym} \int_{-\pi}^{+\pi} \prod \frac{d\theta_i}{2\pi R} \mathcal{Z}^{(vec)}_{1-loop}, \tag{I.9}$$

where

$$\mathcal{Z}^{(vec)}_{1-loop} = \prod_{i\neq j} \prod_{n=-\infty}^{\infty} \prod_{J=0}^{\infty} \frac{J + |\frac{m_i - m_j}{2}| + i\left(\frac{l}{R}n - \frac{l}{R}\frac{\theta_i - \theta_j}{2\pi}\right)}{J + 1 + |\frac{m_i - m_j}{2}| - i\left(\frac{l}{R}n - \frac{l}{R}\frac{\theta_i - \theta_j}{2\pi}\right)}. \tag{I.10}$$

Note that the result (I.10) does not depend on the coupling constant $g_{\rm YM}$. This is the consequence caused by a fact, the Lagrangian (11.4) is *SUSY-exact*. Here, n represents the Kaluza-Klein mode and J corresponds to the angular momentum with respect to the S^2. The

[53] See [71] for more systematic approach.

meaning of θ_i, m_i is explained in Section 11. We can simplify (I.10) by using the symmetry $n \to -n$, and $\theta_i \leftrightarrow \theta_j$ as follows

$$\begin{aligned}(\text{I.10}) &= \prod_{i\neq j}\prod_{n=-\infty}^{\infty}\Big(0+|\frac{m_i-m_j}{2}|+i\big(\frac{l}{R}n-\frac{l}{R}\frac{\theta_i-\theta_j}{2\pi}\big)\Big)\\ &\xrightarrow{\zeta\text{-reg}}\prod_{i>j}\Big|2\sin\Big(\frac{\theta_i-\theta_j}{2}+i\frac{\pi R}{l}\frac{m_i-m_j}{2}\Big)\Big|^2,\end{aligned} \tag{I.11}$$

where we use the zeta function regularization in the final step.

Matter multiplet We can also define the matter multiplets $\Phi=(\phi,\psi,F), \overline{\Phi}=(\overline{\phi},\overline{\psi},\overline{F})$ which couple with the vector multiplet via the gauge symmetry [72]. As well known, we can assign arbitrary $\mathcal{R}$-charge Δ_Φ with Φ. We have to tune the S^1 boundary conditions for the component fields as follows,

$$\phi(\vartheta,\varphi,y+2\pi R)=e^{-\Delta_\Phi\frac{\pi R}{l}+\mu}\phi(\vartheta,\varphi,y), \tag{I.12}$$
$$\psi(\vartheta,\varphi,y+2\pi R)=e^{-(\Delta_\Phi-1)\frac{\pi R}{l}+\mu}\psi(\vartheta,\varphi,y), \tag{I.13}$$
$$F(\vartheta,\varphi,y+2\pi R)=e^{-(\Delta_\Phi-2)\frac{\pi R}{l}+\mu}F(\vartheta,\varphi,y), \tag{I.14}$$
$$\overline{\phi}(\vartheta,\varphi,y+2\pi R)=e^{\Delta_\Phi\frac{\pi R}{l}-\mu}\overline{\phi}(\vartheta,\varphi,y), \tag{I.15}$$
$$\overline{\psi}(\vartheta,\varphi,y+2\pi R)=e^{(\Delta_\Phi-1)\frac{\pi R}{l}-\mu}\overline{\psi}(\vartheta,\varphi,y), \tag{I.16}$$
$$\overline{F}(\vartheta,\varphi,y+2\pi R)=e^{(\Delta_\Phi-2)\frac{\pi R}{l}-\mu}\overline{F}(\vartheta,\varphi,y), \tag{I.17}$$

in order to preserve supersymmetry. Through the well known argument, we have no degenerate vacua with respect to Φ with the Lagrangian (11.5). Therefore, the only nontrivial contribution comes from by inserting the following function into (I.9),

$$\mathcal{Z}^{mat}_{\text{1-loop}}=\prod_{\rho\in R}\prod_{n=-\infty}^{\infty}\prod_{J=0}^{\infty}\frac{J+1-i\big(\frac{l}{R}n-\frac{l}{2\pi R}(\rho(\theta)+i\mu)\big)-\frac{\Delta_\Phi}{2}+|\frac{\rho(m)}{2}|}{J+i\big(\frac{l}{R}n-\frac{l}{2\pi R}(\rho(\theta)+i\mu)\big)+\frac{\Delta_\Phi}{2}+|\frac{\rho(m)}{2}|}. \tag{I.18}$$

There is no coupling constant as same as the case of the vector multiplet, and it comes from the SUSY-exactness of the matter Lagrangian (11.5). Unfortunately, one cannot simplify it as we do in (I.11). In order to overcome this situation, we consider not only one Φ, but two matter multiplets Φ_1,Φ_2 as we explained in Section 11. In addition Δ is taken to be integer as follows, in order to simplify the result. In this case, we obtain,

$$\begin{aligned}&\mathcal{Z}^{mat1,2}_{\text{1-loop}}=\mathcal{Z}^{mat1}_{\text{1-loop}}\times\mathcal{Z}^{mat2}_{\text{1-loop}}\\ &=\prod_{\rho\in R}\prod_{n=-\infty}^{\infty}\prod_{J=0}^{\infty}\Big(\frac{J+1-i\big(\frac{ln}{R}-\frac{l(\rho(\theta)-\alpha)}{2\pi R}\big)-\frac{\Delta}{2}+|\frac{\rho(m)}{2}|}{J+i\big(\frac{ln}{R}-\frac{l(\rho(\theta)-\alpha)}{2\pi R}\big)+\frac{\Delta}{2}+|\frac{\rho(m)}{2}|}\Big)\Big(\frac{J+1-i\big(\frac{ln}{R}+\frac{l(\rho(\theta)-\alpha)}{2\pi R}\big)-\frac{\Delta}{2}+|\frac{\rho(m)}{2}|}{J+i\big(\frac{ln}{R}+\frac{l(\rho(\theta)-\alpha)}{2\pi R}\big)+\frac{\Delta}{2}+|\frac{\rho(m)}{2}|}\Big)\\ &\xrightarrow{\zeta\text{-reg}}\begin{cases}\prod_{\rho\in R}\prod_{J=1-\frac{\Delta}{2}}^{\frac{\Delta}{2}-1}\Big|2\sin\Big(\frac{(\rho(\theta)-\alpha)}{2}+i\frac{\pi R}{l}\big(|\frac{\rho(m)}{2}|+J\big)\Big)\Big|^2 & (\Delta-1\in\mathbb{N})\\ 1 & (\Delta=1)\\ \prod_{\rho\in R}\prod_{J=\frac{\Delta}{2}}^{-\frac{\Delta}{2}}\Big|2\sin\Big(\frac{(\rho(\theta)-\alpha)}{2}+i\frac{\pi R}{l}\big(|\frac{\rho(m)}{2}|+J\big)\Big)\Big|^{-2} & (1-\Delta\in\mathbb{N})\end{cases}.\end{aligned} \tag{I.19}$$

We take $\Delta-1\in\mathbb{N}$ throughout this work.

References

[1] C. N. Yang and R. L. Mills, "Conservation of Isotopic Spin and Isotopic Gauge Invariance," Phys. Rev. **96**, 191 (1954).

[2] D. J. Gross, R. D. Pisarski and L. G. Yaffe, "QCD and Instantons at Finite Temperature," Rev. Mod. Phys. **53**, 43 (1981).

[3] S. Chandrasekharan and N. H. Christ, "Dirac spectrum, axial anomaly and the QCD chiral phase transition," Nucl. Phys. Proc. Suppl. **47**, 527 (1996) [hep-lat/9509095].

[4] S. Weinberg, "The quantum theory of fields. Vol. 2: Modern applications," Cambridge, UK: Univ. Pr. (1996) 489 p

[5] K. Fujikawa and H. Suzuki, "Path integrals and quantum anomalies," Oxford, UK: Clarendon (2004) 284 p

[6] T. D. Cohen, "The High temperature phase of QCD and U(1)-A symmetry," Phys. Rev. D **54**, 1867 (1996). [hep-ph/9601216].

[7] T. D. Cohen, "The Spectral density of the Dirac operator above T(c) rep," nucl-th/9801061.

[8] Y. Nambu and G. Jona-Lasinio, "Dynamical Model of Elementary Particles Based on an Analogy with Superconductivity. 1.," Phys. Rev. **122**, 345 (1961).

[9] A. A. Belavin, A. M. Polyakov, A. S. Schwartz and Y. S. Tyupkin, Phys. Lett. B **59**, 85 (1975).

[10] H. Forkel, "A Primer on instantons in QCD," hep-ph/0009136.

[11] T. Banks and A. Casher, "Chiral Symmetry Breaking in Confining Theories," Nucl. Phys. B **169**, 103 (1980).

[12] M. F. Atiyah and I. M. Singer, "The Index of elliptic operators. 1," Annals Math. **87**, 484 (1968).

[13] S. Aoki, H. Fukaya and Y. Taniguchi, "Chiral symmetry restoration, eigenvalue density of Dirac operator and axial U(1) anomaly at finite temperature," Phys. Rev. D **86**, 114512 (2012). [arXiv:1209.2061 [hep-lat]].

[14] K. G. Wilson, "Confinement of Quarks," Phys. Rev. D **10**, 2445 (1974).

[15] M. Creutz, "Monte Carlo Study of Quantized SU(2) Gauge Theory," Phys. Rev. D **21**, 2308 (1980).

[16] 青木 慎也, "格子上の場の理論" , シュプリンガー現代理論物理学シリーズ, (2012)

[17] G. Cossu [JLQCD collaboration], S. Aoki, H. Fukaya, S. Hashimoto, T. Kaneko, H. Matsufuru and J. I. Noaki, "Finite temperature study of the axial U(1) symmetry on the lattice with overlap fermion formulation," Phys. Rev. D **87**, no. 11, 114514 (2013). [arXiv:1304.6145 [hep-lat]].

[18] T. W. Chiu, W. P. Chen, Y. C. Chen, H. Y. Chou and T. H. Hsieh, "Chiral symmetry and axial U(1) symmetry in finite temperature QCD with domain-wall fermion," arXiv:1311.6220 [hep-lat].

[19] A. Bazavov *et al.* [HotQCD Collaboration], "The chiral transition and $U(1)_A$ symmetry restoration from lattice QCD using Domain Wall Fermions," Phys. Rev. D **86**, 094503 (2012). [arXiv:1205.3535 [hep-lat]].

[20] M. I. Buchoff, M. Cheng, N. H. Christ, H.-T. Ding, C. Jung, F. Karsch, Z. Lin and R. D. Mawhinney *et al.*, "The QCD chiral transition, U(1) symmetry and the Dirac spectrum using domain wall fermions," Phys. Rev. D **89**, 054514 (2014).

[21] H. Ohno, U. M. Heller, F. Karsch and S. Mukherjee, PoS LATTICE **2011** (2011) 210 [arXiv:1111.1939 [hep-lat]].

[22] H. Ohno, U. M. Heller, F. Karsch and S. Mukherjee, "$U_A(1)$ breaking at finite temperature from the Dirac spectrum with the dynamical HISQ action," PoS LATTICE **2012**, 095 (2012). [arXiv:1211.2591 [hep-lat]].

[23] G. Cossu, J. Noaki, S. Hashimoto, T. Kaneko, H. Fukaya, P. A. Boyle and J. Doi, "JLQCD IroIro++ lattice code on BG/Q," arXiv:1311.0084 [hep-lat].

[24] R. C. Brower, H. Neff and K. Orginos, "Mobius fermions: Improved domain wall chiral fermions," Nucl. Phys. Proc. Suppl. **140** (2005) 686; [hep-lat/0409118].

[25] R. C. Brower, H. Neff and K. Orginos, "The Móbius Domain Wall Fermion Algorithm," arXiv:1206.5214 [hep-lat].

[26] R. C. Brower, H. Neff and K. Orginos, "Mobius fermions," Nucl. Phys. Proc. Suppl. **153** (2006) 191. [hep-lat/0511031].

[27] H. Fukaya *et al.* [JLQCD Collaboration], "Overlap/Domain-wall reweighting," PoS LATTICE **2013**, 127 (2013). [arXiv:1311.4646 [hep-lat]].

[28] R. D. Pisarski and F. Wilczek, Phys. Rev. D **29**, 338 (1984).

[29] P. H. Ginsparg and K. G. Wilson, Phys. Rev. D **25**, 2649 (1982).

[30] S. Ejiri and N. Yamada, "End Point of a First-Order Phase Transition in Many-Flavor Lattice QCD at Finite Temperature and Density," Phys. Rev. Lett. **110**, no. 17, 172001 (2013) [arXiv:1212.5899 [hep-lat]].

[31] C. Bonati, P. de Forcrand, M. D'Elia, O. Philipsen and F. Sanfilippo, "Constraints on the two-flavor QCD phase diagram from imaginary chemical potential," PoS LATTICE **2011**, 189 (2011) [arXiv:1201.2769 [hep-lat]].

[32] M. Holthausen, J. Kubo, K. S. Lim and M. Lindner, "Electroweak and Conformal Symmetry Breaking by a Strongly Coupled Hidden Sector," JHEP **1312** (2013) 076 [arXiv:1310.4423 [hep-ph]].

[33] Y. Hosotani, "Dynamical Mass Generation by Compact Extra Dimensions," *Phys.Lett.* **B126** (1983) 309.

[34] Y. Hosotani, "Dynamics of Nonintegrable Phases and Gauge Symmetry Breaking," *Annals Phys.* **190** (1989) 233.

[35] A. Davies and A. McLachlan, "GAUGE GROUP BREAKING BY WILSON LOOPS," *Phys.Lett.* **B200** (1988) 305.

[36] A. Davies and A. McLachlan, "Congruency Class Effects in the Hosotani Model," *Nucl.Phys.* **B317** (1989) 237.

[37] H. Hatanaka, T. Inami, and C. Lim, "The Gauge hierarchy problem and higher dimensional gauge theories," *Mod.Phys.Lett.* **A13** (1998) 2601–2612, arXiv:hep-th/9805067 [hep-th].

[38] G. Burdman and Y. Nomura, "Unification of Higgs and gauge fields in five-dimensions," *Nucl.Phys.* **B656** (2003) 3–22, arXiv:hep-ph/0210257 [hep-ph].

[39] C. Csaki, C. Grojean, and H. Murayama, "Standard model Higgs from higher dimensional gauge fields," *Phys.Rev.* **D67** (2003) 085012, arXiv:hep-ph/0210133 [hep-ph].

[40] C. Lim, "The Higgs Particle and Higher-Dimensional Theories," *PTEP* **2014** no. 2, (2014) 02A101, arXiv:1308.5579 [hep-ph].

[41] K. Agashe, R. Contino, and A. Pomarol, "The Minimal composite Higgs model," *Nucl.Phys.* **B719** (2005) 165–187, arXiv:hep-ph/0412089 [hep-ph].

[42] A. D. Medina, N. R. Shah, and C. E. Wagner, "Gauge-Higgs Unification and Radiative Electroweak Symmetry Breaking in Warped Extra Dimensions," *Phys.Rev.* **D76** (2007) 095010, arXiv:0706.1281 [hep-ph].

[43] Y. Hosotani, K. Oda, T. Ohnuma, and Y. Sakamura, "Dynamical Electroweak Symmetry Breaking in SO(5) x U(1) Gauge-Higgs Unification with Top and Bottom Quarks," *Phys.Rev.* **D78** (2008) 096002, arXiv:0806.0480 [hep-ph].

[44] M. Serone, "Holographic Methods and Gauge-Higgs Unification in Flat Extra Dimensions," *New J.Phys.* **12** (2010) 075013, arXiv:0909.5619 [hep-ph].

[45] Y. Hosotani, S. Noda, and N. Uekusa, "The Electroweak gauge couplings in SO(5) x U(1) gauge-Higgs unification," *Prog.Theor.Phys.* **123** (2010) 757–790, arXiv:0912.1173 [hep-ph].

[46] S. Funatsu, H. Hatanaka, Y. Hosotani, Y. Orikasa, and T. Shimotani, "LHC signals of the $SO(5) \times U(1)$ gauge-Higgs unification," arXiv:1404.2748 [hep-ph].

[47] N. Maru and N. Okada, "$H \to Z\gamma$ in gauge-Higgs unification," *Phys.Rev.* **D88** no. 3, (2013) 037701, arXiv:1307.0291 [hep-ph].

[48] K. Kashiwa and T. Misumi, "Phase structure and Hosotani mechanism in gauge theories with compact dimensions revisited," *JHEP* **1305** (2013) 042, arXiv:1302.2196 [hep-ph].

[49] G. Cossu, H. Hatanaka, Y. Hosotani, and J.-I. Noaki, "Polyakov loops and the Hosotani mechanism on the lattice," arXiv:1309.4198 [hep-lat].

[50] G. Cossu, E. Itou, H. Hatanaka, Y. Hosotani, and J.-I. Noaki, "Hosotani mechanism on the lattice," arXiv:1311.0079 [hep-lat].

[51] K. Kashiwa, H. Kouno, T. Makiyama, T. Misumi, T. Sasaki, *et al.*, "Phase structure and Hosotani mechanism in QCD-like theory with compact dimensions," arXiv:1311.4918 [hep-ph].

[52] N. Irges and F. Knechtli, "Non-perturbative Gauge-Higgs Unification: Symmetries and Order Parameters," arXiv:1312.3142 [hep-lat].

[53] E. Itou, K. Kashiwa, and N. Nakamoto, "Phase structure of pure SU(3) lattice gauge theory in 5 dimensions," arXiv:1403.6277 [hep-lat].

[54] A. Roberge and N. Weiss, "Gauge Theories With Imaginary Chemical Potential and the Phases of QCD," *Nucl.Phys.* **B275** (1986) 734.

[55] V. Pestun, "Localization of gauge theory on a four-sphere and supersymmetric Wilson loops," *Commun.Math.Phys.* **313** (2012) 71–129, arXiv:0712.2824 [hep-th].

[56] A. Kapustin, B. Willett, and I. Yaakov, "Exact Results for Wilson Loops in Superconformal Chern-Simons Theories with Matter," *JHEP* **1003** (2010) 089, arXiv:0909.4559 [hep-th].

[57] F. Benini and S. Cremonesi, "Partition functions of N=(2,2) gauge theories on S^2 and vortices," arXiv:1206.2356 [hep-th].

[58] N. Doroud, J. Gomis, B. Le Floch, and S. Lee, "Exact Results in D=2 Supersymmetric Gauge Theories," *JHEP* **1305** (2013) 093, arXiv:1206.2606 [hep-th].

[59] J. Kallen, J. Qiu, and M. Zabzine, "The perturbative partition function of supersymmetric 5D Yang-Mills theory with matter on the five-sphere," *JHEP* **1208** (2012) 157, arXiv:1206.6008 [hep-th].

[60] S. Kim, "The Complete superconformal index for N=6 Chern-Simons theory," *Nucl.Phys.* **B821** (2009) 241–284, arXiv:0903.4172 [hep-th].

[61] D. Gang, "Chern-Simons theory on L(p,q) lens spaces and Localization," arXiv:0912.4664 [hep-th].

[62] Y. Imamura and S. Yokoyama, "Index for three dimensional superconformal field theories with general R-charge assignments," *JHEP* **1104** (2011) 007, arXiv:1101.0557 [hep-th].

[63] C. Romelsberger, "Counting chiral primaries in N = 1, d=4 superconformal field theories," *Nucl.Phys.* **B747** (2006) 329–353, arXiv:hep-th/0510060 [hep-th].

[64] H.-C. Kim, S. Kim, S.-S. Kim, and K. Lee, "The general M5-brane superconformal index," arXiv:1307.7660 [hep-th].

[65] A. Tanaka, H. Mori, and T. Morita, "Superconformal index on $\mathbb{RP}^2 \times \mathbb{S}^1$ and mirror symmetry," arXiv:1408.3371 [hep-th].

[66] P. Goddard, J. Nuyts, and D. I. Olive, "Gauge Theories and Magnetic Charge," *Nucl.Phys.* **B125** (1977) 1.

[67] H. Hatanaka and Y. Hosotani, "SUSY breaking scales in the gauge-Higgs unification," *Phys.Lett.* **B713** (2012) 481–484, arXiv:1111.3756 [hep-ph].

[68] S. Sugishita and S. Terashima, "Exact Results in Supersymmetric Field Theories on Manifolds with Boundaries," *JHEP* **1311** (2013) 021, arXiv:1308.1973 [hep-th].

[69] K. Hori and M. Romo, "Exact Results In Two-Dimensional (2,2) Supersymmetric Gauge Theories With Boundary," arXiv:1308.2438 [hep-th].

[70] D. Honda and T. Okuda, "Exact results for boundaries and domain walls in 2d supersymmetric theories," arXiv:1308.2217 [hep-th].

[71] C. Closset, T. T. Dumitrescu, G. Festuccia, and Z. Komargodski, "Supersymmetric Field Theories on Three-Manifolds," *JHEP* **1305** (2013) 017, arXiv:1212.3388 [hep-th].

[72] N. Hama, K. Hosomichi, and S. Lee, "Notes on SUSY Gauge Theories on Three-Sphere," *JHEP* **1103** (2011) 127, arXiv:1012.3512 [hep-th].

[73] K. Yamawaki, "Dynamical symmetry breaking with large anomalous dimension," hep-ph/9603293.

[74] V. A. Miransky, "Dynamical symmetry breaking in quantum field theories," Singapore, Singapore: World Scientific (1993) 533 p

[75] S. Weinberg, Cambridge, UK: Univ. Pr. (1995) 609 p

[76] 今村洋介, 調和関数による 3 次元分配関数の計算, 2013, 講義ノート (京都大学理学部集中講義)